POLITECNICO DI MILANO
School of Industrial and Information Engineering

Department of Energy – Laboratory of Catalysis and Catalytic Processes
Master of Science in Chemical Engineering

Applications of Ru-based catalyst for CO_2 methanation: modeling study

Supervisor:
Prof. Carlo Giorgio Visconti

Co-Supervisor:
PhD. Alessandro Porta

Candidate:
Chiara Marcon - 916067

Academic Year 2019 – 2020

To those who encouraged me

Abstract

The growing atmospheric concentration of carbon dioxide is the main anthropic cause of climate change due to the greenhouse gas effect. Among the different possibilities that can be applied as solution, the use of CO_2 as carbon source to obtain added-value products is acquiring interest. In particular, CO_2 hydrogenation to methane is one of the most promising routes. It is generally defined as Power-To-Gas technology and it allows to combine the excess renewable electric energy with the recycling of carbon dioxide. The purpose of this work is to develop a consistent model able to adequately describe experimental data already obtained on laboratory scale under isothermal conditions. Once the model has been validated, it is possible to extend the investigation of operative conditions and identify the most suitable process configuration that maximize CO_2 conversion and CH_4 purity. The results show that the optimal arrangement is composed by two reactors in series with intermediate water condenser since it is possible to operate at different temperatures enhancing the kinetics in the first reactor and achieving thermodynamic equilibrium conditions in the second one. The analysis of this configuration is then extended valuing also the reactor modeling and the assessment of operative effects on performance in order to verify whether the process scheme can be applied on the industrial scale. The problem of thermal management is then addressed because the first reactor works with enhanced reaction rate and thus presents more critical issues.

Abstract (Italian)

La crescente concentrazione atmosferica di anidride carbonica è la principale causa antropica del cambiamento climatico dovuto all'effetto serra. Tra le diverse possibilità che possono essere applicate come soluzione, l'uso di CO_2 come fonte di carbonio per ottenere prodotti di valore aggiunto sta acquisendo interesse. In particolare, l'idrogenazione di CO_2 a metano è una delle vie più promettenti. È generalmente definita come tecnologia Power-To-Gas e permette di combinare l'energia elettrica rinnovabile in eccesso con il riciclo di anidride carbonica. Lo scopo di questo lavoro è quello di identificare la configurazione di processo più adatta per massimizzare la conversione di CO_2 e la purezza di CH_4. I risultati mostrano che la disposizione ottimale è composta da due reattori in serie con condensatore d'acqua intermedio in quanto è possibile operare a temperature diverse favorendo la cinetica nel primo reattore e raggiungendo condizioni di equilibrio termodinamico nel secondo. L'analisi di questa configurazione viene poi estesa considerando anche la modellazione del reattore e la valutazione degli effetti operativi sulle prestazioni al fine di verificare se lo schema di processo può essere applicato su scala industriale. Viene quindi affrontato il problema di gestione termica all'interno del primo reattore che operando in condizioni di velocità di reazione più spinte presenta maggiori criticità.

List of Figures

List of Tables

Key words

CO_2 methanation, ruthenium, carbon dioxide, ultra-pure methane, modeling, process scheme.

Parole chiave

Metanazione di CO_2, rutenio, anidride carbonica, metano ultra-puro, modellazione, schema di processo.

Table of Contents

Section 1: Introduction

1.1. CO_2 emissions reduction

Climate change is considered to be one of the greatest environmental threats of our times. Recent studies confirmed that the growing atmospheric concentration of carbon dioxide is one of the main causes of global warming, due to its greenhouse gas (GHG) effect. Carbon dioxide concentration in the atmosphere, in fact, has kept on increasing in the last century: the current concentration of 397 ppm is far from the preindustrial levels of 280 ppm [1]. In particular, an average growth of 2 ppm/y has been determined in the last 10 years [2].

The technologies for the reduction of CO_2 emissions can be divided in two separate groups: primary or secondary strategies. The goal of primary strategies is to reduce the emissions directly during CO2 production by improving the energy efficiency of combustion processes and/or by increasing the utilization of non-fossil energy sources. Primary strategies are usually a viable option only with a radical change in technologies as well as in energy policy. Indeed it is predicted that fossil fuels will still remain our main source of energy at least in the coming decades [3]. On the other hand, secondary strategies aim at a CO_2 capture after its production, allowing to maintain the conventional technology and in some case even the process layout. In this way the solution coincides in changing the attitude towards the produced wastes, including carbon dioxide. Once captured, CO_2 can be stored exploiting Carbon Capture and Storage (CCS) technologies or used as chemical feedstock through Carbon Capture and Utilization (CCU) processes.

These two approaches are complementary, while CCS technologies aim at capturing and subsequently storing, chemical utilization allows to generate added-value products. In this context, carbon dioxide can turn out to be an attractive C_1 building block in organic synthesis as it is highly abundant carbon source [4]. The utilization of CO_2, complementary to its storage, is indeed attractive, especially if its conversion to useful bulk products is economically profitable.

Both for CCS and CCU the first step is CO_2 capture. This method, in particular, can be applied to many industrial processes, most notably power plants and metallurgical industries, but in general to all the production sites equipped with burners that intrinsically discarded carbon dioxide during processes of combustion. The most important aspect that must be considered is the concentration of carbon dioxide in the exhaust gases. In the presence of air, during combustion, only the oxygen fraction (21 mol.%) is reactive while the nitrogen (79 mol.%) behaves as an inert. For this reason, downstream of the reactor, a flue gas stream composed in majority of inert nitrogen is founded, with low concentration of CO_2 and water. There are three basic capture technologies: post combustion, oxyfuel post combustion and pre combustion.

Post combustion processes separate CO_2 from exhaust gases. The two main methods are based on absorption in liquid solvents and in solid sorbents. Most commercially available techniques use wet scrubbing with aqueous amine solutions. Carbon dioxide is removed from the flue gases by the amine solvent at relatively low temperatures. The solvent is then regenerated by heating for its reuse, before being cooled and recycled continuously. Once separated, carbon dioxide is dried, compressed and transported to safe storage. The main disadvantage of post combustion capture systems is the dilution of the flue gases with nitrogen and, for this reason, it is necessary to operate with very large units. Moreover, the effect of thermal swing depends on the temperature of the reboiler which is limited by the thermal degradation of the amine solution. The selection of the solvent is thus an important aspect to take into account.

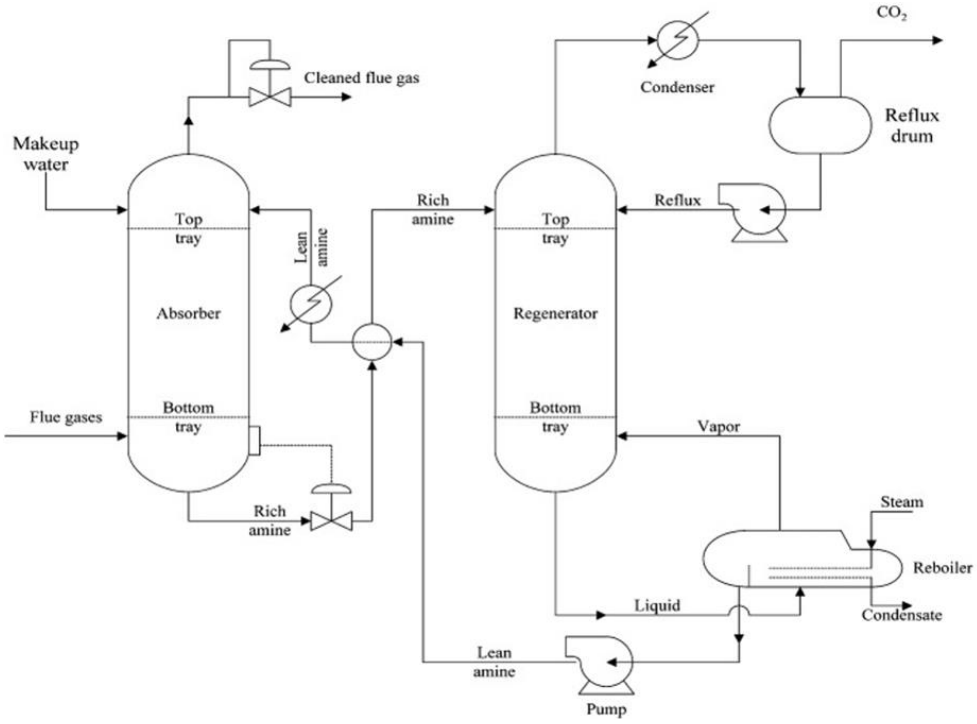

Figure 1.1. Scheme of basic chemical absorption/stripping process for amine-based CO_2 capture.

Advanced amine systems have been developed in order that CO_2 capture technologies can operate with a heat duty less than 2.7 MJ/tCO2 and an equivalent work less than 250 kWh/tCO2 (including compression to 150 bar). The innovation, contributing to the reduction of the energy used, coincides with the discovery of combined solvents, constituted for instance by piperazine (PZ) and methyl diethanolamine (MDEA). These systems allow to obtain thermally stable amines with high heat of CO_2 absorption that maximize the energy performances of thermal swing regeneration [5]. Although the amine scrubbing is the most established post combustion method for carbon dioxide capture, other technologies have been investigated. Membranes can be used to achieve CO_2 removal through the intrinsic selectivity of the material. This method for gas separation is relatively new and the efficiency obtained is generally too low to be promptly commercialized. On the contrary, solid adsorbents such as activated carbons, zeolites and mesoporous silicates have been extensively studied for CO_2 capture. In this case, a dry process occurs and exhibits unique features including low pressure drop, good mechanical properties and

ability to handle dust containing gas streams. While conventional wet solvent processes are widely applied, these methods are currently used in selected applications due to their high cost [6]. The main problem, as for amine solutions, is that high heat duty is required for the CO_2 desorption. Very stable carbonates could be formed using solid systems therefore they require regeneration exploiting very high temperatures or in some cases it is also necessary their replacement.

Oxyfuel post combustion processes mitigate the problem of diluted exhaust gases since carry out the combustion in presence of pure oxygen instead of air. This method was proposed in the early 1980s for the purpose of producing a high purity CO_2 stream to be applied in Enhanced Oil Recovery (EOR) [7]. and simultaneously reduce greenhouse gas emissions from fossil fuel energy generation. Pure oxygen is supplied by an air separation unit (ASU) located upstream of the burner. Although it is expensive, this method allows to obtain the separation of the CO_2 by simple air condensation and, since no nitrogen is present also no NO_x formation occurs. The main drawback is, however, related to high temperatures reached by the system due to the absence of a diluent in the reacting mixture. In order to minimize this issue generally the recirculation of exhaust gases is performed. However, recently oxyfuel fluidized bed combustion (FBC) has also become increasingly important as a potential technology, offering both fuel flexibility and possibility of temperature control. Moreover, to drastically reduce the cost of oxy-combustion, new technologies for oxygen production have begun to be developed. Praxair Inc., in particular, is investigating an alternative approach: instead of a cryogenic ASU, the company has decided to use a membrane within the boiler. Therefore, at high temperature only oxygen can diffuse selectively across this ceramic membrane in order to perform the combustion of the fuel [8].

Pre combustion processes recover carbon dioxide from process streams before the combustion. A very promising approach in this context involves supplemented equipment for Water Gas Shift reaction ($CO + H_2O \rightarrow CO_2 + H_2$). In this case the separation unit for CO_2 is easy because the concentration of the gas is high and it is possible to use physical

separations with cheap solvents, such as capture processes Rectisol® or Selexol®. With physical solvents, capacity is generally proportional to CO_2 partial pressure and the regenerative unit require less energy than post combustion processes since no chemical interaction occurs between carbon dioxide and solvent. The ENCAP project consortium[1] is currently investigating also chemical looping combustion processes. Oxygen is supplied by a solid oxygen carrier and chemical looping is carried out in two fluidized beds. In the first bed, a solid metal-based compound is oxidized while in the second one, the oxide is reduced to its initial state by the fuel, producing a gas with a high concentration of CO_2 that can be then captured and sequestered.

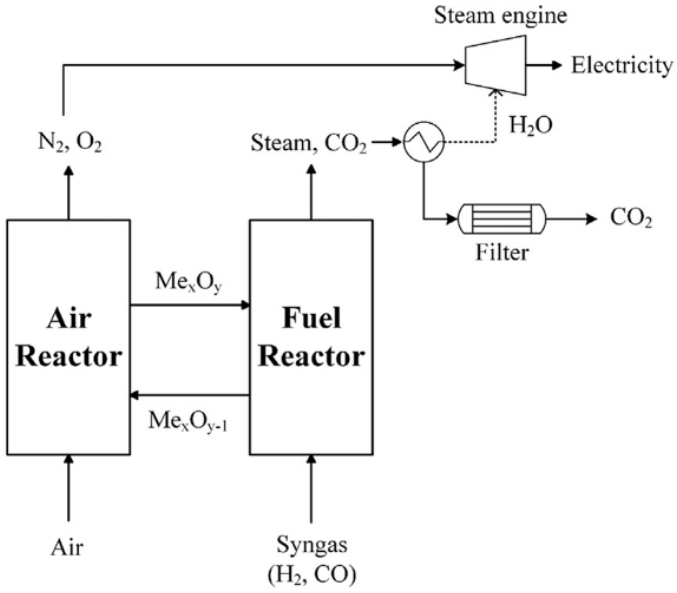

Figure 1.2. Scheme of chemical looping combustion.

[1] ENCAP (ENhanced CAPture of CO_2) is a 22 M€ technology development Programme of the European Commission. It involves energy industries, equipment suppliers, research institutes and universities. The project aims at developing cost efficient pre-combustion CO_2 capture and oxy-fuel technologies for power generation based on fossil fuels, to substantially reduce the cost of CO_2 capture. ENCAP targets at least 90% CO_2 capture rate and 50% CO_2 capture cost reduction, compared to typically 50 – 60 € per ton of CO_2, reported before the project started in 2004.

This application, however, foresees a radical change of the production configuration, making the technology more difficult to be applied to pre-existing plants. Another possible solution of pre combustion CO_2 capture systems is the use of polymer membranes. In comparison to other separation techniques, they are generally less energy intensive. Membrane reactors can also be exploited for improving shift conversion. The catalyst would be placed inside membrane tubes and this would permit the shift reaction to go to completion in a single stage [9].

The application of different CO_2 capture techniques is a balance of fixed and mobile costs. It is important also to highlight that direct air capture (DAC) technologies have recently gained significant attention among researchers, because they could minimize the problems associated with transporting large volumes of CO_2 from point-source emitters to sites suitable for geological sequestration. Although the concept is essentially similar to that of adsorption-based CO_2 capture, the diluted concentration of carbon dioxide in air ($\sim$ 415 ppm) makes the DAC a very challenging technology. Materials with strong binding affinities and high carbon dioxide selectivity are required. For this reason, various aqueous hydroxides and solid materials including alkali and alkali-supported carbonates, anionic-exchange resins and amine functionalized metal oxides have been evaluated. At this moment, the estimated DAC cost is, however, significantly higher than that of capture from large point sources and this makes the technology still difficult to be commercialized [10].

1.1.1 Carbon Capture and Storage

Carbon Capture and Storage (CCS) covers a broad range of technologies that are being developed to transport CO_2 emissions from fossil fuel to safe geological storage, rather than being emitted to the atmosphere. CCS involves the collecting of flue gases produced by large industrial plants, the compression for transportation and the storage of CO_2 in a safe and carefully selected site so that it does not escape in the atmosphere and it is permanently stored. Carbon Capture and Storage is currently considered to be technically feasible at

commercial scale. It is important, however, to highlight that this technology will always require additional energy compared to projects designed without a CCS dedicated section so adequate advantages or incentives must be present in order to adopt this type of route [11].

Once the carbon dioxide has been captured, usually CO_2 is stored in geological areas associated with oil and gas extraction technologies, hence it is necessary to transport it from the carbon capture plant to the specific area. Pipelines are a mature and diffuse technology and it is the most common method for CO_2 transportation. The gas is compressed at high pressure, above 8 MPa, to avoid two-phase flow regimes and to increase the gas density. Since the carbon dioxide dissolved in water can form carbonic acid, which is corrosive for the manganese steels pipelines (standard pipelines), it is necessary to dry the gas stream. However, in order to have greater safety and to avoid any possible breakage, the manganese pipelines are hardly used even if the flue gas has been dehydrated, thus they are typical made by a corrosion resistant alloy with an internal polymer coating. An alternative solution is the transportation by ships, road or rail tankers, but for this type of transportation it is necessary to condense CO_2, either by compression or by cooling. The choice between the different alternatives is typically a function of the distance among the carbon capture plant and the storage zone. For long distances it is always preferable to use pipelines.

With regard to the CO_2 storage technologies, the injection into rock deep underground is generally performed. This kind of storage system is selected for its huge capacity to store and retain the gases. The geological areas that can be used for the purpose of carbon dioxide storage are called ‘sedimentary basins’: they include limestone, sandstone and clays. They have enough pores and voids to allow injection, enhancing movement and spreading of gases. Therefore, in addition to a good permeability, it is necessary to contain the gases for centuries. CO_2 can be injected into oil reservoir to help oil recovery but the most common situation is pumping it into seabed, at depth more than 1 km, since high gas retention capacities are guaranteed. The main concern is to ensure that the fluid pressure does not increase sufficiently to induce fracturing and to ensure that the mobile CO_2 does not find a

permeable path to the surface. Over time, with capillary, dissolution and mineral trapping, storage becomes more secure. To make a significant contribution to reduce atmospheric emissions, however, it will be necessary to store several Gt of CO_2 each year worldwide, especially in large areas with significant industry and fossil-fuel power generation. The determination of storage points, suitable for the CO_2 ton provided during the entire power-plant lifetime, usually met the public opposition (a 'not in my backyard' response) [12]. The only one full-scale CCS project is indeed located in Norway. In particular, it is one of the first industrial plans aimed to develop an open access infrastructure with the intent and the capacity to store significant volumes of CO_2. For the first time ever, at the end of 2019, tests began in the North Sea not to dig for natural resources but to bury CO_2. Project partners Shell and Total, along with operator Equinor, looking to unlock large scale emissions reductions, have recently commenced assessing a reservoir's availability to store CO_2 underground [13]. The main advantage of CCS technology is that investments are generally low compared to CCU and, in particular, the disposed volumes are certainly higher. However, as reported above, the main issue is to obtain permissions to locate buried CO_2. This could be defined as the rate determining step for the Carbon Capture and Storage technology.

1.1.2. Carbon Capture and Utilization

The Carbon Capture and Utilization (CCU) is probably the most interesting technology for the reduction of carbon dioxide concentration in atmosphere since it can turn a waste product, as the CO_2, into valuable products. The utilization of CO_2 a feedstock to make valuable chemicals, materials and transportation fuels is potentially more desirable and provides a better long-term solution than sequestration.

The primary utilization route can be classified as Enhanced Oil Recovery (EOR). It refers to a procedure in which a substance is injected into a reservoir to pressurize rock formation and to release any oil and gas that may have been trapped underground. During the CO_2

EOR process, the injected carbon dioxide mixes with the oil, then stream is pumped to the surface and separated. The recovered carbon dioxide is supplied into the cycle to repeat the process. Basically, CO_2 flooding is one of the most common and efficient methods used in EOR, as it mixes with the oil, expands it and makes it lighter and easier to recover [14]. Numerous facilities have been yet implemented this method in their reservoirs as the Abu Dhabi Company for Onshore Petroleum Operations Ltd. (*ADCO*) that in 2009 built the first CO_2-EOR pilot plant in the Middle East [15].

Outside of EOR, as a raw material, carbon dioxide is commonly used in the beverages industry, in urea production, in water treatment and in enhanced oil recovery with a current global usage of 232 Mt/year. The most important applications of fine chemicals are urea (~160 Mt/year), inorganic carbonates (~60 Mt/year), polyurethane (~18 Mt/year), acrylic acid and acrylates (~10 Mt/year) [16]. However, currently, less than 1% of CO_2 emitted into the atmosphere is utilized [17]. Among all the processes that involve the conversion of carbon dioxide, certainly those which arouse the greatest interest are the productions of fuels and bulk chemicals since the high market demand would contribute to an efficient reduction of emissions. Methane, methanol, syngas, and alkanes are some of the compounds that can be produced by utilizing captured CO_2 as a feedstock. Knowing that carbon dioxide is a thermodynamically stable molecule, its utilization requires the application of a large amount of heat and catalyst inventory to obtain high fuel yields. In the context of fuels production from captured CO_2, hydrogenation and dry reforming of methane (DRM) are the two most important pathways. Dry reforming of methane has attracted significant research interest in terms of using CO_2 for syngas production and, typically, the purity of syngas that is produced by DRM is higher than that produced by partial oxidation and steam reforming. The main hurdle, however, lies in the design and the development of catalysts that not only exhibit high activity under different reaction conditions, but that are also resistant to coke formation and show long-term chemical and structural stability. On the other side, among all the reactions of hydrogenation of carbon dioxide, probably the most promising ones are the methane and the methanol synthesis. In the CO_2 hydrogenation, however, the source of hydrogen from fossil fuel appears to be

problematic, as this can itself lead to an increase of emissions to the atmosphere. The required quantity of hydrogen in the feed stream is high thus it is necessary to reduce as much as possible the cost as well as the environmental impact related to the production. For this reason, renewable energy (e.g., solar, wind, biomass) must be used as alternative to fossil fuels in order to carry out electrolysis process. Recently, for example, Audi motor company, together with plant builder SolarFuel, designed an e-gas plant in Germany. It is the world's first industrial facility to use CO_2 and renewable electricity to generate synthetic natural gas [18].

Another interesting solution of CO_2 utilization is the desalination of water. Actually, most plants do not employ carbon dioxide to perform desalination owing to economic constraints but new technologies are being developed for an efficient utilization of carbon dioxide in this process. This method started to be investigated since sea water, mixed with ammonia, exposed to CO_2, forms weak bonds, which leads to the removal of the ions from the water phase. The products formed, Na_2CO_2 and NH_4Cl, are also heavy and, thus, can easily settle to the bottom of the tank . Then they are recycled or used as a feedstock for the synthesis of ammonia and chlorine. Laboratory experiments using natural seawater are currently underway having shown a number of proofs of reliability, however the estimated desalination costs are currently higher than agricultural or municipal water costs [19]. Even the utilization of CO_2 as feed for crops of microalgae, in order to produce bio-oils and chemicals, can be considered as CCU process. The advantages offered by this approach include higher growth rate and no competition on land with other plants, however, captured CO_2 should be purified before feeding into a photobioreactor. In any case, adopting these emerging technologies depends to a great extent upon their cost effectiveness.

In general, only small fraction of captured carbon dioxide from gas effluents has been actually used to produce other value-added products. Although there is a great interest in turning captured carbon dioxide into chemicals, the proposed laboratory scale technologies are still far from an industrial large-scale commercialization. The reason is partly because, in most cases, CO_2 conversion rates and overall yields of main products are low and thus

do not meet the requirements for a wide deployment. The estimated high costs along with low efficiency of these technologies are two key factors responsible for such a slow progress. However, there is huge potential in various industries to market the utilization of captured CO_2 as a renewable resource instead of permanently sequestering it underground or in oceans. It is expected that with future developments, the majority of proposed techniques related to CO_2 utilization will continue to have lower costs, making CCU technologies more addressable to the market [20].

1.2. Hydrogen production and storage

Hydrogen is present in its molecular form only as meager traces in areas with volcanic activity, while is widely available as atomic component in many compounds. Therefore, its utilization should include an extraction from one of these sources requiring a high energy expenditure. In order that the executed process is completely sustainable it is necessary to consume as low as possible energy input and hydrogen must be produced from renewable sources. Large availability and low cost of hydrogen are the main requirements to obtain a process of CO_2 utilization that can be economically profitable.

The main sources for the production of hydrogen are primary sources (fossil fuels), intermediate chemical compounds (refinery products but also ammonia or methanol), alternative sources (biomass) and secondary sources (electric energy). Nowadays, 45 million of ton/year of hydrogen are produced industrially worldwide, of which approximately 90% is derived from fossil fuels [21]. There are three primary techniques: steam reforming of methane (SRM), partial oxidation (POX), and autothermal reforming (ATR). With a market share of 48%, steam reforming is at present the most commonly used technology, since it is the less polluting option to obtain hydrogen from fossil fuels and its efficiency range is comprehend from 70% to 80%. SRM occurs at 700 - 1100°C generating syngas, composed by H_2 and CO.

$$CH_4 + H_2O \rightarrow CO + 3H_2 \quad \Delta H_R^0\,(298K) = 206\ kJ/mol$$

The reaction is favored at high temperatures and low pressures. Despite the thermodynamics, it occurs at high pressures since, in this way, the volumes are reduced and hydrogen is directly obtained under pressure. One issue is the possible formation of coke. Its presence is, however, limited by operating at high vapor/methane ratios in the feed. Moreover, in this process additional hydrogen may be obtained from carbon monoxide by the Water Gas Shift reaction. Other important techniques to produce hydrogen include partial oxidation of hydrocarbons, as methane. Alternatively, there is also the process of catalytic partial oxidation of hydrocarbons. In this case, the Ni or Rh catalyst allows to operate in mild conditions but the control of temperature is more restrictive to avoid coke formation or hot spot phenomenon, which could lead to the deactivation of catalyst. Finally, the last possibility of production of hydrogen from hydrocarbons is present in the autothermal reforming. This process is a combination of both steam reforming (endothermic) and partial oxidation (exothermic) reactions. ATR has the advantages of not requiring external heat and being simpler than other technologies, however steam reforming presents a higher hydrogen efficiency. For this reason, the autothermal reformers have a limited commercial application.

Other methods applied, besides the reforming, are the biomass-based processes. The current technologies include gasification and pyrolysis. The gasification allows to convert carbon sources, such as biomasses, into carbon monoxide, hydrogen and other gaseous compounds. It is a thermal degradation that operates at high temperatures, 700-800°C, in the presence of an oxidizing agent in order to produce syngas. Pyrolysis, on the contrary, operates in absence of oxygen and air, hence the advantage of this process is the reduction of CO_x emissions. The reaction can be generally described by the following equation: C_nH_m + heat $\rightarrow n$C + 0.5 mH$_2$. One of the challenges with this approach is the potential fouling caused by the carbon formation. Gasification and pyrolysis are also applied to heat treatment of waste because they can degrade almost any organic materials. However, reactors need to be built on large scale and require massive amounts of material to be

continuously fed. Currently, the high logistics costs typically limit the plants to be located. The price of hydrogen obtained is about three times greater than the price of hydrogen obtained by the steam reforming process. It is necessary also to point out that the content of hydrogen present in the biomasses is quite modest (below 10%) [22].

Regarding the technologies used for the production of hydrogen directly from water, the electrolysis is the most exploited one. It consists of circulating a direct current through water to separate its molecules into hydrogen and oxygen. The current flows between two separated electrodes immersed in an electrolyte to raise the ionic conductivity. The process requires the implementation of a diaphragm or separator to avoid the recombination of the compounds generated at the electrodes. The hydrogen obtained with this technology has a high purity: up to 99.999 vol.% can be achieved after drying but the major challenges encountered in the production of hydrogen from renewable sources are the electricity costs, operating expenses, and the investment costs of the electrolyte. From a technological point of view, the advanced alkaline cells are at present sufficiently developed to start the production of renewable hydrogen at significant rates. They are already used in commercial operations, but they are not suitable for dynamic applications and their efficiency ranges stay between 55 and 75% [23]. Polymer electrolyte membrane (PEM) devices are commercially available, but their cost is high due to the presence of noble metal such as Pt and Ir necessary as eletrolyzers. Their efficiency is comparable to that of alkaline electrolyzers 50-80% but this technology seems more suitable for low-scale flexible applications. Solid oxide electrolyzers (SOEs), for hydrogen production from steam, are instead at R&D stage. They are less costly than PEMs and allow efficiency as high as 100%. They show great potential since the use of high temperature reduces their electricity usage but dynamic operation result in high thermal stresses that can threaten their long term stability [24]. Continuous improvements have been made to these technologies and this has led also to the development of a zero-gap design cell. This technique achieves a gap between the two electrodes equal to ~ 0.5 mm, thus reducing the ohmic resistance contribution of the electrolyte. In addition, a gas diffusion layer provides an electrical connection from the porous electrode to the bipolar plate, whilst simultaneously allowing

a feed of electrolytic solution and the removal of the gas products. This permits to obtain cells with a very compact design and high efficiency [25]. In addition, they have a high degree of modularity, what makes them suitable for decentralized applications in residential, commercial, and industrial areas.

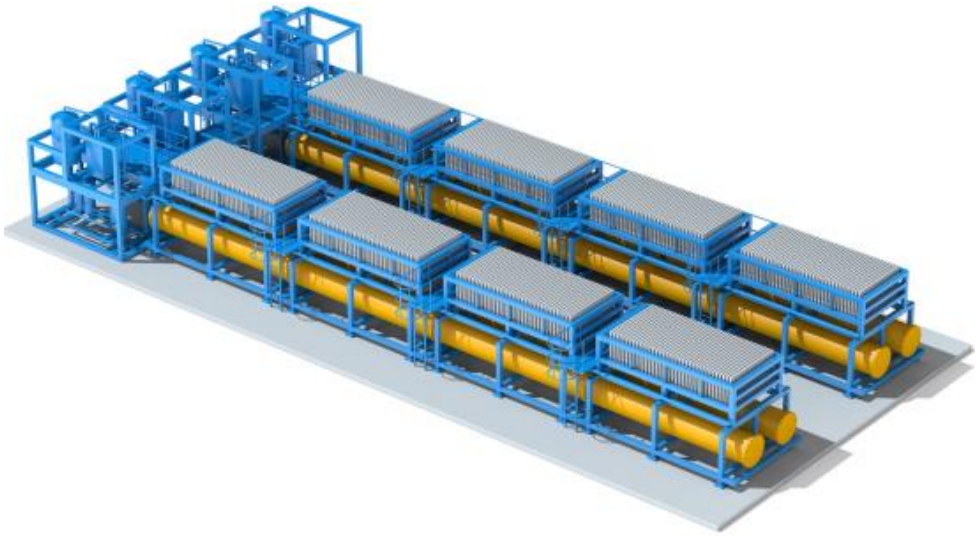

Figure 1.3. Large-scale electrolysis, 20 MW module.

Addressing the issue of the production of hydrogen from renewable sources, today the most consolidated technology coincides with the generation of electric energy from photovoltaic cells or wind turbines and the subsequent application of this energy in the electrolysis process of water. The high necessity of electric energy is, however, the main limit because it strongly affects the operative costs. Support policies and recent technological progress are contributing to cost reduction and knowledge improvement. In general hydrogen production from renewable energy is becoming more and more cost competitive. Indeed, the growing amount of electric energy coming from intermittent renewable sources in EU countries is leading to daily and seasonal overproduction periods, during which the energy cannot be supplied to the electrical grid for stability purposes [26]. This problem is expected to be relevant especially in developed countries, where the electricity mix is going to shift towards renewable sources [27]. Different techniques have been investigated to store this

excess renewable electricity during times of low demand and high production. The chemical conversion of excess electric energy into an energy vector which can be stored and moved without the restriction imposed by the power grid is the most attractive process to store the surplus energy [28].

Besides the electrolysis, other technologies are used for the production of hydrogen directly from water. In photoelectrolysis, for instance, is present a semiconducting photoelectrode that absorbs solar energy and simultaneously creates the necessary voltage for the direct decomposition of water molecule into oxygen and hydrogen. The light absorption of the semiconductor material is directly proportional to the performance of the device. Although this process is still in the phase of experimental development, it seems to be an effective method of hydrogen production from renewable resources. In thermochemical water splitting, also called thermolysis, heat alone is used to decompose water to hydrogen and oxygen. Water will decompose at 2500°C but materials stable at this temperature are not easily available [29].

Storage and transport of hydrogen must guarantee safety since hydrogen is a flammable gas and it can react roughly with oxidants and unsaturated hydrocarbons causing highly exothermic reactions. There are various possibilities of transport. One method is distribution by pipeline. This solution is frequently exploited for onsite supply but hydrogen can be transported also for long distances via pipeline and this is generally performed for consistently high consumption, as in the case of industrial areas. Linde AG, for instance, operates a pipeline network long more than 100 km in Germany [30]. Equipped trucks transport hydrogen over long distances. In this case, gaseous hydrogen is stored under high pressure in special trailers. The most common methods include compression or liquefaction. The storage is generally at 200-250 bar and taking into account that at atmospheric pressure hydrogen does not liquefy until -253 °C, much energy must be employed [31]. Ideal materials of a highly pressurized cylinder must have very high tensile strength, low density and do not react with hydrogen or allow hydrogen to diffuse into them. Most pressurized cylinders used austenitic stainless steel (e.g. AISI 316 and 304), Cu

or Al alloys, which are largely immune to hydrogen effects at ambient temperatures. The large amount of energy necessary for liquefaction and the continuous boil-off of hydrogen limit the possible use of liquid hydrogen storage systems only to applications where the cost of hydrogen is not an issue and the gas is consumed in a short time, such as in space application. In 2018 NASA Kennedy Space Center's Launch Complex 39B started to build the world's largest liquid hydrogen storage tank [32]. Alongside well-established high pressurized cylinders for laboratory applications and liquid hydrogen storage methods for specific applications, metal hydrides and complex hydrides are under development as new materials to offer safe and efficient solutions for the hydrogen storage. The storage of H_2 as solid or liquid hydride has given promising results, but the cost, weight of the storage material and reversibility of the H_2 storage are still an issue [33].

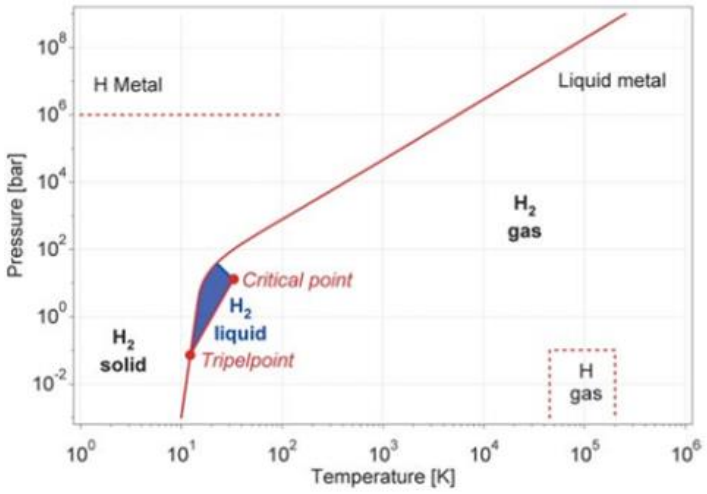

Figure 1.4. Primitive phase diagram for hydrogen.

1.3. Power to Gas

Combining what has been presented with regard to the CO_2 utilization and the current issues of H_2 storage, synthetic hydrocarbons such as methanol, methane, or liquid hydrocarbons could be considered as promising storage media able to efficiently store excess renewable energy as well as recycle the CO_2 content approaching carbon neutrality.

In particular, the technologies that allow the storage of excess renewable energy in a liquid or gaseous carrier are referred to as Power-to-X (PtX) [34,35]. The hydrogenation of carbon dioxide to methane is particularly appealing. It produces a fuel identified as Substitute or Synthetic Natural Gas (SNG) through the Sabatier reaction. With respect to other fuels, CH_4 has a rather low added value and requires the highest amount of H_2 per mol of product. However, a few advantages may be pointed out. First of all, the Sabatier reaction is a selective process, and, despite the thermodynamic limitations, high CH_4 yields per pass can be achieved [36]. This allows in principle to avoid the recirculation of unreacted gases with the associated costly separation of the products that instead could be present in other CO_2 utilization processes, such as the combination of Reverse Water Gas Shift and Fischer-Tropsch reactions for the production of liquid fuels or the methanol synthesis [37]. Furthermore, the produced SNG can be injected into the existing natural gas pipeline network to be stored, transported and used as needed [38]. A large number of PtG plants are currently in operation in Europe, most of them in a demonstrative/pilot scale [39]. A schematic representation of the process is reported in Figure 1.5.

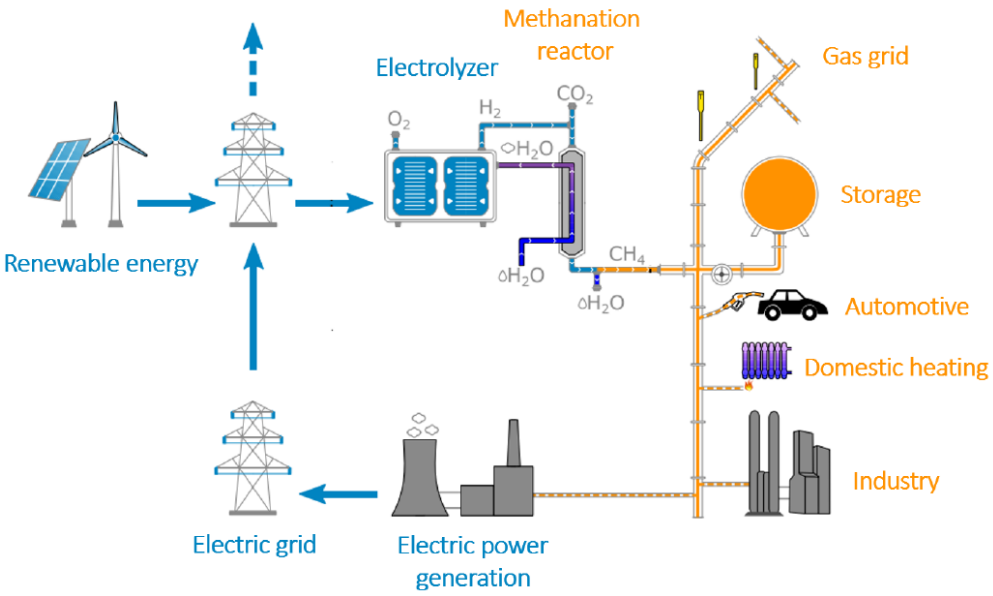

Figure 1.5. Schematic representation of the PtG concept.

1.3.1. CO_2 methanation reaction fundamentals

The reaction of CO_2 methanation (1) was discovered in 1897 by the French chemist Paul Sabatier. It comprises the reduction of carbon dioxide to methane, while the electron donor hydrogen is oxidized to water.

$$CO_2 + 4H_2 \leftrightarrow CH_4 + 2H_2O \quad (1)$$

$$\Delta H^0_R(298K) = -165 \text{ kJ/mol} \quad (1.1)$$

$$\Delta G^0_R(298K) = -113 \text{ kJ/mol} \quad (1.2)$$

It is exothermic, reversible and spontaneous at ambient temperature. Gibb's free reaction energy is negative but increases significantly with temperature becoming also positive at temperature over 600°C. Overcoming this value the reverse reaction is favoured.

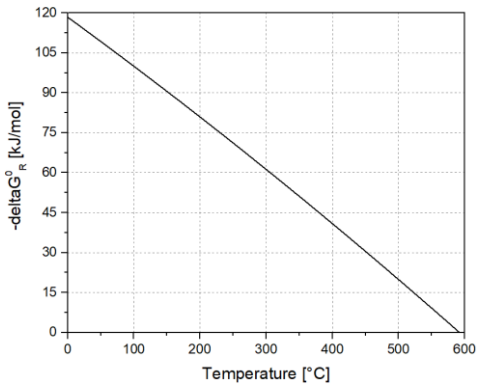

Figure 1.6. Gibb's free reaction energy as function of temperature.

Therefore, it is preferable in order to obtain high CO_2 conversion to operate at low temperatures. However, decreasing temperature more and more, the kinetics of the reaction could become limited. The thermodynamic study of the process is necessary to know conversion constraints and yields achievable under different situations. In order to fully define the thermodynamics of the reaction system, two reactions involving 5 species (CO_2,

CO, CH_4, H_2, H_2O) must be considered. The reactions investigated for the thermodynamic analysis are the Sabatier (1) and the Reverse Water-Gas Shift (2):

$$CO_2 + H_2 \leftrightarrow CO + H_2O \tag{2}$$

$$\Delta H^0_R(298K) = 41 \text{ kJ/mol} \tag{2.1}$$

$$\Delta G^0_R(298K) = 29 \text{ kJ/mol} \tag{2.2}$$

It is of interest know the variation of CO_2 conversion (3) and the carbon selectivity of CH_4 (4) and CO (5) as function of temperature and pressure working with an inlet H_2/CO_2 ratio in the feed equal to the stoichiometric one, 4 mol/mol.

$$X_{CO_2} = \frac{\dot{n}_{CO_2,in} - \dot{n}_{CO_2,out}}{\dot{n}_{CO_2,in}} \cdot 100 \tag{3}$$

$$S_{CH_4} = \frac{\dot{n}_{CH_4,out}}{\dot{n}_{CH_4,out} + \dot{n}_{CO,out}} \cdot 100 \tag{4}$$

$$S_{CO} = \frac{\dot{n}_{CO,out}}{\dot{n}_{CH_4,out} + \dot{n}_{CO,out}} \cdot 100 \tag{5}$$

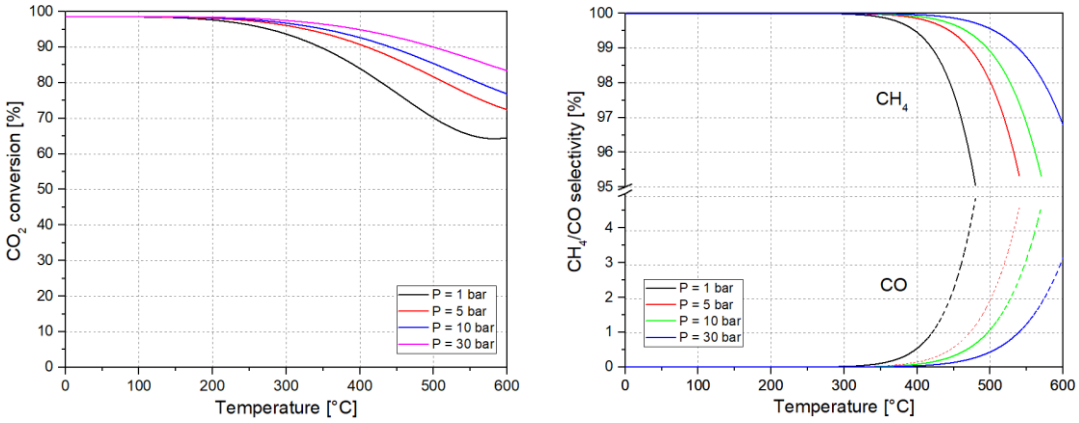

Figure 1.7. CO_2 conversion and selectivity of CH_4 and CO at thermodynamic equilibrium as function of temperature and pressure.

CO_2 conversion increases at higher pressures, as the reaction occurs with a reduction in number of moles.

The pressure dependence is confirmed by the equilibrium constant K_P, being inversely proportional to the square of pressure.

$$K_P = \frac{P_{CH_4} P_{H_2O}^2}{P_{H_2}^4 P_{CO_2}} = \frac{1}{P^2} \frac{x_{CH_4} x_{H_2O}^2}{x_{H_2}^4 x_{CO_2}} \quad (6)$$

In addition, the Sabatier reaction is exothermic thus the methanation process is less favored by increasing temperature. However, at atmospheric pressure and high temperatures (close to 550°C), the conversion begins to increase. This happens because the contribution of the endothermic reaction of RWGS (2) becomes more relevant, bringing to a significant raise in the production of CO and a consequent decrease in selectivity of methane. It occurs at atmospheric pressure but it is not valid in higher pressure situations, in which only a decreasing conversion trend is observed. Indeed, unlike the methanation reaction, the RWGS is an equimolar reaction that does not have a dependence of the equilibrium compositions on pressure.

$$K_P = \frac{P_{CO} P_{H_2O}}{P_{H_2} P_{CO_2}} = \frac{x_{CO} x_{H_2O}}{x_{H_2} x_{CO_2}} \quad (7)$$

At high pressures, indeed, the increasing conversion rate becomes less noticeable, since RWGS has no significant effect. Overall, from a thermodynamic point of view, if the purpose is to obtain high CO_2 conversion, the Sabatier reaction has to be conducted at high pressures and low temperatures.

Concerning the effect of H_2/CO_2 inlet ratio on thermodynamic equilibrium at constant atmospheric pressure, CO_2 conversion is favored at high ratios H_2/CO_2. In particular, it is highly favoured by the presence of an increasing amounts of H_2 at temperatures below 300°C. If the ratio results lower than the stoichiometric one, hydrogen becomes the limiting reagent and, consequently, the conversion decreases. When the inlet composition of H_2/CO_2 is between 2 and 4, as the temperature increases, the conversion initially decreases, but at certain point, when the reaction of RWGS begins to be favored, it increases more markedly. On the contrary, at stoichiometric or over-stoichiometric ratios, at the begin CO_2 conversion is 100 % and gradually decreases, as temperatures become higher, because of

the exothermic nature of the methanation reaction. These considerations are in accordance also with the selectivity plots, as carbon monoxide production increases at high temperatures while curves describing the selectivity of methane depict a negative trend.

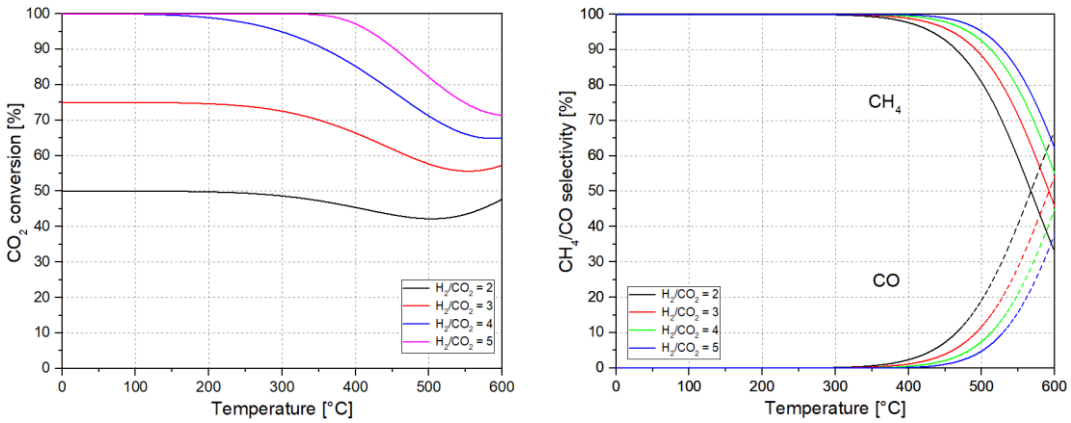

Figure 1.8. CO_2 conversion and selectivity of CH_4 and CO at thermodynamic equilibrium as function of temperature and reagents ratios.

Concerning the best selection of parameters to obtain high CO_2 conversion based on thermodynamic analysis, besides low temperatures and high pressures also high H_2/CO_2 ratios are preferable. As regards the H_2/CO_2 ratio of the feed mixture, to avoid having too low conversions, ratio greater than or equal to 4 is preferable. However too high values mean large hydrogen flows and, therefore, additional costs as reported in previous chapters. Moreover, in case of over-stoichiometric H_2/CO_2 ratios, indeed, the high amount of remaining H_2 in product stream has to be removed in a following separation step, which is much more expensive and complicated than CO_2 removal using an adsorption method. High pressures represent an increase in compression costs, which are not necessarily repaid by a more quantitative production. Moreover, operate at low temperatures means that low reaction rates will be involved. Although the reaction is spontaneous, it proceeds slowly with a negligible kinetics, hence, a proper catalyst should be used and it is necessary that it is active at low temperatures in order to achieve high CO_2 conversion values.

Next to the direct conversion of CO_2 to CH_4, also the Reverse Water Gas Shift (RWGS) reaction, possibly followed by CO methanation, chain-growth reactions on basis of CO_2 or CO as well as carbon deposition might be catalyzed. For this reason, in addition to good activity, the catalyst must be as selective as possible towards the Sabatier reaction.

	ΔH_R^0 [kJ/mol]	ΔG_R^0 [kJ/mol]
Reverse water-gas-shift reaction (RWGS)		
$CO_2 + H_2 \rightleftharpoons CO + H_2O$	41	29
CO methanation		
$CO + 3\,H_2 \rightleftharpoons CH_4 + H_2O$	-204	-142
chain growth (CO_2)		
$CO_2 + 3\,H_2 \rightleftharpoons -CH_2- + 2\,H_2O$	~ -110	-
chain growth (CO)		
$CO + 2\,H_2 \rightleftharpoons -CH_2- + H_2O$	~ -150	-
Carbon deposition/Boudouard reaction		
$2\,CO \rightleftharpoons C + CO_2$	-172	-120

Table 1.1. Possible reactions occurring within the system.

Various studies have been done on supported catalysts for the CO_2 hydrogenation to methane showing that the reaction is kinetically favoured with VIII group metal-based supported catalysts. Metals, such as ruthenium, rhodium and nickel on various supports are considered effective catalysts. In contrast, Pt preferably catalyzes the RWGS [40], while Co and Fe are active for chain growth reactions and for this reason exploited in Fischer-Tropsch synthesis [41]. Among all the catalysts that have been investigated in recent years, Ni and Ru are currently rated as the most promising for Sabatier reaction.

Over the last period, Ni-based catalysts have been intensively studied because of their wide availability. In view of economic feasibility, concerning large scale technical applications, Ni-based catalysts allow fast reaction rates at relatively low cost. However, literature reports that high activation temperatures are needed to achieve the maximum CO_2 conversion, which results in undesirable influences on the catalyst stability as well as in increase of energy consumption [42]. Different studies have been done to enhance the activation at low temperature but another problem occurs in this condition because strong interactions between the metal particle and CO are present, which induce the formation of

undesired nickel carbonyls (Ni(CO)x), resulting in sintering as well as fouling due to carbon whisker formation. It is necessary that over their lifetime catalysts remain functional and active for prolonged operative times, avoiding any type of deactivation phenomenon, such as fouling, sintering and poisoning [43]. Fouling coincides with the deposition of species onto the catalysts surface, provoking the blockage of active sites and consequently a decrease of activity. Mostly carbon or coke deposits occur in heterogeneous catalytic systems. They may block reversibly the access of reactants to active sites on catalyst surface by chemisorbing as a monolayer or physically adsorbing with a multilayer arrangement. The decrease of active sites may occur also at high temperatures, due to irreversible chemical transformation of catalytic phases to non-catalytic phases or to particle growth, resulting in the modification of particle dimensions and thus in a minor dispersion of the active material. These mechanisms are often referred to sintering processes, which cause an irreversible deactivation of the catalyst. Methanation reaction is strongly exothermic and so an optimal temperature control is required to inhibit possible thermal runaway condition. Finally, poisoning describes the adsorption of components on the active sites of catalyst. Sulfur poisoning, in particular, was studied for the CO_2 methanation [44]. The results show that the adsorption of sulfur species could block active sites provoking also changes in surface geometry.

In recent years, noble metals have been discovered more active than nickel in the CO_2 hydrogenation. Studies proved that 96% yield to methane with no CO coproduction can be obtained at 300 °C on 3% Ru/γ-Al_2O_3, while the maximum CH_4 yield for 20% Ni/γ-Al_2O_3 is 80% at 400 °C with some CO coproduction [45]. Therefore, since they present higher catalytic activity and stability compared with transition metals, supported noble metal catalyst as palladium, platinum and ruthenium based one have been started to be investigated. In particular, Ruthenium is the most promising noble metal for the catalytic hydrogenation of carbon dioxide in term both of activity and selectivity of methane. This statement is a result of an investigation [46] between different noble metals supported with γ-alumina: the higher activity is, indeed, obtained by Ru and Rh based catalyst, while Pd and Pt are more reactive for Reverse Water Gas Shift reaction. Moreover, Ruthenium

results to be two/three times more active in Sabatier reaction than Rh and two order of magnitude more effective if compared with Pt and Pd. High activity and selectivity are always important parameters for catalytic systems but also their stability over time must be considered for industrial applications.

It is necessary to point out that the performance of the metals are strongly influenced also by the support since it could modify the active phase dispersion and the particle size distribution, thus the reactivity of the catalytic system. For this reason, apart from the metal, also various oxides have been employed as carrier. The effect of the support on the activity of ruthenium catalyst was investigated in a study conducted by Kowalczyk et al. [47], which report that the catalytic system of Ru/Al_2O_3 is actually the more active. Low activity could be found for example in carbon supported systems because carbon tends to cover the active phase particle reducing the number of available sites for CO_2 adsorption. Most catalyst studies address the preparation of classical supported metal catalyst systems by impregnation techniques, characterized by a relative low metal content, which, however, allow high metal dispersion. Ruthenium is used in percentages range from 0.5 to 5% by weight. It can be observed that by increasing the load of the metal, it is possible to work at progressively lower temperatures [48]. Moreover, by feeding reduced flow rates, the conditions of contact between reactants and catalyst are increased and it is thus possible to push the conversion and selectivity to values very close to those of equilibrium. Another advantage of noble metals as active material is their low deterioration due to low sulphur and carbon deposition. Unlike the Nickel-based catalyst, active at 300-500 °C, Ru-based catalyst proves to be active even at lower temperatures, a factor which ideally would allow to avoid the phenomenon of deactivation due to sintering. According to all the considerations reported above, Ru-based catalysts are optimal candidates for CO_2 methanation.

Regarding the reaction pathway of CO_2 methanation it is still under debate and there is evidence that the nature of the metal, the typology of the support and process conditions can affect the reaction mechanism. Some authors propose that CO_2 is adsorbed on the

catalyst surface to form CO and O adsorbed species, which are then hydrogenated, while other studies suggest the H-assisted CO_2 dissociation through the formation of carbonate and other species on the support [49, 50, 51]. Moreover, it was confirmed that the presence of a high amount of water does not deactivate the catalyst but could inhibit the Sabatier reaction kinetics. This makes in-situ strategies for water removal appealing and worth to be investigated.

1.4. CO_2/H_2 methanation technologies

Fixed-bed reactors are the most widely adopted for CO_2 methanation process. They are, in particular, the only reactors present in commercial scale for this process due to their easy design, flexibility and reliability respect to other types. Fluidized bed reactors, for instance, could operate in isothermal conditions due to the movement of catalyst particles, enhancing heat transfer, but they suffer of catalyst abrasion and more difficult scale-up. At pilot scale, fluidized beds have been proposed and demonstrated using Ni-based catalysts [52, 53]. However, Ru-based catalysts are less indicated for this reactor technology, because the high mechanical stress in reacting conditions results in a relevant loss of catalyst which needs to be periodically integrated. Hence, externally cooled packed bed reactors are regarded as the most promising solution [54].

Process schemes for CO_2 methanation generally consist of at least two reactors in series. In this chapter some examples present in literature that allow to obtain methane content higher than 90% in the product stream will be introduced.

The first technology coincides with the patented process of ETOGAS GmbH, formerly named Solar Fuel GmbH, started in 2009 for the catalytic methanation of feed gases containing carbon dioxide and hydrogen. Preferable total pressures are between 2 and 8 bar, while gas hourly space velocities (GHSV) are 2000-4000 h^{-1} for the first stage and 1500-4000 h^{-1} for the second stage. The feed gas contains hydrogen and carbon dioxide in stoichiometric ratio.

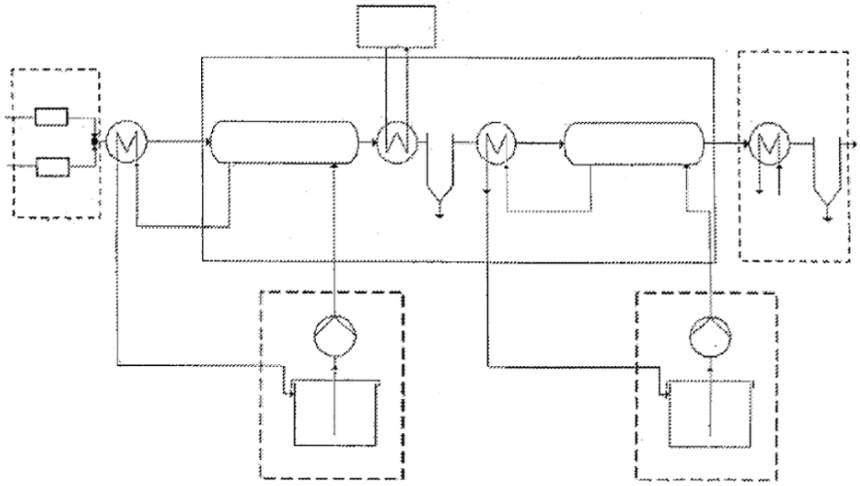

Figure 1.9. Solar Fuel's patented process.

The first reactor works in the range of 300°C-400°C while the second one at 200-300°C. In particular, in the sample reported, the system operates at 6 bar with two reactors in series, loading with Ni-based catalysts and externally counter-current cooled. The feed enters in the first reactor at 270°C, does not exceed 450°C and exits at a temperature of almost 300°C. The space velocity initially is set 3500h^{-1} but it decreases after the first flash, that operates at 120°C, since water content is partially removed. Second reactor works at lower temperatures than the first one to shift the equilibrium conversion. The final condenser is suggested to be set to 30°C in order to purify the product, obtaining a high methane content. As report in the patent, "according to the embodiment, the conversion of the carbon dioxide in the first reactor stage is approximately 95% while the conversion of the carbon dioxide in the second reactor stage is slightly more than 90%, so that the methane content in the final product is approximately 99%" [55].

The second configuration, which was considered at least to be mentioned, includes the whole system of CO_2 utilization from the production of raw materials to the final purification of methane. This project was commissioned by the Kinetics Technology S.p.A. and Maire Tecnimont Group in order to design a process suitable to convert surplus of renewable energy into Synthetic Natural Gas (SNG). Referring only to the methanation

section, it was selected a scheme of three reactors with intermediate coolers but no condensers and a multi-feed of hydrogen, split on first and second reactors. In this way a moderate temperature increment is assessed maintaining the catalyst integrity and minimizing the presence of reverse reactions. Although a maximum threshold value of temperature must not be exceeded, there is also an issue related to operate at too low temperatures due to kinetic limitations and possible formation of highly toxic nickel carbonyls since Ni-based catalysts are involved [56]. This configuration has been taken into account especially to report a type of scheme present in literature which encloses an intrinsic complexity because not only three reactors are used but also a cryogenic distillation column is present to achieve a value over 96% of CH_4 purity at the end.

It is also important to report a single reactor configuration patented in 2011 by MAN Diesel & Turbo SE. The equipment is designed as a multi-tubular reactor with at least two separate reactor zones. Tubes are filled with catalyst pellets and externally cooled. The first zone is operated at higher temperatures to facilitate fast reaction rates for stream with large fractions of H_2 and CO_2, while the temperature in the last zone, where the gas composition is closer to equilibrium, is reduced so that the reaction is shifted towards the products in order to obtain higher methane contents. The heat carrier in the first zone is imposed equal to 550°C in order to bring the system at temperature as high as possible while in the second zone it operates at 250°C in order to achieve thermodynamic equilibrium conditions and prevent unwanted side reactions. The inlet mixture is composed only by the reactants, hydrogen and carbon dioxide, in under-stoichiometric conditions with a ratio H_2/CO_2=3.85. The space velocity is set equal to $5000h^{-1}$ and pressure is lower than 20 bar. The patent states that the dry outlet mixture in these conditions should be composed by 92.3% CH_4, 4.3% CO_2, 3.4% H_2 [57]. Regarding the heat exchange, in the first zone it is placed a smaller hydraulic diameter that could be advantageous for the minimization of radial transport limitations, enhancing the heat transfer with the cooling medium. In the last zone, on the contrary, only a small fraction of the reaction heat is released and for this reason larger hydraulic diameters can be exploited to facilitate the approach to thermodynamic equilibrium. Maintaining the same tube diameter over the whole length of the reactor, the

hydraulic diameter in the first zone could be reduced for instance by centrally placing a tube of smaller diameter not filled with catalyst pellets. In particular, the reactor tube diameter is maintained in the range of 10 mm to 22 mm.

1.5. Motivations and thesis structure

After been reported the techniques to obtain raw materials, the reaction fundamentals and the technologies already validated, the present work aims to investigate further the topic of CO_2 methanation. The recent increased interest in hydrogenation reactions is related to the development of a technology for CO_2 emissions reduction. In this context, the Sabatier process has a crucial role. The purpose is to develop a process setup in order to achieve high CO_2 conversion rates and outlet streams with high purity of methane. Usually, CO_2 methanation refers to the technology of Power to Gas (PtG) that provides a solution for storing and using the surplus electricity by transforming it into synthetic natural gas, composed mainly by methane. PtG applications aim at the production of a CH_4 stream that requires no additional purifications other than water removal. Indeed, if the produced SNG is to be injected in the natural gas grid, it has to meet stringent specifications, varying from country to country. Generally a dry CH_4 purity of more than 96% is required, but in some cases, values can be above 98%. A few percentages CO_2 are normally tolerated, while a maximum concentration of 0.1% is normally required for CO [58]. H_2 shows a higher variability. It is tolerated up to few percentages in some countries: 2% for Switzerland and Germany, between 4 and 6% in the case of Austria, Spain and France. In other cases the limits for H_2 blending in natural gas pipelines are below 1%: 0.2% for Japan, UK, Belgium and California, 0.5% for Italy [59]. The interest of the research project coincides with the exploitation of CO_2 hydrogenation in order to achieve high methane purity in the product stream directly by catalytic pathway. The target is to establish the maximum performances achievable in terms of methane purity and obtain in the final current a methane content at least of 98% for the application of Power to Gas technologies exploiting the possibility to directly enter the product stream into the natural gas grid network.

Section 1 has given a basic introduction including motivations and objectives of the work. In particular, the preparation of raw materials have been described, including carbon dioxide capture technologies and production of hydrogen from renewable sources. The reaction fundamentals was present in order to set the thermodynamic limits and introduced the involved catalytic system.

Section 2 lays down the theoretical setting of the thesis: the tools and the models that will be exploited throughout the work are described. After a brief introduction of the experimental set-up, the modeling procedures conducting in the involved software are present in detail.

Section 3 provides the results obtained from simulations performed in Aspen Plus® V10 according to different process scheme. The purpose is to achieve a model validation through the comparison with experimental data. In this way it becomes possible also to extend the operative conditions and identify the most suitable process configuration for obtaining high CO_2 conversion and CH_4 purity.

Section 4 focuses on gPROMS ModelBuilder® V5.0.2 simulations that have the final purpose to verify if the process scheme, identified in Section 3, can be industrialized. The high exothermicity of the Sabatier reaction requires an efficient thermal management. Therefore, during the modelling of the reactor and the selection of operative conditions, the thermal aspects are taken into account and evaluated.

Section 5 summarizes the results and provides a conclusion to the work. Future developments are also reported.

Section 2: Tools and methods

In this Section all the tools and methods exploited will be described. In particular, the experimental set up will be introduced in order to have a higher comprehension of how the experimental data reported within the work were obtained. Moreover, the modeling procedure conducted in both the involved software, Aspen Plus® V10 and gPROMS ModelBuilder® V5.0.2, will be present in detail.

2.1. Experimental set-up

Sabatier reaction tests are carried out in an automated lab-scale rig operating 24/7. The catalysts are loaded in a fixed-bed reactor (I.D. 1.1 cm, length 23 cm) placed in an electric furnace. The experimental set up allows to work with one or two fixed bed reactors operating in series, with or without water condensation. The gaseous mixture leaving the reactor(s) is sent to a heat exchanger followed by a cold trap to condense the water produced by the reaction. Condensing traps were made by standard 50 cm3 stainless steel sampling tanks with external cooling tubes. The final dried stream is then analyzed with an on-line gas chromatograph able to identify and quantify different chemical species present in the gaseous mixture.

The reacting mixture is stored in cylindrical tanks of 50 liters respectively and is fed by high-pressure lines to the test rig. The cylinders are located in a separate room that is used for the storage of high-pressure flammable chemical substances for safety reason. In order

to allow the SNG low pressure rig to work at atmospheric pressure, on the high pressure lines two different reduction stages are provided, the first step is responsible of a high-medium pressure variation (from the cylinder pressure to 20 barg) and a second step for medium-low variation (from 20 barg to 5 barg). Low-pressure auxiliary lines (0-10 barg) supply hydrogen, nitrogen and other auxiliary gases such as Argon.

Figure 2.1. Final plant lab-scale layout.

The reference catalyst of this work is a calcinated 5% Ru-based catalyst prepared by homogeneous impregnation over alumina support during research activities in the Laboratory of Catalysis and Catalytic Processes (LCCP) of Politecnico di Milano. A high density industrial γ-Al_2O_3 powder, with an average pore diameter of 10 nm, is employed. Once prepared, the desired amount of catalyst is loaded into the reactor diluted with inert

100 μm α-Al_2O_3 to facilitate the thermal control of the reaction and avoid hotspots. On the bottom of the reactor, a porous septum acts as support for all catalytic and inert materials that fill the reactor. For every experiment conducted for this work 1 g of catalyst is used for each reactor.

At the beginning of each run, the catalyst is reduced in situ in hydrogen flow at 400°C for 3h and atmospheric pressure. The reactor is then cooled down to 250°C and H_2 is substituted with N_2 to sweep the catalyst surface. Nitrogen is in turn slowly replaced by the reactive mixture. The catalyst is then conditioned by increasing the temperature up to 350°C. This temperature is maintained until CO_2 conversion and CH_4 selectivity reached steady values. Once the catalyst is conditioned, the temperature is varied stepwise in the range 150-430°C, maintaining each temperature for at least 2h. A test, typically at the temperature of 350°C, is repeated at least twice during the run as activity check.

After the tests, all catalysts are cooled down in inert atmosphere and exposed at room temperature to 2% v/v O_2 in He. Kinetically relevant CO_2 conversion and CH_4 selectivity data are collected in the following ranges of process conditions: T = 150-410 °C, GHSV = 0.25-50 NL/h/g_{cat}, H_2/CO_2= 2-5 v/v.

2.2. Aspen Plus procedure

The preliminary simulations are conducted in equilibrium and in isothermal conditions exploiting the process simulator Aspen Plus® V10. The physical properties of the following components used for this purpose are provided in the database: carbon dioxide (CO_2), carbon monoxide (CO), methane (CH_4), hydrogen (H_2), water (H_2O) and argon (Ar).

The introduction of the additional flash model (V-DRUM1) represents a single stage separator, which performs a phase equilibrium calculation. As suggested from various studies a Peng-Robinson equation of state (EoS) is selected [60,61]. The Van der Waals

equation of state is certainly not able to represent the volumetric behaviour of fluids with sufficient accuracy for engineering assessments. The Peng-Robison EoS is one of the variants developed, which allows to better predict the components interactions and it is often used for the calculation of the properties of hydrocarbons and inorganic gases. However, also a Soave-Redlich-Kwong (SRK) equation of state can be used since the results are comparable, as reported in literature [62]. All the binary interaction parameter values, needed for the model, were provided also in this case by the Aspen Plus® V10 database.

2.2.1. Thermodynamic analysis

Regarding the simulations at thermodynamic equilibrium, Gibbs reactors (RGibbs) are chosen. The Gibbs model provides reactor calculations at equilibrium conditions without the need for a detailed reaction stoichiometry or kinetics model since it is only necessary to define inlet parameters as composition, pressure and temperature.

Pressure drops in all the cases performed within the work will be considered negligible.

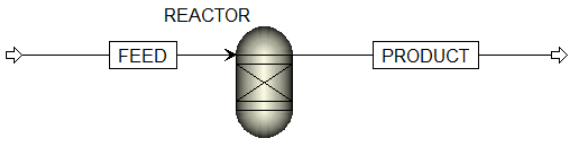

Figure 2.2. Single RGibbs reactor configuration.

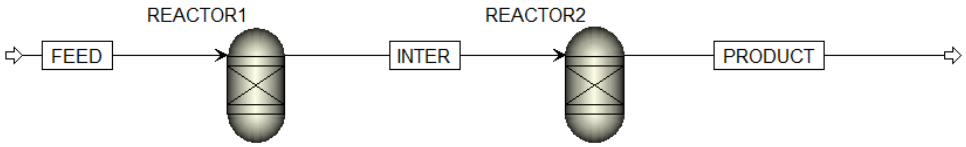

Figure 2.3. Series of two RGibbs reactors configuration.

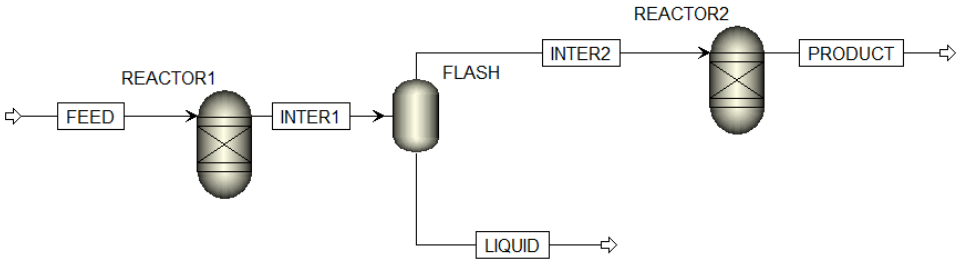

Figure 2.4. Series of two RGibbs reactors with intermediate flash (V-DRUM1) configuration.

The analysis that the process simulator conducts in few seconds for each reactor, that works at specified temperature, consists with the evaluation of a complete model of each reaction j based on its Gibbs free energy:

$$\Delta G^0_{R_j}(T) = \Delta H^0_{R_j}(T) - T \cdot \Delta S^0_{R_j}(T) = -RTlnK_{eq_j}$$

$\Delta G^0_{R_j}(T)$ is actually the variation of reaction Gibbs free energy defined at reference pressure as:

$$\Delta G^0_{R_j}(T, P_{rif}) = \sum_{i=1}^{NC} \nu_{i,j} \cdot \Delta g^0_{f_i}(T, P_{rif})$$

where $\Delta g^0_{f_i}(T, P_{rif})$ is the Gibbs free energy of formation of the compound i as function of temperature.

	A	B	C
CO_2	-393,36	-3,82E-03	1,33E-06
H2	0	0	0
H_2O	-241,74	4,17E-02	7,43E-06
CH4	-75,262	7,59E-02	1,87E-05
CO	-109,885	-9,22E-02	1,455E-06

Table 2.1. Thermodynamic data to calculate $\Delta g^0_{f_i}(T, P_{rif}) = A + B \cdot T + C \cdot T^2$. Ref.: Carl L.Yaws, Chemical Properties Handbook, McGRAW-HILL.

The equilibrium partial pressures for both reactions can be then derived from the equilibrium constant equation:

$$K_{p_j} = \prod_{i=1}^{NC} P_i^{\nu_{i,j}}$$

where NC is the number of components involved, P_i is the partial pressure of the component i and ν_i is the stoichiometric coefficient of component i for the reaction j. The thermodynamic equilibrium is calculated using the ideal gas assumption. Therefore, a system of two equations $K_{eq_j} = K_{p_j}$ is imposed and solved through the extent of reaction method.

$$n_i = n_i^0 + \sum_{j=1}^{NR} \nu_{i,j} \cdot \lambda_j$$

From the number of moles, the molar fractions of every compound can be easily computed and the resolution of the equilibrium system, since temperature and pressure are assigned, gives the two values λ_j. Consequently, the equilibrium concentration of each component is obtained.

2.2.2. Kinetic model implementation

For the evaluation of the reaction rate of the process it is considered the kinetic model proposed by Lunde and Kester [63] for the Sabatier reaction. It is known that carbon dioxide and hydrogen can also react to form carbon monoxide and water thanks to the Reverse Water Gas Shift reaction, however, CO appears only at temperatures higher than 700 K. In particular, in Ni-based catalysts also undesired coproduction of CO can become relevant depending on metal loading, preparation method and pretreatment conditions [64]. On the contrary, the presence of CO in the products of a Ru-based catalyzed system, is below 1% in most of the investigated process conditions. Regarding the possible CO chain growth reactions, previous studies conducted by LCCP report that the most relevant reaction, among all the possible Fischer-Tropsch synthesis, coincides with the production of ethane. However, this compound results to be present in few traces only using a nitrate Ru-based catalyst [65].

As the highly selective Ru-based calcined catalyst will be used throughout the analysis, all these results legitimate the consideration of the Sabatier reaction on its own.

$$r_{Sabatier}\left[\frac{mol}{s \cdot g_{cat}}\right] = k\left\{P_{CO_2}^{n} P_{H_2}^{4n} - \frac{P_{CH_4}^{n} P_{H_2O}^{2n}}{(K_{eq}(T))^{n}}\right\} \quad (8)$$

The calculation of reaction rate is based on component partial pressures P_i in $[atm]$. R is the gas constant with value 8.314 $\left[\frac{J}{mol \cdot K}\right]$. T is the reaction temperature in $[K]$. Even if the model proposed has been fitted by different authors under different conditions, the same rate equation has been successively used to fit experimental data collected in a large range of CO_2 conversion [66]. It has been shown, in particular, that the value of the parameter *n* can drastically change in order to describe the catalyst performance at high CO_2 conversion.

The rate constant k is treated as Arrhenius type (8.1):

$$k = k_0 \, exp\left(\frac{-E_a}{R \cdot T}\right) \quad (8.1)$$

The value of equilibrium constant K_{eq} is evaluated using the empirical correlation (8.2) reported by Lunde and Kester:

$$K_{eq}(T) = exp\left[\left(\frac{1}{1.987}\right)\left(\frac{56000}{T^2} + \frac{34633}{T} - 16.4 \ln T + 0.00557 \cdot T\right) + 33.165\right] \quad (8.2)$$

Therefore, three parameters have to be defined, which are the rate constant k_0 $\left[\frac{mol}{s \cdot g_{cat} \cdot atm^{5n}}\right]$, the activation energy E_a $\left[\frac{kJ}{mol}\right]$ and the reaction order n. These are established through a non-linear regression over experimental data using a Fortran subroutine. The dataset used by colleagues as input for the regression is composed by previous tests obtained at different space velocities (GHSV = 0.25, 0.5, 1, 5, 10, 50 Nl/h/g_{cat}), temperature range T = 150–310°C, atmospheric pressure and an inlet H_2/CO_2 ratio of 3.94. In these way it is possible to obtain suitable coefficients for the current investigation.

$k_0 \ \left[\frac{mol}{s \cdot g_{cat} \cdot atm^{5n}}\right]$	1.91E+02
$E_a \left[\frac{J}{mol}\right]$	7.00E+04
n	1.96E-01
$AVG\ absolute\ error$	9.434711E-03
$AVG\ \%\ error$	2.803763E+00
$Correlation\ index$	9.994385E-01

Table 2.2. Results of parameters necessary to be implemented on the kinetic expression.

A comment must be made also on the ability of the model to describe data collected under pressure. Considering the P-effect on thermodynamics, it is reported that the performance of the CO_2 methanation reactor may be optimized operating with a pressure in the 5–20 bar range. Under these conditions the thermodynamic constraints are less strict and equipment volumes are decreased. However, in the literature it is very rare to find data on the effect of pressure of CO_2 methanation with Ru-based catalyst. Experimental data collected in the laboratory LCCP of Politecnico di Milano not include until now the effect of pressure in a 5%wt. Ru/γ-Al_2O_3 catalyst indeed the kinetics has not yet been validated with pressurized data. It is possible, however, to take as reference a study on 0.5%Ru/γ-Al_2O_3 catalyst where the Lunde and Kester kinetic model results able to describe the effect of pressure on CO_2 conversion [67].

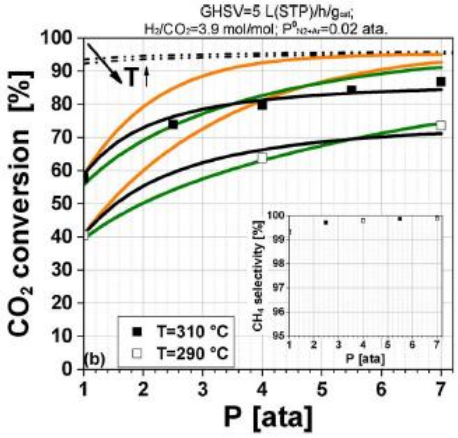

Figure 2.5. Comparison of CO_2 conversion computed with Lunde and Kester model and experimental data varying pressure at 290°C and 310°C.

The analysis can therefore be considered as a first estimate of the effect of pressure on the performances since it is used a value of order of reaction similar to those exploited in this work. The widely adopted kinetic expression proposed by Lunde and Kester in 1973 thus emerges adequate to describe the kinetics of the Sabatier reaction at least up to few bar.

Once established the kinetic model that will be used in the simulations, the selection of the correct reactor is assessed. The choice coincides with a Plug Flow Reactor model (RPlug) that, in this case, describes a system of five components: carbon dioxide (CO_2), hydrogen (H_2), methane (CH_4), water (H_2O) and argon (Ar). Carbon monoxide is not present because the catalyst, as described above, could be considered highly selective. Argon, instead, is present in all the simulations conducted in Aspen Plus® V10 both in equilibrium and isothermal conditions. It is not involved in the Sabatier reaction but it is present during all the experiments performed in lab-scale since it is necessary for final product analysis with gas chromatographer as inert tracer. Therefore, to have a valid comparison with experimental data, it is also included in the simulations.

The reactor model is composed by five ordinary differential equations, expressing the material balances of the main species involved in the process with their initial conditions.

$$\frac{dF_i}{dW_{cat}} = \nu_i \cdot r_{CO_2} \tag{9}$$

$$F_i = F_i^{IN}\big|_{W_{cat}=0} \tag{9.1}$$

F_i and F_i^{IN} are, respectively, the molar flows of the generic species i along the reaction axis and at reactor inlet, W_{cat} is the catalyst weight, ν_i is the stoichiometric coefficient of the component i and r_{CO_2} is the Sabatier reaction rate.

There are no presence of energy balances since the reactor is maintained as isothermal in lab-scale so also the simulations are performed at specified temperature. The RPlug reactor model requires configuration properties as well as the catalyst loading and the bed voidage.

Reactor dimensions: ID = 0.011 [m], L = 0.23 [m]

Catalyst loading = 1 g_{cat}

Bed voidage = 0.4

To fully obtain an exact representation of the reaction rate a proper CUSTOM (Reaction class) function is implemented within the process simulator.

$$r = [Kinetic\ factor][Driving\ force][Custom\ Term]$$

Being the kinetic model slightly different from a simple power-law, a *Custom Term* coupled with *Kinetic factor* is defined neglecting the *Driving force* description. Within the *Kinetic factor* the parameters of rate constant and activation energy are introduced. The reaction order, instead, is inserted in the reaction rate expression written as equation within the *Custom Term*.

Calculations of CO_2 conversion and CH_4 purity are performed with the following equations. These two parameters, in particular, are maintained for the whole analysis as indicator of process performances.

$$X_{CO_2} = \frac{\dot{n}_{CO_2,in} - \dot{n}_{CO_2,out}}{\dot{n}_{CO_2,in}} \cdot 100 \quad (10)$$

$$Pu_{CH4} = \frac{\dot{n}_{CH_4}}{\dot{n}_{CH_4} + \dot{n}_{H_2} + \dot{n}_{CO_2}} \cdot 100 \quad (11)$$

Being the dry CH_4 purity defined as reported (11), it can be noticed that CO_2 and H_2 appears in the final product. Argon, instead, is neglected because in industrial applications it will be not present while in the experimental setup is need in the inlet stream for analysis purposes. Also water is not present in this definition since it certainly will be removed from the product with a simple final condensation.

Process scheme evaluated in the work are reported below.

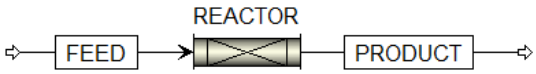

Figure 2.6. Single RPlug reactor configuration.

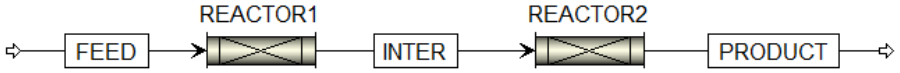

Figure 2.7. Series of two RPlug reactors configuration.

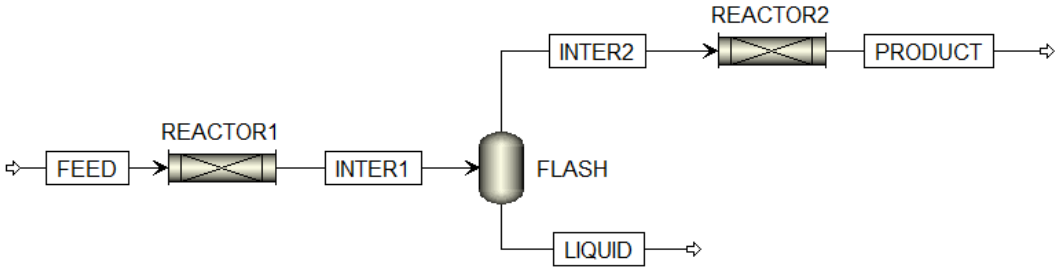

Figure 2.8. Series of two RPlug reactors with intermediate flash (V-DRUM1) configuration.

2.3. gPROMS model description

In a multi-tubular packed bed reactor model is encountered the interplay of fluid flows through a variety of coupled heat and mass transfer mechanisms. Three phenomena of heat transfer can be distinguished and categorized within a packed bed reactor: convection by fluid (1), solid-fluid transfer (2), conduction through solid (3a), contact conduction (3b), conduction through stagnant film (3c), conduction through fluid (3d), radiation between adjacent solid (4a) and radiation between solid surfaces separated by more than a void space (4b). In the CO_2 methanation process, the convection in axial direction and the radial dispersion as well as the solid-fluid transfer are considered the main relevant mechanisms

involved. This occurs also for the mass transfer even if added intraporous diffusion limitations are present and therefore assessed. As Figure 2.9. shows, indeed, the reagent concentrations and temperature profile changes according to a non-isothermal and isobaric pellet model. Moreover, the situation adjacent to the inner tube wall is reported and it is different to the core zone because both temperature and concentration will evolve in the radial direction.

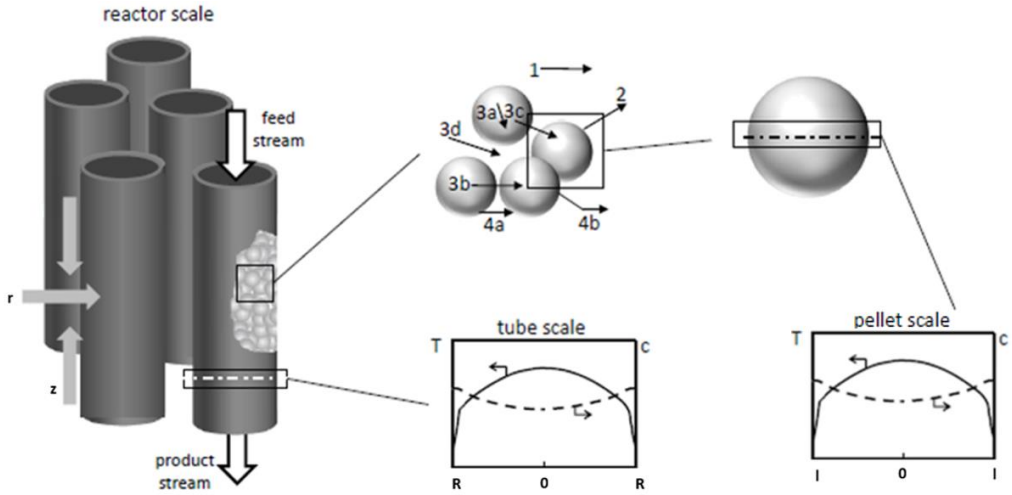

Figure 2.9. Model proposed of packed-bed reactor.

A detailed description of flow and temperature evolution of the cooling medium is omitted. Instead it is assumed that the temperature of the coolant is constant over the whole tube circumference and length. Process conditions require a heat transfer media with temperatures in the range of 150-300 °C therefore water in transition phase close to its boiling point seems to be a suitable solution also from the economical point of view. In particular, outside tubes a natural circulation flow is established due to the difference in density, which means that circulating pumps are often not required. On top the fluid is collected within a drum that separates saturated steam, reused as external duty, and liquid that is recirculated in the reactor jacket. To regulate the boiling point of water it is necessary to install a pressure controller generally coupled with a level one to maintain a minimum value of liquid inside the equipment. Another advantage is that the flow direction of coolant

does not play a role. In the developed model it has been supposed that also the inner tube wall temperature is equal to the coolant one, uniform along the tube length.

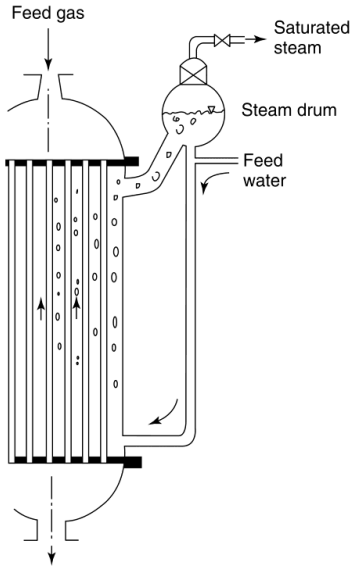

Figure 2.10. Multi-tubular reactor with external boiling-water.

A 2D steady state pseudo-continuous description of the concentration and temperature gradients is adopted in order to represent the cylindrical tube along its axial and radial coordinate. In this analysis the reactor is considered isobaric. The commercial software gPROMS ModelBuilder® V5.0.2 is used to make calculations since the reactor is defined by a system of partial differential equations describing mass and energy balances.

2.3.1. Model equations

- Mass balances:

gas phase $$-W_t \frac{\partial \omega_{i,g}}{\partial z} + \rho_g D_{eff,i} \left(\frac{\partial^2 \omega_{i,g}}{\partial r^2} + \frac{1}{r} \frac{\partial \omega_{i,g}}{\partial r} \right) + \rho_g K_{m,i} a_v \left(\omega_{i,s} - \omega_{i,g} \right) = 0$$

interphase continuity $$\rho_g K_{m,i} a_v \left(\omega_{i,g} - \omega_{i,s} \right) + \rho_{bed} MW_i \nu_i r_{Sabatier}^{eff} = 0$$

- Energy balances:

gas phase $-W_t c_{p,g} \frac{\partial T_g}{\partial z} + \lambda_{eff}^{g} \left(\frac{\partial^2 T_g}{\partial r^2} + \frac{1}{r} \frac{\partial T_g}{\partial r} \right) + h a_v (T_s - T_g) = 0$

interphase continuity $h a_v (T_g - T_s) + \rho_{bed} r_{Sabatier}^{eff} (-\Delta H_R) = 0$

Boundary conditions for mass balances:

inlet condition (@ z=0) $\omega_{i,g} = {\omega_{i,g}}^0$

symmetry in the radial coordinate within the tube (@ r=0) $\frac{\partial \omega_{i,g}}{\partial r} = 0$

no flux at the wall (@ r=d_t/2) $\frac{\partial \omega_{i,g}}{\partial r} = 0$

Boundary conditions for energy balances:

inlet condition (@ z=0) $T_g = {T_g}^0$

symmetry in the radial coordinate within the tube (@ r=0) $\frac{\partial T_g}{\partial r} = 0$

flux at the wall (@ r= d_t/2) $h_w (T_g - T_{cool}) = -\lambda_{eff,r}^{g} \frac{\partial T_g}{\partial r}$

Notation:

$W_t = total\ mass\ flux\ \left[\frac{kg}{m\ s^2}\right] = \frac{Q_0 \left[\frac{m^3}{s}\right] MW gas \left[\frac{kg}{mol}\right]}{v_0 \left[\frac{m^3}{mol}\right] S_{tot}[m^2]}$

$\omega_{i,g} = massive\ fraction\ gaseous\ component\ i\ (BULK)[-] = \frac{x_{i,g}\, MW_i}{\sum_{i=1}^{NC} x_{i,g}\, MW_i}$

$z = axial\ coordinate\ [m], z\ \epsilon\ (0, L]$

$\rho_g = gas\ mixture\ density\ \left[\frac{kg}{m^3}\right]$

$a_v = surface\ area\ per\ unit\ volume\ of\ reactor\ \left[\frac{m^2}{m^3}\right] = \frac{S_p}{V_p}(1-\varepsilon)$

$\omega_{i,s} = massive\ fraction\ component\ i\ (CATALYST\ SURFACE)\ [-]$

$\rho_{bed} = catalyst\ bed\ density\ \left[\frac{kg}{m^3}\right] = \rho_{cat}(1-\varepsilon)$

$c_{p,g} = gas\ mixture\ specific\ heat\ \left[\frac{J}{kg\ K}\right]$

$T_g = gas\ temperature\ [K]$

$r = radial\ coordinate\ [m], r\ \epsilon\ (0, R]$

$T_s = solid\ temperature\ [K]$

$\Delta H_R = reaction\ enthalpy\ \left[\frac{J}{mol}\right]$

$MW_i = component\ molecular\ weight\ \left[\frac{g}{mol}\right]$

$D_{eff,i} = radial\ effective\ diffusivity\ \left[\frac{m^2}{s}\right]$

$\lambda_{eff}^{g} = radial\ conductivity\ \left[\frac{W}{m\ K}\right]$

$K_{m,i} = mass\ transfer\ coefficient\ \left[\frac{m}{s}\right]$

$h = heat\ transfer\ coefficient\ \left[\frac{W}{m^2 K}\right]$

$h_w = wall\ heat\ trasfer\ coefficient\ \left[\frac{W}{m^2 K}\right]$

$T_{cool} = coolant\ temperature\ [K]$

$\omega_{i,g}{}^{0} = massive\ fraction\ gaseous\ component\ i\ at\ inlet\ [-]$

$T_g{}^{0} = gas\ temperature\ at\ inlet\ [K]$

The Multiflash 3.9. package for gPROMS ModelBuilder® V5.0.2 is adopted for the reactor configuration in order to evaluate individual gas and mixture properties.

From the kinetic point of view, $r_{Sabatier}^{eff}\ \left[\frac{mol}{kg_{cat}\,s}\right]$ refers to the effective reaction rate that is present along the axial and radial coordinate of the reactor tube. It have been defined as integral of the reaction rate that depends also on radial coordinate of the catalyst pellet calculated over the diffusion characteristic length $l\ [m]$ of the catalyst.

$$r_{Sabatier}^{eff} = \frac{\int_0^{l=\frac{V_p}{S_p}} r_{Sabatier}^{p}(x,z,r)\,dx}{V_p/S_p}$$

$r_{Sabatier}^{p}(x,z,r)\ \left[\frac{mol}{kg_{cat}\,s}\right]$ is described in the 1D pellet model.

Indeed, in order to characterize the pore diffusion and the intraphase heat transfer within the catalyst particle a 1D isobaric and pseudo-homogeneous pellet model is extended to the heterogeneous reactor model. Therefore, coupled balances for reactor and pellet are solved.

Mass balance

solid phase $\quad \frac{\partial}{\partial x}\left(D_{eff,i}^{p}\frac{\partial C_i}{\partial x}\right) + \rho_{cat}\nu_i r_{Sabatier}^{p} = 0$

Energy balance

solid phase $\quad \lambda_{eff}^{p}\ \frac{\partial^2 T}{\partial x^2} + \rho_{cat} r_{Sabatier}^{p}(-\Delta H_R) = 0$

Boundary conditions for mass balance:

symmetry within the pellet (@ x=0) $\quad \frac{\partial C_i}{\partial x} = 0$

flux continuity (@ x=l) $\quad C_i = C_{i,surf}$

Boundary conditions for energy balance:

symmetry within the pellet (@ x=0) $\frac{\partial T}{\partial x} = 0$

flux continuity (@ x=l) $T = T_{surf}$

Notation:

$C_i = species\ concentration\ (WITHIN\ CATALYST)\ \left[\frac{mol}{m^3}\right]$

$C_{i,surf} = species\ concentration\ (CATALYST\ SURFACE) = \frac{P\ x_{i,s}}{R\ T_s}\ \left[\frac{mol}{m^3}\right]$

$T = temperature\ (WITHIN\ CATALYST)\ [K]$

$T_{surf} = temperature\ (CATALYST\ SURFACE)\ [K]$

$x = radial\ coordinate\ along\ the\ catalyst\ pellet\ [m], x\ \epsilon\ (0, l]$

$D^p_{eff,i} = effective\ diffusivity\ coefficient\ for\ intraporous\ limitations\ \left[\frac{m^2}{s}\right]$

$\lambda^p_{eff} = effective\ thermal\ conductivity\ for\ intraporous\ limitations\ \left[\frac{W}{m\ K}\right]$

Kinetics involved:

As reported in Section 2.2.2., for the evaluation of the reaction rate of the process it is considered the kinetic model proposed by Lunde and Kester for the Sabatier reaction.

$r^p_{Sabatier} = k\left\{P^n_{CO_2} P^{4n}_{H_2} - \frac{P^n_{CH_4} P^{2n}_{H_2O}}{(K_{eq}(T))^n}\right\}$

$k = k_0\ exp\left(\frac{-E_a}{R\ T}\right)$

$$K_{eq}(T) = exp\left[\left(\frac{1}{1.987}\right)\left(\frac{56000}{T^2} + \frac{34633}{T} - 16.4\ \ln T + 0.00557 \cdot T\right) + 33.165\right]$$

$r^{p}_{Sabatier}\left[\frac{mol}{kg_{cat}\, s}\right]$ refers to the reaction rate as function of axial and radial coordinate of the reactor tube as well as of radial coordinate along the catalyst pellet.

$$P_i = P_i\left(n_{comp}, x, z, r\right) = component\ partial\ pressure\ [Pa]$$

$$T = T_s\ (x, z, r) = solid\ temperature\ [K]$$

2.3.2. Transport correlations

All the transport correlations involved within the system of partial differential equations are reported below.

The radial effective dispersion coefficients are given by the equation [68]:

$$D_{eff,i} = \ \varepsilon\ \left(D_{mix,i}\sqrt{\varepsilon} + 0.1\ d_{p,e}u\right)$$

where u [m/s] is the gas velocity and $d_{p,e}$ [m] is calculated as diameter of an equivalent sphere with the same volume to surface ratio with respect to the catalyst pellet. ε is equal to the reactor void fraction [-] and it is defined through the Dixon correlation [69] in order to describe the packing of cylindrical pellets.

For $\frac{d_{p,v}}{d_t} < 0.6$ is valid: $\varepsilon = 0.36 + 0.1\left(\frac{d_{p,v}}{d_t}\right) + 0.7\left(\frac{d_{p,v}}{d_t}\right)^2$

Moreover, for the calculation of gas mixture properties, Blanc's correlation [70] has been chosen as mixing rule for estimating the molecular diffusion coefficients:

$$D_{mix,i} = \left(\sum_{j=1, j\neq i}^{NC} \frac{x_{j,g}}{D_{i,j}}\right)^{-1}$$

Then binary diffusion coefficients $D_{i,j}$ [m^2/s] have been evaluated by using the Fuller's equation. The empirical correlation permits the determination of the diffusivity without the necessity of involving Lennard-Jones parameters, as the energy of molecular interaction for binary system and the collision diameter.

$$D_{i,j} = \frac{0.0143\, T_g^{1.75}}{P\sqrt{\frac{2000}{\frac{1}{MW_i}+\frac{1}{MW_j}}\left[(\sum v_i)^{1/3}+(\sum v_j)^{1/3}\right]^2}}$$

v [cm^3/mol] is the atomic diffusion volume. In particular, the table reported in the reference [71] is used to determine the required different values: v_{CO_2}= 26.9, v_{H_2}= 7.07, v_{H_2O}= 12.7, v_{CH_4}= 29.9 ,v_{Ar}= 16.1.

The bed radial effective conductivity weight both the conductive and the convective contributions [72].

$$\lambda_{eff}^{g} = \lambda_{gas}\left\{\varepsilon + \frac{1-\varepsilon}{0.22\,\varepsilon^2+\frac{2}{3}\left(\frac{\lambda_{gas}}{\lambda_{cat}}\right)} + \frac{Re_{d_{p,e}} d_{p,a}\, Pr}{8.65\left[1+19.4\left(\frac{d_{p,a}}{d_t}\right)^2\right]\frac{d_{p,v}}{d_{p,a}}}\right\}$$

where λ_{gas} is the gas mixture thermal conductivity [W/m/K] and λ_{cat} is the catalyst thermal conductivity, assumed equal to 1 [W/m/K] since it is a typical value for porous alumina based catalysts.

$d_{p,a}$= diameter of an equivalent sphere with the same surface as the catalyst pellet [m]
$d_{p,v}$= diameter of an equivalent sphere with the same volume as the catalyst pellet [m]
d_t= tube diameter [m]

The dimensionless numbers are calculated through their standard definitions:

$$Re_{d_{p,e}} = \frac{W_t\, d_{p,e}}{\mu_{gas}}$$

$$Pr = \frac{c_{p,g}\,\mu_{gas}}{\lambda_{gas}}$$

Regarding the gas-solid heat and mass transfer coefficients, they are derived from Sherwood and Nusselt numbers. However, the heat and mass transport in packed bed systems has the necessity to be described according to the bed voidage present in the reactor tubes in order to assess some inertial effects that can be caused by higher velocities. The analytical relationships for the dimensionless number are thus derived from a study on multiparticle system [73].

Gas-solid mass transfer:

$$K_{m,i} = \frac{Sh_i\,D_{mix,i}}{d_{p,e}}$$

$$Sh_i = 1.26\,Re_{d_{p,e}} Sc_i^{\frac{1}{3}} \left(\left(\frac{1-(1-\varepsilon)^{\frac{5}{3}}}{2-3(1-\varepsilon)^{\frac{1}{3}}+3(1-\varepsilon)^{\frac{5}{3}}-2(1-\varepsilon)^2} \right)^{-0.5} Re_{d_{p,e}} \right)^{-\frac{2}{3}}$$

$$Sc_i = \frac{\mu_{gas}}{\rho_g\,D_{mix,i}}$$

Gas-solid heat transfer:

$$h = \frac{Nu\,\lambda_{gas}}{d_{p,e}}$$

$$Nu = 1.26\,Re_{d_{p,e}} Pr^{\frac{1}{3}} \left(\left(\frac{1-(1-\varepsilon)^{\frac{5}{3}}}{2-3(1-\varepsilon)^{\frac{1}{3}}+3(1-\varepsilon)^{\frac{5}{3}}-2(1-\varepsilon)^2} \right)^{-0.5} Re_{d_{p,e}} \right)^{-\frac{2}{3}}$$

The wall heat transfer coefficient can be expressed as the sum of a stagnant (or conductive) contribution and a turbulent (or convective) contribution [74].

$$h_w = (h_w)_0 + (h_w)_G$$

The conductive contribution counts the bed void fraction present near the wall zone and considers the heat transferred through the solid phase according to two mechanisms in series. In particular, both conduction through stagnant fluid near the particle-wall contact surface and conduction through solid phase are taken into account.

$$h_w = \frac{\lambda_{gas}}{d_{p,v}}\, 2\varepsilon + \frac{1-\varepsilon}{0.0024\left(\frac{d_t}{d_{p,v}}\right)^{1.58} + \frac{1}{3}\left(\frac{\lambda_{gas}}{\lambda_{cat}}\right)} + h_{w,conv}$$

On the other side, two equations are introduced to describe the convective contribution.

$$h_{w,conv} = \begin{cases} \frac{\lambda_{gas}}{d_{p,a}}\, 0.0835\, Re_{d_{p,a}}^{0.91} & if\ Re_{d_{p,a}} < 1200 \\ \frac{\lambda_{gas}}{d_{p,a}}\, 1.23\, Re_{d_{p,a}}^{0.53} & if\ Re_{d_{p,a}} \geq 1200 \end{cases}$$

An effective diffusivity coefficient is introduced within the mass balance equation of the 1D pellet. The mass flow rate is, indeed, determined by the Fick's law. The driving force is the component concentration that changes moving along the coordinate of the pellet, x.

$$N_i = D_{eff,i}^{p} \frac{\partial C_i(x)}{\partial x}$$

The diffusivity is named "effective" since it considers both the porosity and the tortuosity present inside the catalyst. However, depending on its definition, it can be considered constant or not along the coordinate. According to the comparison between the molecular free path (λ) and the pore radius (r_p) different phenomena could be classified and thus different correlations can be involved. The average distance the particle travels between collisions with other ones, defined as mean free path, could be derived from the kinetic theory of gases. However, although the pore radius can be easily obtained through a catalyst characterization, the molecular free path is more complex to be identified.

$$r_p = 5 \cdot 10^{-9}\,[m] \qquad (Alumina\ porous\ support)$$

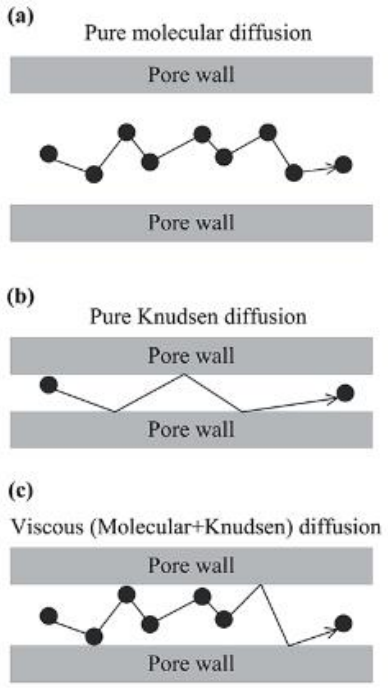

Figure 2.11. Basic mechanisms of gas diffusion in porous media.

If $\lambda \ll r_p$, the pores could be considered large. The collisions with other molecules are thus more facilitate than diffusion. This is a situation that includes only the molecular diffusion coefficient. On the contrary, when the relation between molecular free path and pore radius is inverted, the intraporous diffusion falls within the Knudsen domain and molecules have no space to collide with others: compounds unavoidably impact on the walls of the pore. The best way to consider both Knudsen and molecular diffusion is to evaluate the mass transport limitation as a resistance to the diffusive flow. The overall effective diffusion coefficient within the particle can be therefore calculated by a series arrangement.

$$D_{eff,i} = \frac{\frac{\varepsilon_p}{\tau}}{\frac{1}{D_{K,i}} + \frac{1}{D_{i,mix}}}$$

$\frac{\varepsilon_p}{\tau}$ is a constant coefficient that encounters both the porosity and the tortuosity of the pellet catalyst. The higher the porosity, the faster the diffusion while this will be slower if the tortuosity has a high value. This coefficient is assumed equal to 0.123 [75].

For the calculation of gas mixture properties, Blanc's correlation has been chosen as mixing rule for estimating the molecular diffusion coefficients $D_{mix,i}$ [m^2/s] while binary diffusion coefficients $D_{i,j}$ [m^2/s] have been evaluated with Fuller's correlation, as done for the 2D reactor model.

$$D_{mix,i} = \left(\sum_{j=1,j\neq i}^{NC} \frac{x_{j,s}}{D_{i,j}}\right)^{-1}$$

$$D_{i,j} = \frac{0.0143\, T^{1.75}}{P\sqrt{\frac{2000}{\frac{1}{MW_i}+\frac{1}{MW_j}}}\left[(\sum v_i)^{1/3}+(\sum v_j)^{1/3}\right]^2}$$

In the Knudsen flow, when the gas density is low or pores are quite small, molecules hitting the wall are momentarily adsorbed and then give off in random directions. The gas flux is reduced by the wall resistance which causes a delay because of both the diffuse reflection and the finite time the molecule is adsorbed. Kinetic theory of gases provides the following relation [76]:

$$D_{K,i} = 9700\, r_p \sqrt{\frac{T_s}{MW_i}}$$

The symbols refer to a single component since molecular collisions in this case are negligible. It is important, however, to point out that reducing the pressure in the system, Knudsen phenomenon could become relevant also at higher pore radius [77]. Therefore, it is expected that the intraphase diffusion limitations related to the Knudsen domain will prevail.

The effective thermal conductivity is present in the energy balance to describe the heat transported by conduction within the pellet considering the solid catalyst as partially porous. Therefore, it is not equal to the conductivity of the catalyst but it takes into account also the fraction void that does not contribute to the heat transfer. In particular the specific pore volume of the 5%wt. Ru/γ-Al_2O_3 catalyst is 0.38 cm^3/g. The effective thermal conductivity is thus calculated and imposed equal to 0.335 W/m/K.

In addition to the transport correlations used within the system, below will be reported also two empirical criteria that allow to neglect mass and heat axial dispersion maintaining a sufficient reliability in the balance equations.

The empirical correlation for absent axial mass dispersion requires that: $\frac{D_{eff,axial}}{v\ L} \ll 1$. The axial effective diffusivity can be described by the same equation of the radial one, as established by the reference text.

$$D_{eff,axial} = \varepsilon\ \left(D_{mix,i}\sqrt{\varepsilon} + 0.1\ d_{p,e}u\right) \cong 10^{-4}\ m^2/s$$

The result is: $\frac{D_{eff,axial}}{v\ L} \cong 10^{-6}$

In analogy, the axial heat dispersion can be neglected if: $\frac{\lambda^g_{eff,axial}}{\rho_g c_{p,g}\ v\ L} \ll 1$. Unlike before, however, the axial effective thermal conductivity is defined by a different correlation respect to the radial one. For packed bed reactors it can be evaluated using the correlation [78]:

$$\frac{\lambda^g_{eff,axial}}{\lambda_{gas}} = \frac{\lambda^0_{eff,g}}{\lambda_{gas}} + 0.7\ Re_{d_{p,e}}Pr$$

where the ratio $\frac{\lambda^0_{eff,g}}{\lambda_{gas}}$ coincides with a static thermal conductivity, calculated as:

$$\frac{\lambda^0_{eff,g}}{\lambda_{gas}} = \varepsilon + \frac{1-\varepsilon}{0.22\ \varepsilon^2 + \frac{2}{3}\left(\frac{\lambda_{gas}}{\lambda_{cat}}\right)}$$

Substituting all the parameters: $\frac{\lambda^g_{eff,axial}}{\rho_g c_{p,g}\ v\ L} \cong 10^{-4}$

The criteria for negligible axial mass and heat dispersion can be thus considered satisfied.

Section 3: Effect of the process configuration on the performances

It is necessary, as first thing, to identify the more adequate process scheme that allows to achieve high CO_2 conversion and CH_4 purity. The analysis is executed with isothermal reactors following the tests (#138, #143, #149) already conducted in the laboratory scale at atmospheric pressure. With the aim of finding the proper conditions to produce as much methane as possible ($g_{methane}/h/g_{cat}$) and to obtain high purity in the outlet stream, the plant has been investigated with different configurations up to the construction of two reactors with intermediate flash. In this way it is possible to verify the alignment of the predictions simulated in Aspen Plus® V10 with the experimental data and also extend the investigated ranges to fields not already studied, exploiting the flexibility of the model. Once the configuration has been identified, possible changes in operating conditions will also be evaluated with the aim of intensifying process performance. In particular, an increase in productivity by raising the GHSV and an increase in the value of methane purity through simulations conducted at pressures higher than the atmospheric will be investigated.

3.1. Single reactor

The experimental dataset (test #138) available for a single reactor configuration allows to investigate the model adequacy in a wide range of operative conditions. Temperature was selected between 125°C and 400°C and the space velocities involved were 0.25, 0.5, 1, 5, 50 $NL/h/g_{cat}$. Ratio H_2/CO_2 was 3.94 in the inlet stream with 2.05% of Argon.

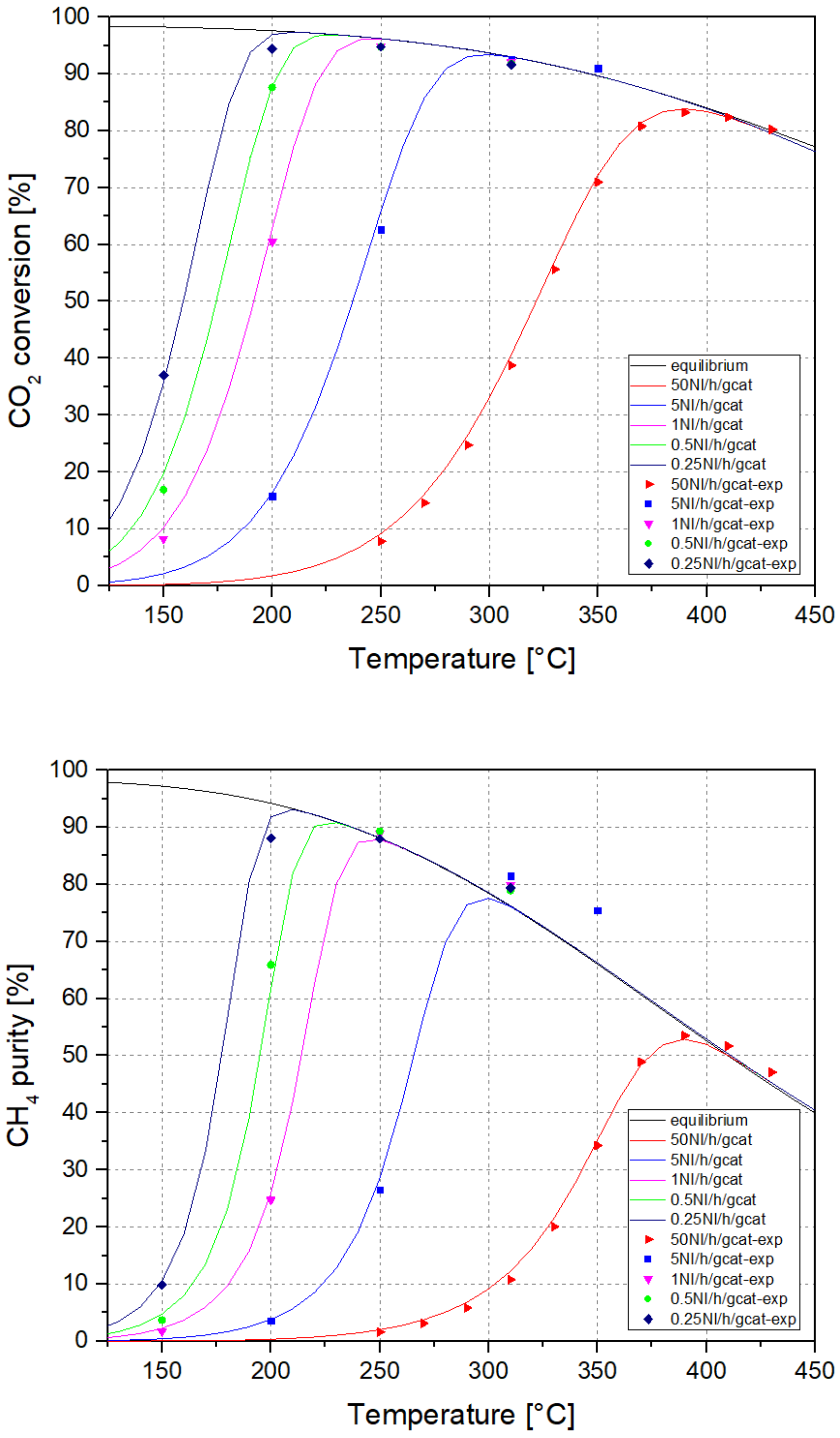

Figure 3.1. CO_2 conversion and CH_4 purity compared to experimental data obtained from test #138.

In this work the kinetic model Lunde and Kester is implemented for the first time in Aspen Plus® V10. Therefore, the plots of CO_2 conversion and CH_4 purity shown in Figure 3.1. verify the predictive ability of the simulator to describe quantitatively the data collected in the laboratory tests. Two added considerations must be taken into account for a detailed description of the obtained results. The first one is that at temperatures usually higher than 410°C it is not found a perfect overlapping between the equilibrium curve and the kinetic model. This is due to the fact that actually the kinetic model has been validated within a certain range. A comparison is performed between the equilibrium constant calculated through the kinetic expression of Lunde and Kester model and the one calculated with the knowledge of Gibb's free energy of formation of compounds. The relative error committed with the utilization of the empirical expression of the equilibrium constant becomes relevant, higher than 0.05, only at temperatures above 410°C. The empirical expression of Lunde and Kester, in particular, is no longer valid at temperature over 410°C because it neglects the conversion contribution of the Reverse Water Gas Shift (RWGS) reaction. Indeed, at high temperatures secondary reactions can become relevant, as the RWGS, due to its endothermic nature. As second consideration, it is important to point out that some experimental data exhibit slightly higher values above the thermodynamic equilibrium line. This is based on the possible non isothermal condition that may occur at high temperatures in the laboratory reactor. Indeed, measurements of temperature profile in the catalytic bed verified that it is possible to have a maximum difference of ΔT_{max} = 15°C. Shifting the temperature to lower values will thus increase CH_4 production, due to the exothermic nature of the reaction.

This preliminary analysis is not only useful to establish a comparison between the model and the experimental data but it allows also to evaluate the effect of the operating conditions on system performances. Regarding the space velocity of the inlet stream, an increase of it produces low conversions due to the low contact time between gas and catalyst. For instance, by increasing GHSV (Gas Hourly Space Velocity) from 0.5 to 5 $NL/h/g_{cat}$, CO_2 conversion decreases from 88% to 15% at 200 °C. Being the reactor approximated to a plug flow, an increase in space velocity is equivalent to a decrease in the residence time of the

reactants in the catalytic bed. To increase the process yield, it is possible to increase the contact time, for instance with larger quantity of catalyst, maintaining the same flow rates. However, it requires bigger reactors and necessarily implies an increase in the purchase and eventual replacement costs of catalyst. Another possibility, at expense of productivity but in favour of methane purity, is to work at low GHSV with lower inlet stream maintaining the required quantity of catalyst sufficiently small. Taking into account these aspects and the target of the research, the identification of the process scheme is analyzed at GHSV equal to 0.25, 0.5, 1 NL/h/g_{cat}. The purpose is to maximize the residence time of gas streams in the catalytic bed and thus CO_2 conversion and methane purity. All the different configurations will be investigated in these conditions in order to perform a valid comparison of the performances. For this reason, the situations of single reactor operating at 0.25, 0.5,1 NL/h/g_{cat} are again reported in separated plots (Figure 3.2.).

GHSV = 1 NL/h/g_{cat}

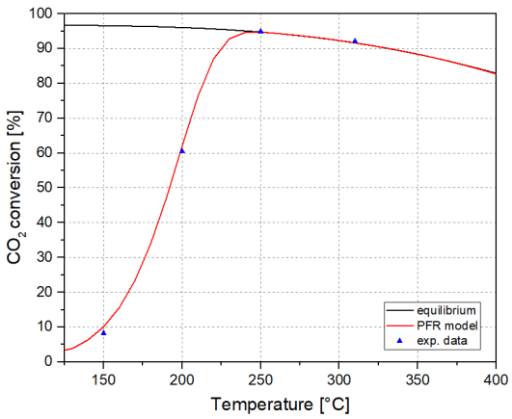

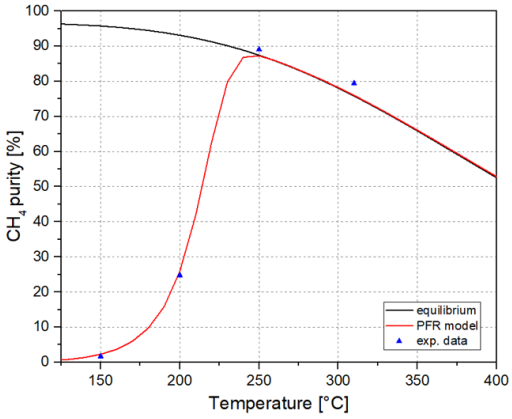

GHSV = 0.5 NL/h/g_{cat}

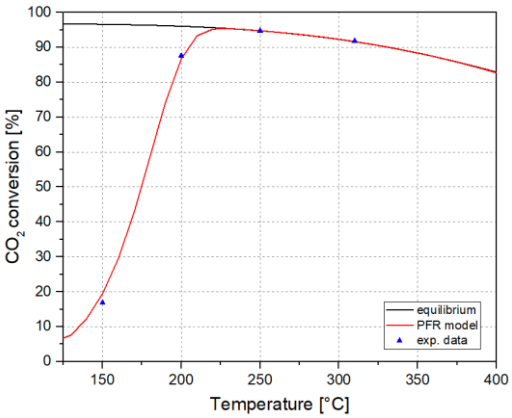

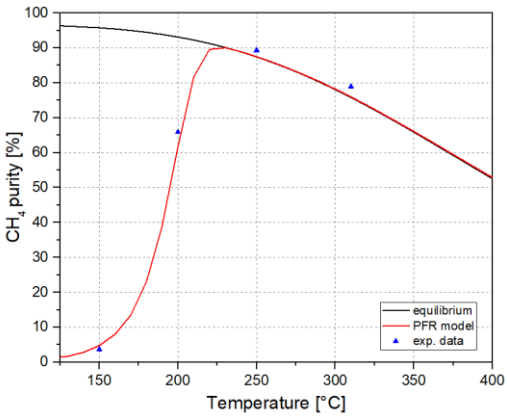

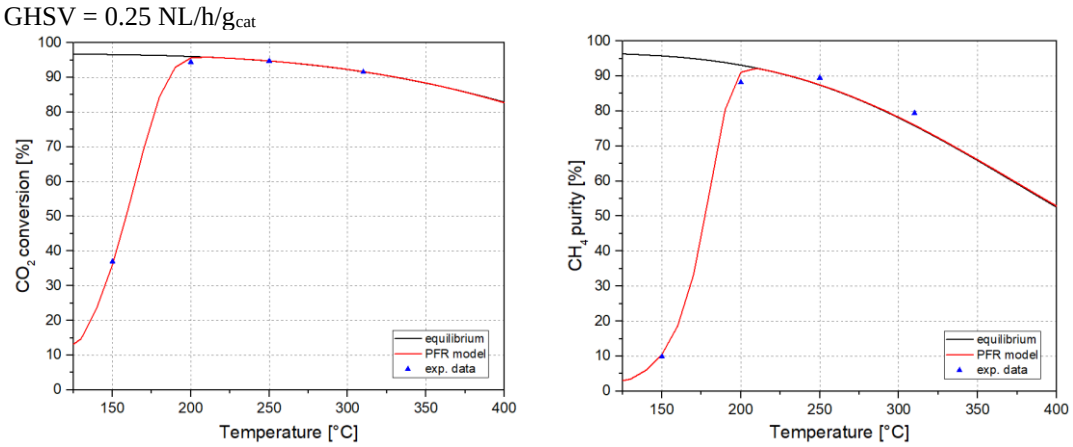

Figure 3.2. CO_2 conversion and CH_4 purity as function of temperature for different GHSV.

Concerning the effect of temperature on CO_2 conversion it can be seen that the curves follow the classic exponential behaviour at temperatures below 250°C for all space velocities. For higher temperature, kinetic results are disposed on the equilibrium line. In particular, for these simulations, the maximum values of CO_2 conversion are equal to 94.7% at 250°C for GHSV=1 NL/h/g_{cat}, 95.4% at 230°C for GHSV=0.5 NL/h/g_{cat} and 95.8% at 210°C for GHSV=0.25 NL/h/g_{cat}. In Figure 3.2., also the CH_4 purity is reported. In the whole temperature range, high values are observed even if they hardly overcome 90% of methane purity.

Once possible solution to achieve higher values of purity of methane is to perform an additional and optional removal of carbon dioxide present in the outlet gaseous product. This step could be executed bringing to high efficiency of separation. CO_2 is generally removed using a solvent by chemical or physical absorption. Physical absorption is convenient compared to the chemical one in the case of removal of components in high pressure streams and the most commonly used methods are, for example, the washing in water, the separation by use of methanol, through Rectisol process, and other techniques involving organic solvents. Among the chemical absorption processes, which are generally favoured at low partial pressure of components, the most used method for CO_2 removal is the washing with amines. However, the method that most probably will be performed for

this situation is the adsorption of carbon dioxide through activated alumina, silica gel or activated carbon at high pressures and low temperatures, which is widely used for the elimination of residual gases.

Assuming an ideal efficiency of 100%, with a complete removal of CO_2, the calculated CH_4 purity results equal to 91.7% for GHSV=1 NL/h/g_{cat}, 94.2% for GHSV=0.5 NL/h/g_{cat} and 96.02% for GHSV=0.25 NL/h/g_{cat}. The use of this technology will certainly depend on economic considerations. Although this option is not completely discarded, it does not offer for this scenario sufficient methane purity values. Other configurations are therefore assessed.

3.2. Series of two reactors

To study the effect of multiple reactors, a second PFR reactor is added to the base process scheme. The main reason for implementing this scenario is to promote CO_2 conversion and CH_4 purity in the product stream by working at different temperatures. In this way, it is possible to operate at higher temperatures in the first rector, enhancing the system kinetics, while in the second one, lower temperatures allow to achieve thermodynamic equilibrium conditions, pushing the final CO_2 conversion to higher values. For the concerning work with two reactors in series, temperature of first reactor was set up experimentally at 250°C and 310°C, while the temperature range of the second reactor varied from 100°C to 200°C.

Figure 3.3. reports graphs for CO_2 conversion and CH_4 purity, at temperature of first reactor of 250°C and 310°C. In both cases, experiments (test #143) were conducted with variation of temperature of second reactor and GHSV of inlet stream. The space velocities involved were always 0.25, 0.5, 1 NL/h/g_{cat}. Additionally, also for these scenarios, thermodynamic equilibrium lines are obtained from simulation with two Gibbs reactors in series, considering thus both reactors in equilibrium conditions.

GHSV = 1 NL/h/g_{cat}

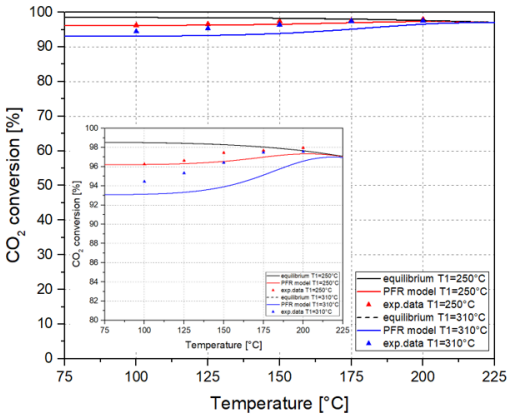

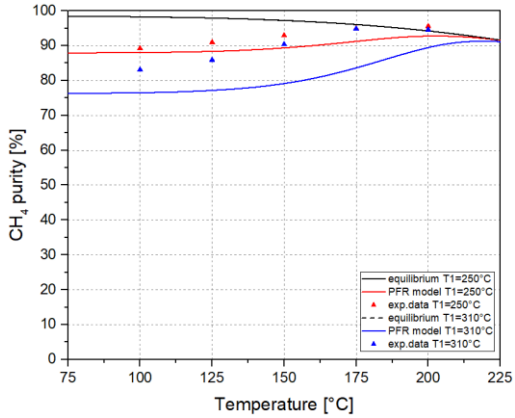

GHSV = 0.5 NL/h/g_{cat}

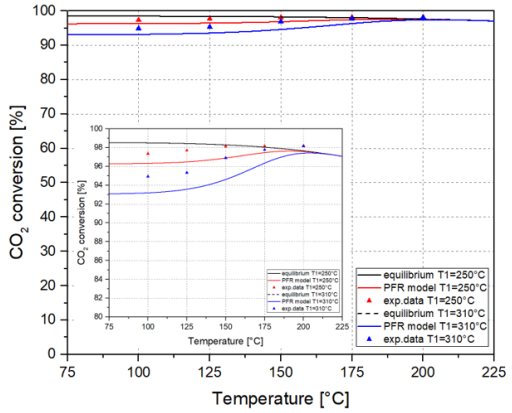

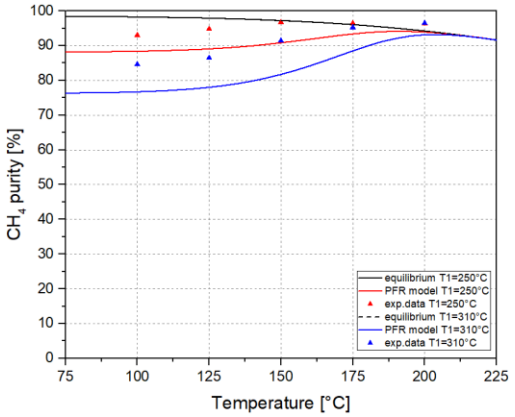

GHSV = 0.25 NL/h/g_{cat}

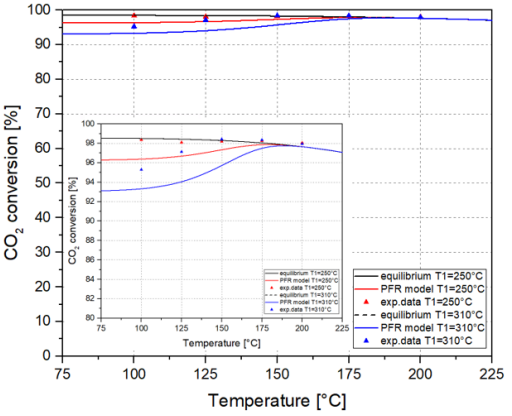

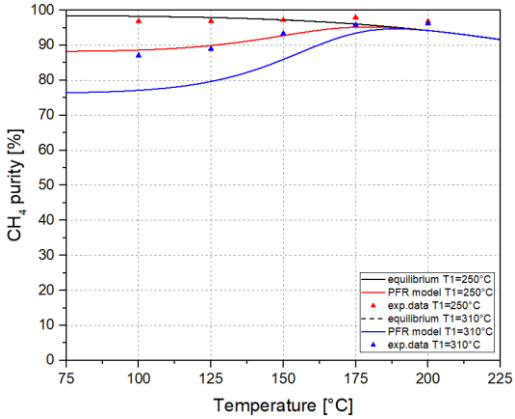

Figure 3.3. CO_2 conversion and CH_4 purity of outlet stream of a series of two reactors when the first one is maintained at 250°C (red line) or at 310°C (blue line).

It is evident from the plots that adding a second reactor, which operates at lower temperatures, promotes CO_2 conversion and CH_4 purity. For instance, in the case of GHSV=1 NL/h/g_{cat}, a single reactor operating at 250°C exhibited CO_2 conversion of 94.7 %, while the results of double reactor configuration, maintaining the first reactor at the same temperature of 250°C, are about 97 %.

It must be point out that in some cases the simulation does not foresee with extreme precision the experimental data. The main reason is that working with two reactors in series at conversion higher than 90% is actually an extrapolation of the kinetic model. These values, indeed, were not previously used for the fitting and it is thus possible to obtain a discrepancy from 2% up to 10% between experimental data and results from simulation. Another possible issue could be a non-complete isothermal conditions during reaction conducted in laboratory and, since two isothermal reactors have been considered, the error may be increased. Taking into account these observations, other information can be extrapolated from the plots reported in Figure 3.3. In single reactor configuration, for instance, by lowering GHSV values, higher CO_2 conversion is obtained, however, this difference is not so marked in the scenario of two reactors in series: values of CO_2 conversion and CH_4 purity are very similar for all the GHSV investigated. It can be clearly noticed that comparing the two solutions, better performances are achieved operating the first reactor at 250°C. For this case, as underline before, the highest values of carbon dioxide conversion and purity of methane are obtained using an inlet stream with space velocity of 0.25 NL/h/$g_{cat.}$ In these conditions, however, the experimental values lie almost on a horizontal line. This could be based on the high contact time of gas stream and catalyst, which is obtained in first reactor, and thus thermodynamic equilibrium is faster approximated in the second reactor at these conditions. However, experimental data, obtained at higher space velocities, describes better the approach of the kinetic model respect to the thermodynamic equilibrium line. The curve trend, moreover, highlights that thermodynamic equilibrium is reached in the temperature range from 180°C up to 225°C of the second reactor.

The results obtained from the configuration of two reactors in series allow to confirm that higher values of CO_2 conversion and CH_4 purity are achieved with respect to the base case process. In this simulation the best value of methane purity is equal to 94.95%. Working at low GHSV values, with temperature of first reactor between 250°C and 310°C and lower temperatures in the second one, enhances performances but it is necessary to investigate if further improvements can be obtained.

3.3. Series of two reactors with intermediate flash

A flash was inserted in the configuration of two reactors in series in order to investigate another possibility of rising the performances. The main reason for implementing this scenario is to promote CO_2 conversion and CH_4 purity in product stream by working at different temperatures in the two reactors but also removing a high amount of H_2O byproduct through condensation. As can be seen in the reported scheme, the stream exiting the first reactor is introduced into a flash separator operating at isothermal conditions (T_{flash}=1°C). Downstream the flash only the vapour outlet stream enters the second reactor. The conversion of the remaining unreacted components is thus performed. The specific temperature values of reactors are maintained equal to the ones exploited in the second scenario. As previously reported for other configurations, Gibbs reactors are used since they are suitable to study the thermodynamic equilibrium conditions of CO_2 methanation. Both the reactors are considered at equilibrium.

GHSV = 1 NL/h/g_{cat}

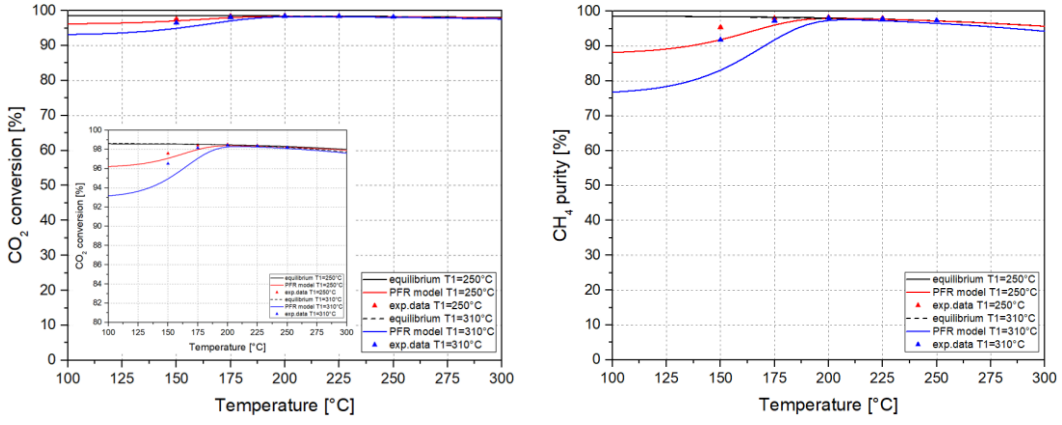

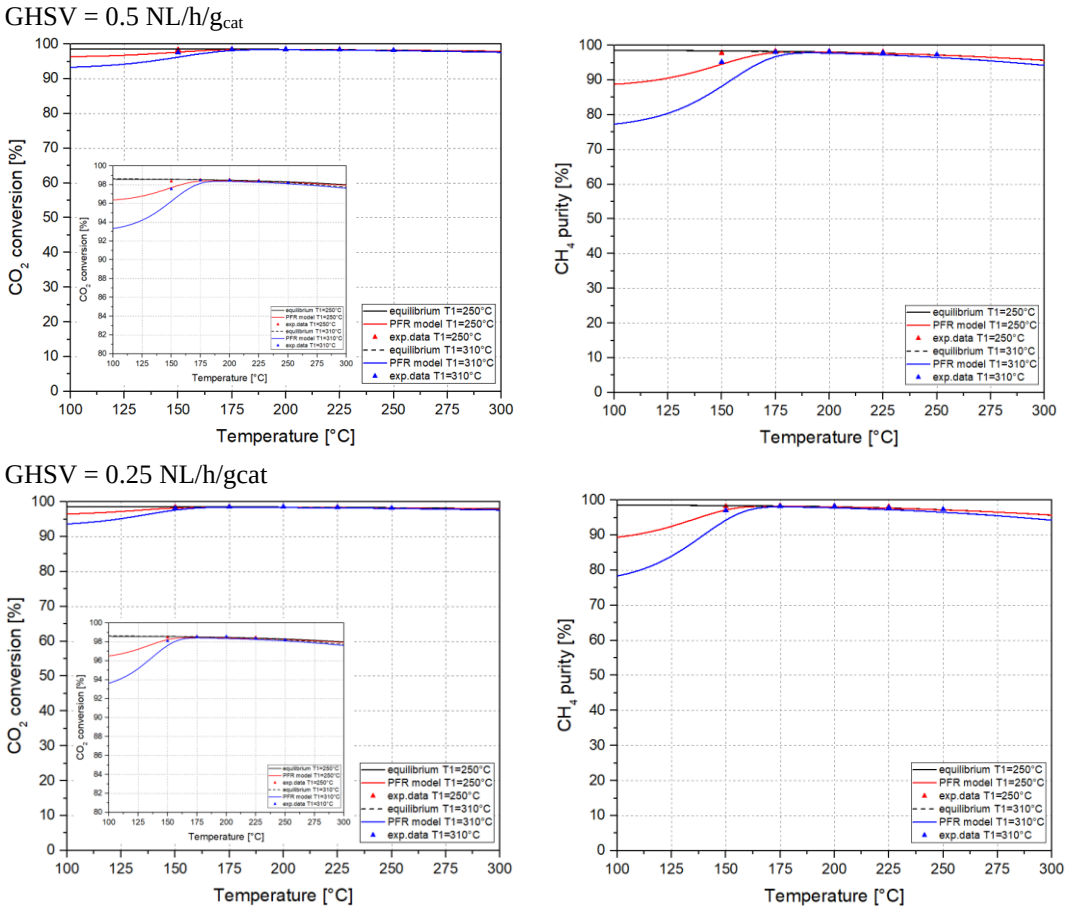

Figure 3.4. CO_2 conversion and CH_4 purity of outlet stream of series of two reactors with intermediate flash. First reactor is maintained at 250°C (red line) and at 310°C (blue line). GHSV = 1,0.5,0.25 NL/h/gcat.

The configuration with a multiple cascade of reactors with condenser unit in between to separate liquid stream from gas feed stream, shows the possibility to enhance CO_2 conversion and to obtain product stream with a high content of methane. The water removal, indeed, allow to shift the reaction towards the products and the presence of a second reactor, working at lower temperatures, makes possible the complete conversion of carbon dioxide, according to the thermodynamic equilibrium. As can been noticed in Figure 3.4., having inlet gas streams with H_2/CO_2 ratio near the stoichiometric value and temperatures of first reactor at about 250°C, with lower values of temperature for the second reactor, is beneficial. The experiments (test #149) were conducted at lab-scale at temperature of first reactor equal to 250°C and 310°C but the results have slightly smaller

values of methane purity working at higher temperature in the first reactor. The conversions achieved from the third scenario are similar also for each case of gas hourly space velocities: values of 98% are generally reached. The most interesting parameter is, nevertheless, the methane purity. More accurately, the values achieved at various GHSV must therefore be assessed. In particular, a methane purity of 98.25% is obtained from the configuration of 0.25 $NL/h/g_{cat}$ inlet stream with the second reactor working at 170°C. It is the maximum value achieved with the two reactors in series with intermediate flash. At higher space velocities the amount of CH_4 in the product never overcome 98%. As suggested in Section 4.1, in this case it might be useful to perform calculations for an optional CO_2 removal, downstream the second reactor. Considering an efficiency of separation equal to 100% thus operating in the best ideal case, maximum value of 99.8% of methane purity can be assessed. This result is a great confirm of the possible achievement of outlet methane stream.

3.4. Analysis of possible improvements for performances intensification

Once identify the process scheme reasonable to obtain high methane purity, two possibilities are present as further possible improvements for performances intensification. From the point of view of an increase of specific productivity, in terms of $g_{methane}/h/g_{cat}$, it can be useful investigate higher inlet gas space velocities. On the other side, if the target is maintained equal to assess as much higher methane purity as possible, the beneficial effect of an increase of pressure should be considered.

3.4.1. Gas Hourly Space Velocity (GHSV) effect

As reported in previous sections, to operate with low inlet space velocities means to increase the methane purity, however it also coincides with larger quantity of catalyst if the same inlet flow rates are maintained or with lower inlet flow rates if the same quantity of catalyst is installed. It is therefore important to assess whether increasing gas space

velocities can raise the productivity of methane maintaining reasonable purity values. For this reason, the analysis of two reactors in series with intermediate flash configuration is also exploited at GHSV=3,4 NL/h/g_{cat} working with first reactor at 250°C (Figure 3.5.) and 310°C (Figure 3.7).

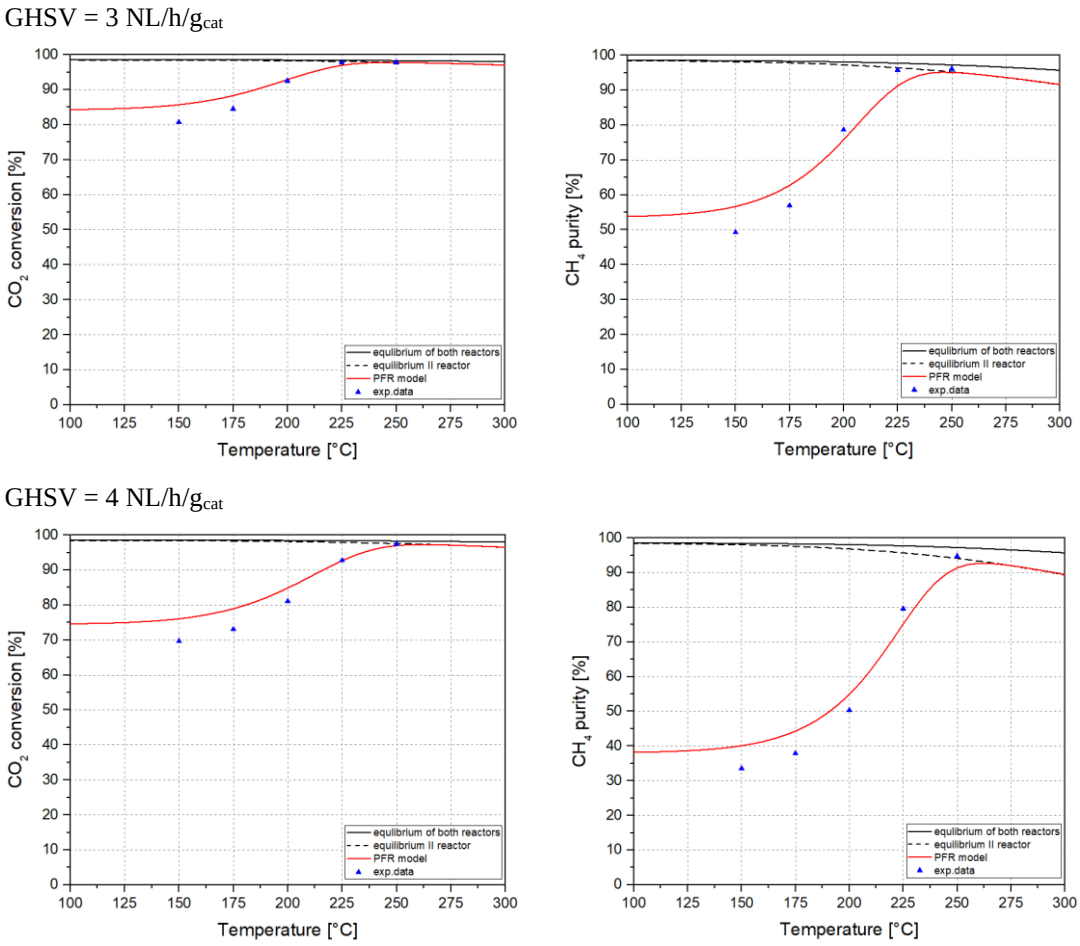

Figure 3.5. CO_2 conversion and CH_4 purity of outlet stream of series of two reactors with intermediate flash when first reactor is maintained at 250°C. GHSV = 3,4 NL/h/gcat.

For the first time, compared to all the simulations performed so far, the case working with first reactor at 250°C present a curve that does not achieve the thermodynamic equilibrium line at high temperature. Until now both the reactors were selected as Gibbs reactors for the conduction of the thermodynamic analysis. However, in this case it is an error consider

that the first reactor is working in thermodynamic equilibrium conditions with a maximum CO_2 conversion. The correct thermodynamic analysis is thus conducted with the first reactor operating at 250°C with only the second one at equilibrium conditions. As a proof of this observation, it is reported the simulation of a single reactor at 5 NL/h/g_{cat} in Figure 3.6. This value of GHSV is chosen in accordance with experimental data available from laboratory tests. CO_2 conversion, indeed, reaches the maximum at almost 310°C.

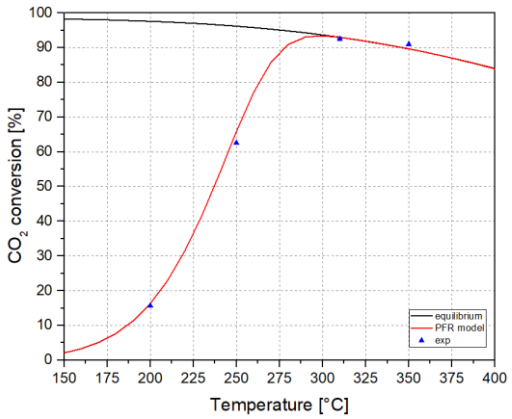

Figure 3.6. CO_2 conversion of a single reactor with GHSV = 5 NL/h/gcat varying temperature.

In any case the result shows that for values of gas space velocities higher than 3 NL/h/g_{cat} is thus necessary to operate with first reactor at 310°C if the performances need to be enhanced.

GHSV = 3 NL/h/g_{cat}

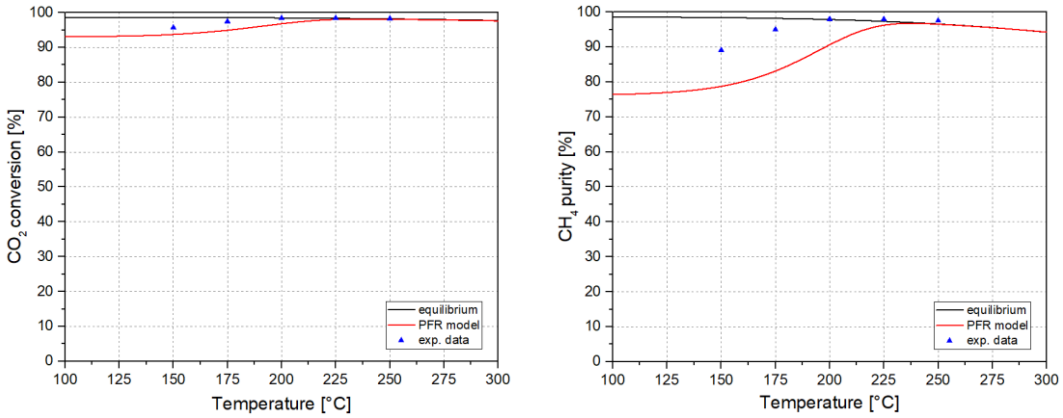

GHSV = 4 NL/h/g_{cat}

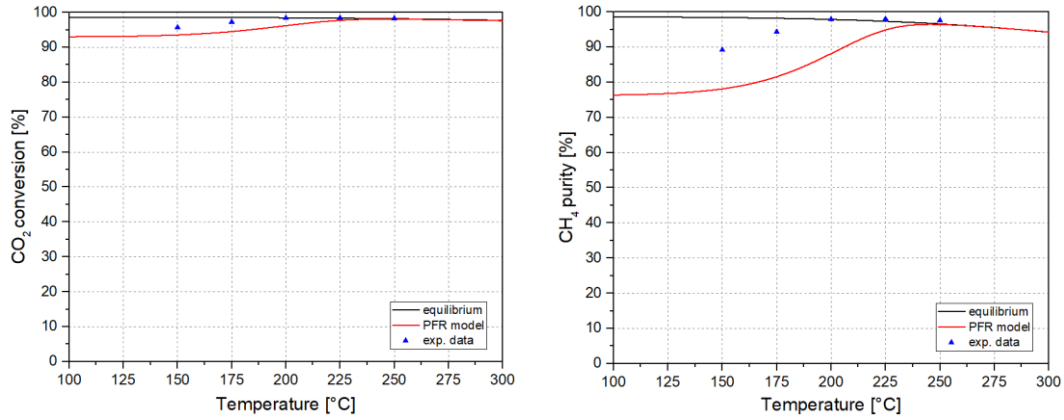

Figure 3.7. CO_2 conversion and CH_4 purity of outlet stream of series of two reactors with intermediate flash when first reactor is maintained at 310°C. GHSV = 3,4 NL/h/gcat.

Figure 3.7. highlights that the same scenario with gas space velocities slightly higher (GHSV=3 or 4 NL/h/g_{cat}), gives different results respect to previous plots reported for GHSV=1,0.5,0.25 NL/h/g_{cat}. The maximum value of methane purity that can be achieved with first reactor operating at 250°C is equal to 94.6%. Unlike simulations at low space velocities, however, performing experiments with first reactor working at 310°C show better results. In particular, 96.7% CH_4 purity can be obtained. This result is not very close to the required target, however, evaluating a final efficient CO_2 removal the productivity of methane can be increased maintaining the methane purity over 98.5%.

3.4.2. Pressure effect

Based on the expected beneficial properties of operating with an increase of pressure in CO_2 methanation reaction, the laboratory rig design is being modified to enable experimental testing also at elevated pressures. Some research at LCCP, Laboratory of Catalysis and Catalytic Processes of Politecnico di Milano, are now focusing on this aspect. It is known that the dataset from which the different parameters for the kinetic expression

are extrapolated, influence the performance of the kinetic model. The values of k_0 $\left[\frac{mol}{s \cdot g_{cat} \cdot atm^{5n}}\right]$, E_a $\left[\frac{kJ}{mol}\right]$ and n, reported in Section 2, were obtained considering only CO_2 conversion data at atmospheric pressure, thus in the future they will be updated through new regression of larger dataset obtained at different pressures. In any case, the analysis reported in Section 2.2.2. regarding the pressure effect on CO_2 methanation kinetics defined by Lunde and Kester model could be taken as reference.

Although this consideration, it was deemed useful to evaluate the performance of the model at pressure higher than the atmospheric one to assess if the results could be in line with expectations at least qualitatively.

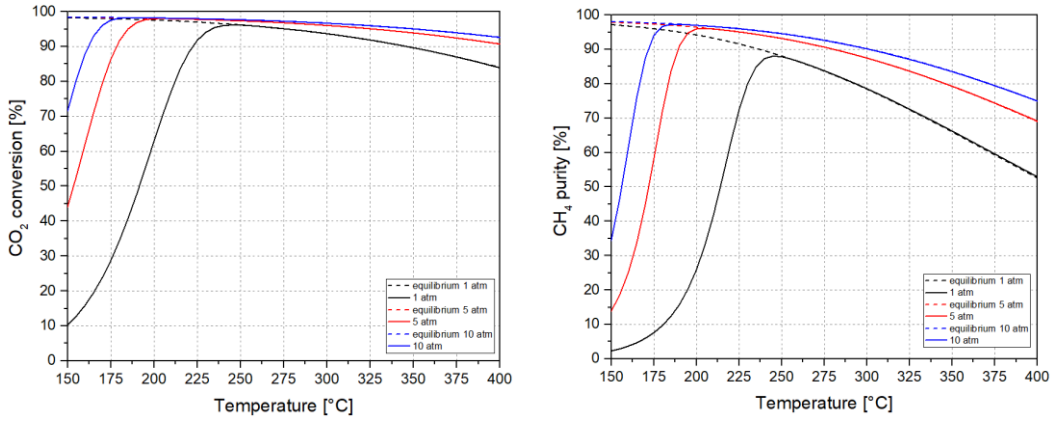

Figure 3.8. Single reactor configuration with GHSV=1 NL/h/gcat varying pressure and temperature.

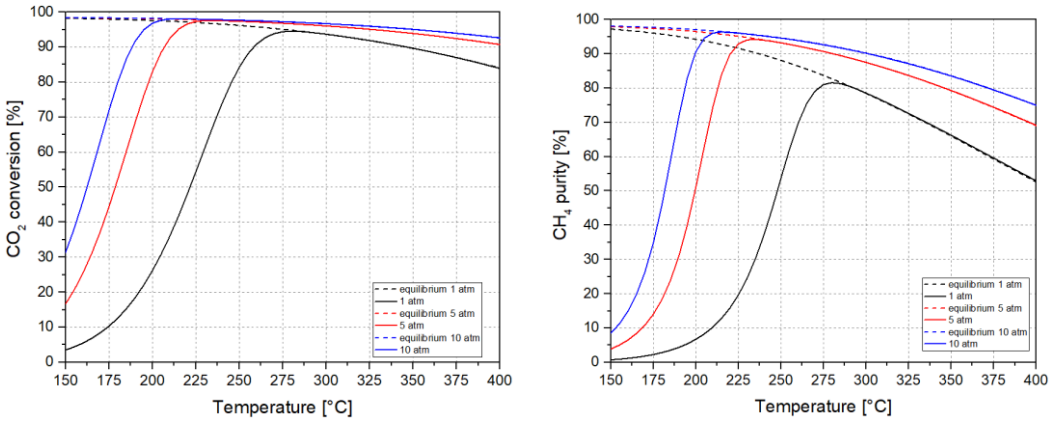

Figure 3.9. Single reactor configuration with GHSV=3 NL/h/gcat varying pressure and temperature.

As expected, increasing pressure the thermodynamic constraints are less strict and it is possible to obtain an improvement in terms of methane purity. Figure 3.10. is added in order to quantify the detachment between the kinetic curves evaluating, for instance, the inlet stream with a space velocity of 3 Nl/h/gcat at 225°C and 250°C. At 250°C CO_2 conversion is kinetically boosted from 84% at atmospheric pressure to 97% at 5 atm, having already reached the thermodynamic equilibrium conditions at 3 atm. The P-effect observed at 225 °C, temperature at which the catalyst works at conditions far from thermodynamic equilibrium at atmospheric pressure, is ever stronger.

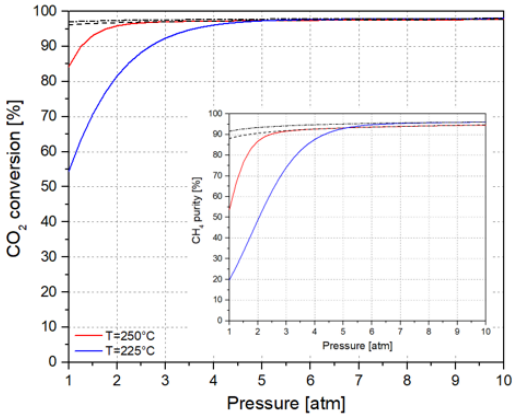

Figure 3.10. CO_2 conversion and CH_4 purity varying pressure at 3 Nl/h/gcat (T=225°C, 250°C).

In addition, pressure upgrades also the CH_4 purity. For this reason, the analysis of the pressure effect has been enlarged also to the other configurations.

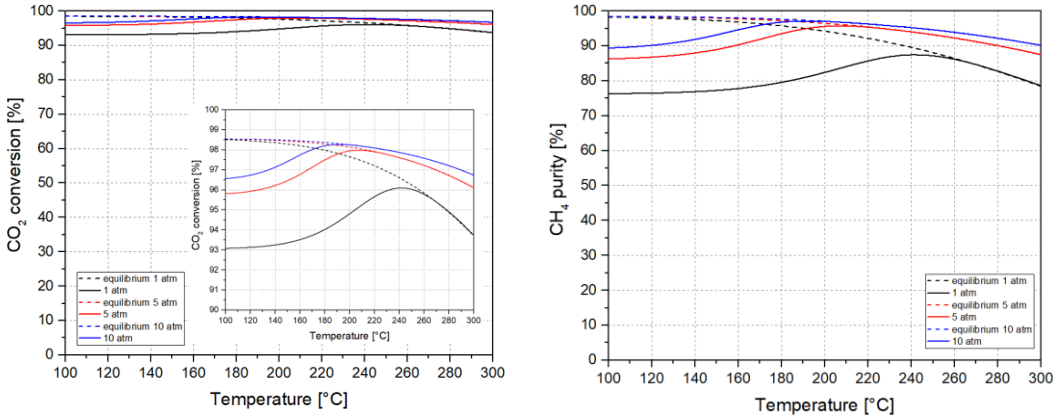

Figure 3.11. CO_2 conversion and CH_4 purity varying pressure in two reactors in series configuration.

The thermodynamic equilibrium line is always present and assessed through the simulation of two Gibbs reactors with or without intermediate flash. Both the reactors are thus considered in equilibrium conditions.

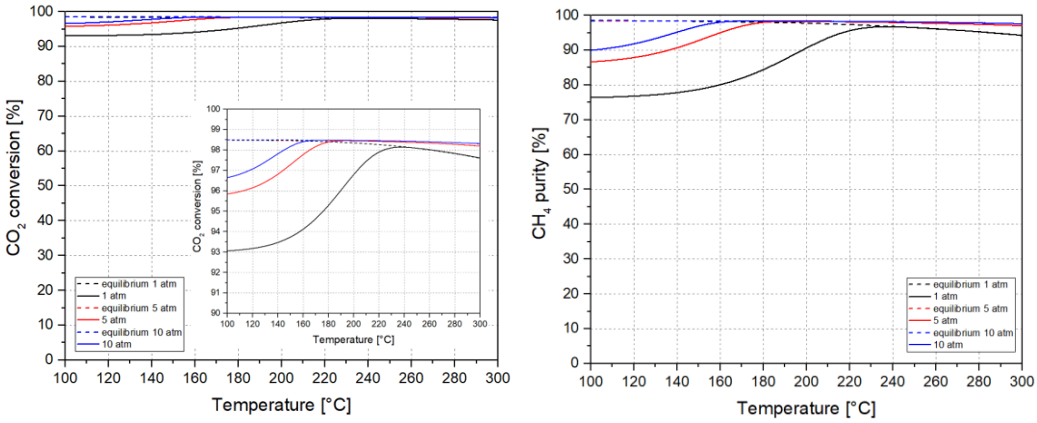

Figure 3.12. CO_2 conversion and CH_4 purity varying pressure in two reactors in series with intermediate flash configuration.

As reported in Section 3.3., in a configuration of two reactors in series with intermediate flash, CH_4 purity achieved a value of 98.5% at atmospheric pressure, with 3 Nl/h/gcat inlet space velocity, only performing an efficient 100% CO_2 removal. However, without the necessity of this final separation, 98.5% of methane purity can also be reached by the same system increasing pressure at about 10 atm. The operative condition, in particular, coincides with the first reactor working at 310°C and with the second one set to about 180°C. If the raise of pressure and the insertion of CO_2 removal step are then coupled, a value of 99.9% methane purity can be obtained.

3.5. Ru-catalyst application in patented configurations

In previous simulations high values for CO_2 conversion and CH_4 purity confirm that Ru-based catalyst is very active in the Sabatier reaction. The kinetic model at atmospheric pressure has been compared to laboratory tests and it is turn out to be consistent with

experimental data. It can be thus used as flexible tool in extended operative conditions range. The application of Ru-based catalysts in process configuration of series reactors with intermediate water condensation is still unreported in literature. However, significant benefits may derive from its use in terms of higher catalytic activity at low temperatures, where the kinetic constraints limiting the CH_4 yields are almost negligible even at atmospheric pressure. As described in the Introduction (Section 1.4.), there are available the operating conditions used for the CO_2 methanation process in patented technologies. It could be useful to test the performance of the non-commercialized 5%wt.Ru/γ-Al_2O_3 catalyst in these validated schemes that are also comparable with the ones just investigated in isothermal conditions.

In the Solar Fuel patent [55] it is declared that in the selected operative range "according to the embodiment, the conversion of the carbon dioxide in the first reactor stage is approximately 95% while the conversion of the carbon dioxide in the second reactor stage is slightly more than 90%, so that the methane content in the final product is approximately 99%". It is possible to recreate the whole process scheme adding a final water condenser to the two reactors in series with intermediate condenser configuration. As initial step, it is important to identify more accurately the percentage values of conversion and purity that can be reached. For this purpose, simulations at equilibrium are performed, keeping the parameters always within the suggested range. The analysis is conducted by varying the temperature of the first reactor, highlighting per pass CO_2 conversion and maintaining it about 95%. It is necessary also to determine whether the percentage of methane present in the product has been considered in accordance with the definition (11) used up to now.

$$Pu_{CH4} = \frac{\dot{n}_{CH4}}{\dot{n}_{CH4}+\dot{n}_{H2}+\dot{n}_{CO2}+\dot{n}_{H2O}} \quad (11)$$

The results, in thermodynamic equilibrium conditions, show that working in the first reactor with a conversion of almost 95% and in the second one with a conversion slightly more than 90%, the percentage of methane purity in the product never overcome 99%, but could be reasonable close to this value according to the selected working temperatures.

equilibrium					
T_{R1} [°C]	T_{R2} [°C]	conv.CO_2 1°reactor [%]	conv.CO_2 2°reactor [%]	conv.CO_2 total [%]	CH_4 Purity [%]
340	170	95,93	96,46	99,86	98,66
340	175	95,93	96,06	99,84	98,58
340	180	95,93	95,64	99,82	98,50
340	185	95,93	95,18	99,80	98,40
340	190	95,93	94,68	99,78	98,31
340	195	95,93	94,14	99,76	98,20
340	200	95,93	93,56	99,74	98,08
340	205	95,93	92,93	99,71	97,96
340	210	95,93	92,26	99,69	97,83
340	215	95,93	91,54	99,66	97,69
340	220	95,93	90,77	99,62	97,53
340	225	95,93	89,94	99,59	97,37

equilibrium					
T_{R1} [°C]	T_{R2} [°C]	conv.CO_2 1°reactor [%]	conv.CO_2 2°reactor [%]	conv.CO_2 total [%]	CH_4 Purity [%]
320	170	96,78	95,65	99,86	98,68
320	175	96,78	95,16	99,84	98,60
320	180	96,78	94,64	99,83	98,52
320	185	96,78	94,07	99,81	98,43
320	190	96,78	93,46	99,79	98,34
320	195	96,78	92,80	99,77	98,23
320	200	96,78	92,08	99,75	98,12
320	205	96,78	91,32	99,72	98,00
320	210	96,78	90,49	99,69	97,87
320	215	96,78	89,61	99,67	97,73
320	220	96,78	88,66	99,64	97,59
320	225	96,78	87,65	99,60	97,43

Table 3.1. Performances assessed in Solar Fuel patented configuration in equilibrium conditions.

The aim is set the performances limits through a thermodynamic analysis. For this reason, the CO_2 conversion in the first reactor has been selected with slightly excess values of 95%. The reference percentage of maximum performance of CH_4 purity according to the patent's statement, thus considering the conversion in the second reactor at least lower than the first one, can be considered equal to 98.3%. It is established that, in these conditions, even at

maximum catalyst activity this threshold value cannot be exceed. Taking into account these considerations, the activity of the catalyst can be tested. The reactors are selected as isothermal in order to perform a sensitivity analysis regarding the operative temperature that it is expected to be lower than the suggested values adopted for Ni-based catalyst.

GHSV=3500/h					
T_{R1} [°C]	T_{R2} [°C]	conv.CO_2 1°reactor [%]	conv.CO_2 2°reactor [%]	conv.CO_2 total [%]	CH_4 Purity [%]
210	150	98,93	58,76	99,56	97,21
210	155	98,93	65,79	99,63	97,58
210	160	98,93	71,99	99,70	97,90
210	165	98,93	76,85	99,75	98,15
210	170	98,93	80,28	99,79	98,33
210	175	98,93	82,23	99,81	98,43
210	180	98,93	82,93	99,82	98,47
210	185	98,93	82,60	99,81	98,45
210	190	98,93	81,42	99,80	98,39
210	195	98,93	79,76	99,78	98,30
210	200	98,93	77,84	99,76	98,20
210	205	98,93	75,71	99,74	98,09
210	210	98,93	73,43	99,71	97,97

GHSV=3500/h					
T_{R1} [°C]	T_{R2} [°C]	conv.CO_2 1°reactor [%]	conv.CO_2 2°reactor [%]	conv.CO_2 total [%]	CH_4 Purity [%]
330	150	96,36	58,95	98,51	92,38
330	155	96,36	67,15	98,81	93,71
330	160	96,36	74,68	99,08	94,96
330	165	96,36	81,24	99,32	96,07
330	170	96,36	86,47	99,51	96,98
330	175	96,36	90,08	99,64	97,61
330	180	96,36	92,30	99,72	98,00
330	185	96,36	93,38	99,76	98,19
330	190	96,36	93,59	99,77	98,23
330	195	96,36	93,32	99,76	98,18
330	200	96,36	92,78	99,74	98,08
330	205	96,36	92,11	99,71	97,96
330	210	96,36	91,38	99,69	97,83

Table 3.2. Performances assessed in Solar Fuel patented configuration operating with inlet GHSV=3500/h.

The results show that, as awaited, Ru-based catalyst allows to work in the first reactor at almost 100°C less respect to the recommended values of temperatures. However, this condition brings to operate the system with higher conversions thus it requires further investigations especially from the thermal point of view since higher reaction heat could be released. The performed simulations however bring also to the conclusion that if the specific percentage of per pass CO_2 conversion in each reactor is maintained almost equal to 95% and 90%, respectively, it is necessary to operate in the first reactor at temperature above 300°C. Working in the first reactor at 330°C and in the second one at 190°C, a value of 98.23% of methane purity can be reached. This is any case in accordance with the thermodynamic limits and with what stated by the patent. The use of Ru-based catalyst is thus validated within this configuration at conditions different respect to those investigated so far.

The second patent [57] that could be analyzed as application of Ru-based catalyst is the MAN Diesel & Turbo SE technology. In this case the process scheme exploited coincides with two reactors in series. Actually from the constructive point of view they are designed so that the two reaction zones at different temperatures are located within a single equipment. It is performed a sensitivity analysis of pressure since this parameter is the only one not completed specified.

P[bar]	T_{R1} [°C]	T_{R2} [°C]	conv.CO_2 [%]	CH_4 dry [%]	CO_2 dry [%]	H_2 dry [%]
1	550	250	91,21	75,63	7,29	17,08
2	550	250	94,77	89,10	4,92	5,98
3	550	250	95,15	90,75	4,63	4,62
4	550	250	95,31	91,45	4,50	4,04
5	550	250	95,41	91,92	4,42	3,65
6	550	250	95,49	92,28	4,36	3,36
7	550	250	95,55	92,56	4,31	3,13
8	550	250	95,60	92,79	4,27	2,94
9	550	250	95,64	92,98	4,24	2,79
10	550	250	95,68	93,14	4,21	2,65

Table 3.3. Performances assessed in MAN Diesel & Turbo SE technology patented configuration.

Result shown in Table 3.3. is in complete agreement with what declared by the patent. The dry outlet mixture in these conditions is indeed composed by 92.3% CH_4, 4.3% CO_2, 3.4% H_2.

This analysis, conducted after the selection of the adequate process scheme, is therefore used to test the kinetic model under different operating conditions. What is found is a valid application of the Ru-based catalyst in process configurations and operating conditions already validated.

Section 4: Thermal behaviour analysis

In order to produce SNG with high CH_4 molar fraction the CO_2 methanation process must be operated in absence of diluents, with complete conversion of both reactants and with complete methane selectivity. The Sabatier reaction is highly exothermic, and CO_2 conversion as well as CH_4 selectivity are thermodynamically limited at high temperatures. From the process engineering point of view, this requires an efficient thermal management of the reactor. Until now the problem of temperature control has never been addressed although the reaction involved is strongly exothermic. The general approach that has been decided to cross is to investigate firstly the reactor in isothermal conditions in order to compare the model with the data obtained experimentally and then to implement the validated kinetic model in a 2D reactor configuration in gPROMS ModelBuilder® V5.0.2 in order to take into account also the heat exchange with an external coolant exhibited in a packed bed reactor.

4.1. Model validation

This section is present in order to verify that the model is reliable. The only data available experimentally are those used in Section 4. and they are therefore evaluated in isothermal conditions. The available model can describe with greater level of detail the diffusive limitations and the heat exchange inside a 2D configuration however in order to have a valid comparison with the experimental data now these phenomena will be considered negligible. It is therefore possible to approach the approximation of a plug flow reactor by first selecting the coefficients of heat exchange and diffusive limitations with

very high fixed values in order to achieve a complete cooling performed by the boiling water within the reactor and zero variations in concentration gradients within the catalytic particle and along the radial coordinate. All the specific inputs adopted to conduct the simulation are reported below.

Transport correlation coefficients	
$D_{eff,i}\left[\frac{m^2}{s}\right]$	1E+03
$\lambda_{eff}^{g}\ \left[\frac{W}{m\,K}\right]$	1E+03
$K_{m,i}\left[\frac{m}{s}\right]$	1E+06
$h\ \left[\frac{W}{m^2K}\right]$	1E+06
$h_w\ \left[\frac{W}{m^2K}\right]$	1E+06
$D_{eff,i}^{p}\left[\frac{m^2}{s}\right]$	1E+03

Reactor design	
L [m]	8
dt [m]	0.042
Ntubes	1
ρ_{bed} [kg/m$^3_{react}$]	1050
ε	0.4

Pellet design	
dp [m]	0.006
hp [m]	0.0035

Process conditions	
Tin = Tcoolant [°C]	150:10:450
P [atm]	1
H_2/CO_2	3.94
GHSV [NL/h/g_{cat}]	0.25, 0.5, 1, 5, 50

Table 4.1. Input conditions for the model validation.

It must be point out that the parameters present in the reactor and pellet design are not relevant for this analysis. The reactor length, the diameter of the tube and of the pellet as well as its height are set equal to those reported for a packed-bed reactor for methanol synthesis [79]. The only important parameter related to these selected values is actually the process condition of the gas space velocity. The process conditions have been investigated in the temperature range [150:10:350]°C for the GHSV imposed equal to 0.25, 0.5, 1, 5 Nl/h/g_{cat}. In addition also the case at higher space velocity, 50 Nl/h/g_{cat}, is performed but changing the temperature between 250°C and 450°C, being these values more interesting in terms of kinetic performances. All the simulations are executed at atmospheric pressure with inlet composition of H_2/CO_2 =3.94 and 2.05% Ar. Argon is only present in this case to execute a valid comparison with previous analysis performed at laboratory scale.

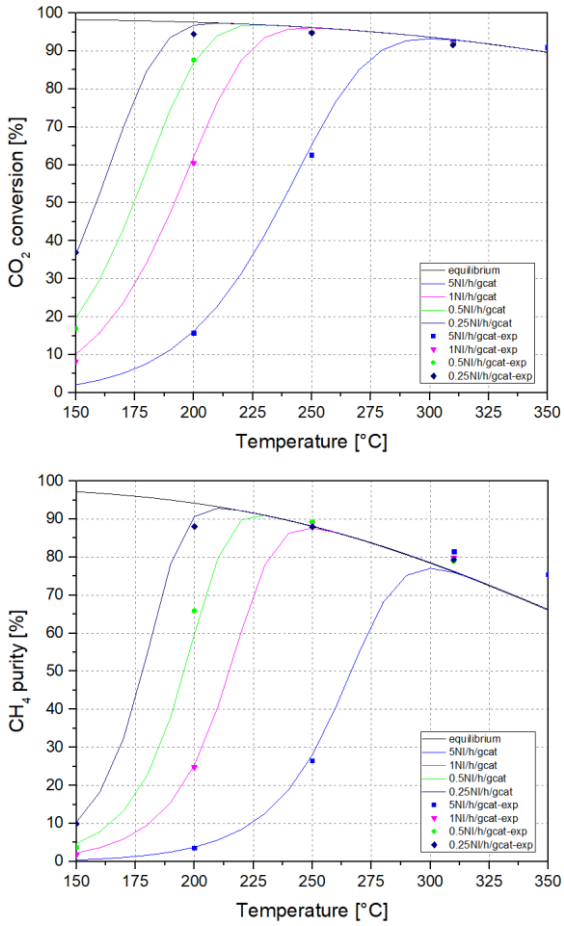

Figure 4.1. gPROMS isothermal single reactor simulations for GHSV=0.25, 0.5, 1, 5 NL/h/gcat.

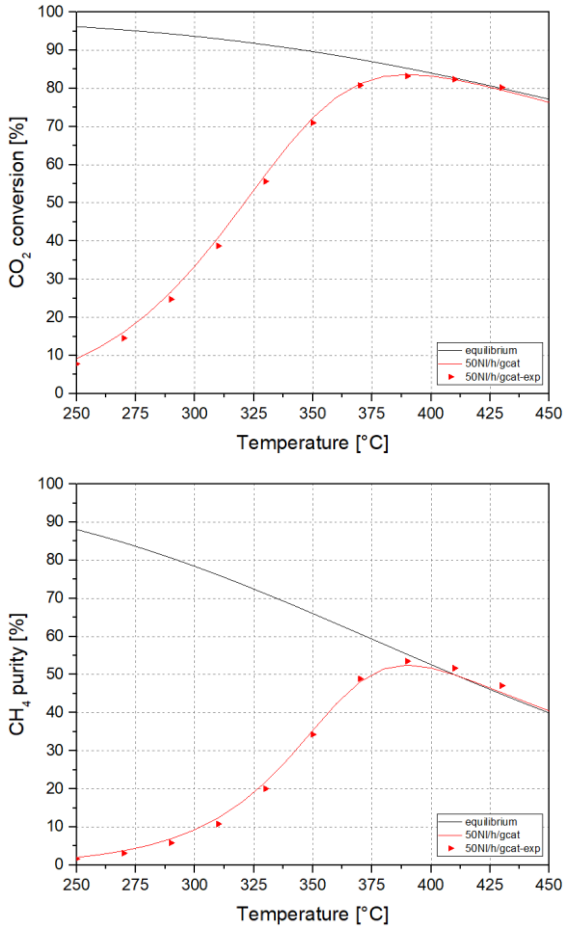

Figure 4.2. gPROMS isothermal single reactor simulations for GHSV=50 NL/h/gcat.

The results of CO_2 conversion and CH_4 purity present in Figure 4.2. confirm that the kinetic model of the Sabatier reaction implemented within the model in gPROMS ModelBuilder® V5.0.2 is able to correctly describe the results obtained experimentally in isothermal conditions at different temperatures. In this way it is possible to obtain a validation of the model even having used the 2D reactor in a simplified way. These simulations are also directly comparable with those presented in Figure 3.1. of Section 3. Therefore, also the problem of non-perfect overlapping between the kinetic curve and the thermodynamic one at equilibrium conditions for temperature above 410°C has already been addressed.

For a better understanding of the results the table of all the tests carried out is also given.

	GHSV=0.25 [Nl/h/gcat]		GHSV=0.5 [Nl/h/gcat]		GHSV=1 [Nl/h/gcat]		GHSV=5 [Nl/h/gcat]			GHSV=50 [Nl/h/gcat]	
Temp. [°C]	**conv. CO_2**	**purity CH_4**	**conv. CO_2**	**purity CH_4**	**conv. CO_2**	**purity CH_4**	**conv. CO_2**	**purity CH_4**	**Temp. [°C]**	**conv. CO_2**	**purity CH_4**
150	36,199	10,368	19,517	4,693	10,113	2,230	2,079	0,428	**250**	9,169	2,005
160	52,164	18,285	29,586	7,877	15,684	3,637	3,279	0,682	**260**	12,254	2,754
170	69,669	32,363	42,846	13,283	23,557	5,893	5,056	1,067	**270**	16,131	3,756
180	84,681	54,554	58,589	22,570	34,119	9,544	7,622	1,645	**280**	20,905	5,095
190	93,590	78,259	74,497	38,016	47,316	15,529	11,237	2,503	**290**	26,643	6,878
200	96,794	90,653	87,051	59,726	62,176	25,353	16,191	3,773	**300**	33,348	9,249
210	97,304	92,909	94,028	79,797	76,484	40,680	22,770	5,652	**310**	40,915	12,388
220	97,147	92,205	96,597	89,807	87,424	60,604	31,179	8,444	**320**	49,090	16,496
230	96,877	91,017	96,885	91,048	93,527	78,042	41,417	12,616	**330**	57,446	21,746
240	96,564	89,665	96,567	89,681	95,754	86,317	53,092	18,855	**340**	65,400	28,148
250	96,207	88,167	96,208	88,168	96,076	87,624	65,250	28,011	**350**	72,319	35,334
260	95,806	86,524	95,806	86,524	95,792	86,469	76,403	40,568	**360**	77,682	42,398
270	95,355	84,739	95,356	84,737	95,354	84,736	85,011	55,236	**370**	81,253	48,097
280	94,853	82,816	94,853	82,817	94,853	82,816	90,306	68,040	**380**	83,131	51,499
290	94,297	80,762	94,298	80,761	94,297	80,762	92,690	75,243	**390**	83,658	52,511
300	93,684	78,584	93,684	78,584	93,684	78,584	93,237	77,055	**400**	83,256	51,736
310	93,010	76,295	93,010	76,295	93,010	76,295	92,915	75,979	**410**	82,288	49,933
320	92,274	73,905	92,274	73,906	92,274	73,905	92,262	73,867	**420**	81,003	47,667
330	91,472	71,430	91,472	71,430	91,472	71,430	91,471	71,424	**430**	79,544	45,254
340	90,604	68,883	90,604	68,883	90,604	68,883	90,604	68,882	**440**	77,978	42,837
350	89,666	66,280	89,666	66,280	89,666	66,280	89,666	66,280	**450**	76,335	40,472

Table 4.2. gPROMS isothermal and isobaric single reactor simulations.

4.2. Effect of GHSV on process temperature

Once the model has been validated, it is possible to remove the isothermal conditions reintroducing all transport correlations related to the heat exchange no longer fixing the coefficients but allowing the software to consider this phenomenon during calculations. The assumption of constant temperature along the axial and radial coordinate of tube is thus removed so it is necessary to investigate the proper reactor configuration able to grant the minimization of all the heat transfer limitations that could bring a negative effect to the performances. For this initial analysis on the thermal effect in a 2D isobaric and non-

isothermal reactor model the intraporous diffusion limitations are still kept at zero. Therefore, for the moment, $D^{p}_{eff,i}\left[\frac{m^2}{s}\right]$ is still maintained equal to 1E+03. The reactor is also considered isobaric since the configuration choices have not yet been ended. This assumption will therefore be maintained throughout this thesis work.

Implementing the Sabatier kinetic model in the rector design present an issue of thermal management. The reactor and pellet design, given the high exothermicity of the CO_2 methanation process, indeed have to be modified. In general, two possibilities are present to reduce as much as possible the temperature gradients: scale down the tube diameter in order to recreate a smaller path for the heat along the radial coordinate or dilute the catalyst with inert material. Although the last option allows to release the heat generated over bigger volume, there is a high probability of bypassing and moreover it is like hindering the activity of the catalyst, developed specifically to obtain high conversions. To begin the analysis, a tube diameter of 1cm is thus set. This diameter is small, comparable to the laboratory diameter, but an industrial standard length of 8 m is always maintained.

In a packed bed reactor configuration it is also important to consider the possible channeling phenomenon. Pellets are randomly disposed within the reactor and for this reason the bed void fraction often is described as function of tube radius. Although in the wall the packing of catalyst is forced, the local variation along the radial coordinate could be consider stable. Moreover, a rule of thumb guarantees to minimize changes in interstitial velocity: $\frac{d_t}{d_p} > 10$.

Once the tube diameter is selected equal to 1cm, the empirical correlation implemented in the model to describe void fraction provides pellet dimensions. Imposing a standard value of porosity in the reactor equal to 0.4 the catalytic particle is about 1 mm.

For $\frac{d_{p,v}}{d_t} < 0.6$ is valid: $\varepsilon = 0.36 + 0.1\left(\frac{d_{p,v}}{d_t}\right) + 0.7\left(\frac{d_{p,v}}{d_t}\right)^2$

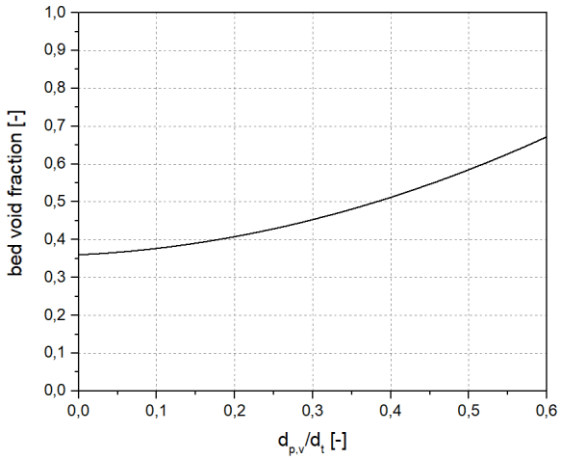

Figure 4.3. Bed void fraction, Dixon empirical correlation.

Regarding the process conditions, the range within investigate the performances has already been identified in the previous Sections. Temperature is selected equal to [200:10:300]°C, both for the inlet gas and for the coolant, while gas hourly space velocity is maintained [1:1:10]NL/h/g_{cat}. The choice to adopt low GHSV values falls into the possibility of keeping contained the absolute value of the heat released being it directly proportional to the converted flow rate. Moreover, a decrease in space velocity allows to obtain high conversions due to the higher contact time between the gas stream and the catalyst. However, too low inlet flow rates could also obstacle an effective heat transfer since one of the major mechanism coincides with the convection by fluid. For this reason, it seems useful to look into all the *n* combinations of temperatures and space velocities to assess the best working conditions. Simulations are conducted for one tube because this analysis aims to study how the interplay of fluid flow will evolve from the thermal point of view. Then it will be simple to scale up the single behaviour to Ntubes, relating them also to an adequate inlet molar stream.

reactor design	
L [m]	8
dt [m]	0.01
Ntubes	1
ρ_{bed} [kg/m^3_{react}]	1050
ε	0.4

pellet design	
dp [m]	0.001862
hp [m]	0.001086

Process conditions	
Tin = Tcool [°C]	200:10:300
P [atm]	1
H_2/CO_2	4
GHSV [NL/h/g_{cat}]	1:1:10

Table 4.3. Input conditions for the analysis of temperature effect in a 2D reactor model.

convCO_2[%]	**200°C**	**210°C**	**220°C**	**230°C**	**240°C**	**250°C**	**260°C**	**270°C**	**280°C**	**290°C**	**300°C**
1 [Nl/h/gcat]	66,255	81,066	91,260	96,070	97,433	97,429	97,113	96,608	96,064	95,474	94,828
2 [Nl/h/gcat]	39,320	53,287	68,350	81,755	90,842	95,155	96,525	96,619	96,103	95,520	94,886
3 [Nl/h/gcat]	27,433	38,293	51,498	65,917	79,195	88,661	93,821	95,712	96,055	95,538	94,913
4 [Nl/h/gcat]	20,976	29,645	40,694	53,823	67,774	80,113	88,892	93,544	95,225	95,480	94,913
5 [Nl/h/gcat]	16,953	24,115	33,458	45,037	58,293	71,565	82,747	90,107	93,733	94,909	94,872
6 [Nl/h/gcat]	14,214	20,298	28,342	38,551	50,749	63,915	76,321	85,819	91,481	93,988	94,755
7 [Nl/h/gcat]	12,233	17,513	24,554	33,625	44,756	57,361	70,173	81,120	88,618	92,611	94,031
8 [Nl/h/gcat]	10,734	15,394	21,645	29,779	39,939	51,821	64,553	76,347	85,342	90,814	93,243
9 [Nl/h/gcat]	9,561	13,729	19,344	26,703	36,010	47,144	59,531	71,722	81,837	88,671	92,189
10 [Nl/h/gcat]	8,618	12,388	17,481	24,192	32,757	43,174	55,087	67,363	78,254	86,270	90,884

Table 4.4. CO2 conversion obtained in a single 2D reactor model.

PuCH_4[%]	**200°C**	**210°C**	**220°C**	**230°C**	**240°C**	**250°C**	**260°C**	**270°C**	**280°C**	**290°C**	**300°C**
1 [Nl/h/gcat]	28,196	46,129	67,617	83,013	88,344	88,312	86,883	85,091	83,160	81,101	78,923
2 [Nl/h/gcat]	11,473	18,576	30,163	47,262	66,485	79,701	84,727	84,945	83,143	81,100	78,923
3 [Nl/h/gcat]	7,029	11,041	17,516	27,891	43,223	60,994	75,224	81,686	82,843	81,055	78,918
4 [Nl/h/gcat]	5,041	7,772	12,067	18,904	29,608	44,618	61,543	74,339	79,942	80,780	78,870
5 [Nl/h/gcat]	3,922	5,976	9,137	14,081	21,846	33,482	48,959	64,559	74,942	78,839	78,692
6 [Nl/h/gcat]	3,208	4,847	7,330	11,149	17,087	26,158	39,196	54,758	68,228	75,760	78,293
7 [Nl/h/gcat]	2,712	4,073	6,111	9,200	13,944	21,201	31,998	46,216	60,894	71,480	75,899
8 [Nl/h/gcat]	2,348	3,511	5,235	7,818	11,738	17,704	26,698	39,231	53,798	66,410	73,400
9 [Nl/h/gcat]	2,071	3,085	4,577	6,791	10,116	15,138	22,732	33,654	47,400	61,019	70,240
10 [Nl/h/gcat]	1,851	2,750	4,065	5,999	8,878	13,191	19,699	29,218	41,851	55,685	66,599

Table 4.5. CH4 purity obtained in a single 2D reactor model.

real/eq.conv	200°C	210°C	220°C	230°C	240°C	250°C	260°C	270°C	280°C	290°C	300°C
1 [Nl/h/gcat]	0,67	0,82	0,93	0,98	1,00	1,00	1,00	1,00	1,00	1,00	1,00
2 [Nl/h/gcat]	0,40	0,54	0,69	0,83	0,93	0,98	0,99	1,00	1,00	1,00	1,00
3 [Nl/h/gcat]	0,28	0,39	0,52	0,67	0,81	0,91	0,97	0,99	1,00	1,00	1,00
4 [Nl/h/gcat]	0,21	0,30	0,41	0,55	0,69	0,82	0,92	0,97	0,99	1,00	1,00
5 [Nl/h/gcat]	0,17	0,24	0,34	0,46	0,60	0,73	0,85	0,93	0,98	0,99	1,00
6 [Nl/h/gcat]	0,14	0,21	0,29	0,39	0,52	0,66	0,79	0,89	0,95	0,98	1,00
7 [Nl/h/gcat]	0,12	0,18	0,25	0,34	0,46	0,59	0,72	0,84	0,92	0,97	0,99
8 [Nl/h/gcat]	0,11	0,16	0,22	0,30	0,41	0,53	0,66	0,79	0,89	0,95	0,98
9 [Nl/h/gcat]	0,10	0,14	0,20	0,27	0,37	0,48	0,61	0,74	0,85	0,93	0,97
10 [Nl/h/gcat]	0,09	0,13	0,18	0,25	0,33	0,44	0,57	0,70	0,81	0,90	0,96

Table 4.6. CO2 conversion reached respect to the equilibrium one in a single 2D reactor model.

From the matrices reported above it is possible to assess the performances at different process conditions. In particular conversion over 95% can be obtained only working at temperatures between 230-290°C within the range of these investigated GHSV. In Figure 4.4. it is depicting the CO_2 conversion and the CH_4 purity as function of different space velocities underling the approach to the equilibrium line at each temperature considered suitable for the analysis.

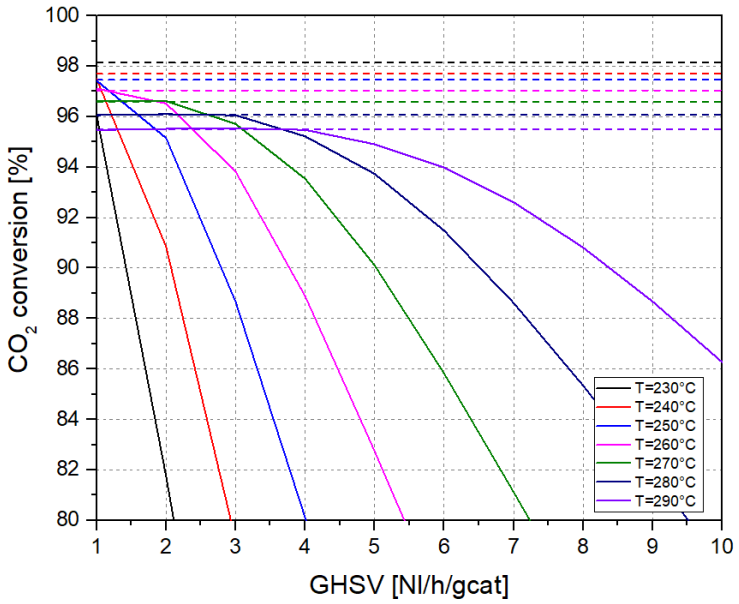

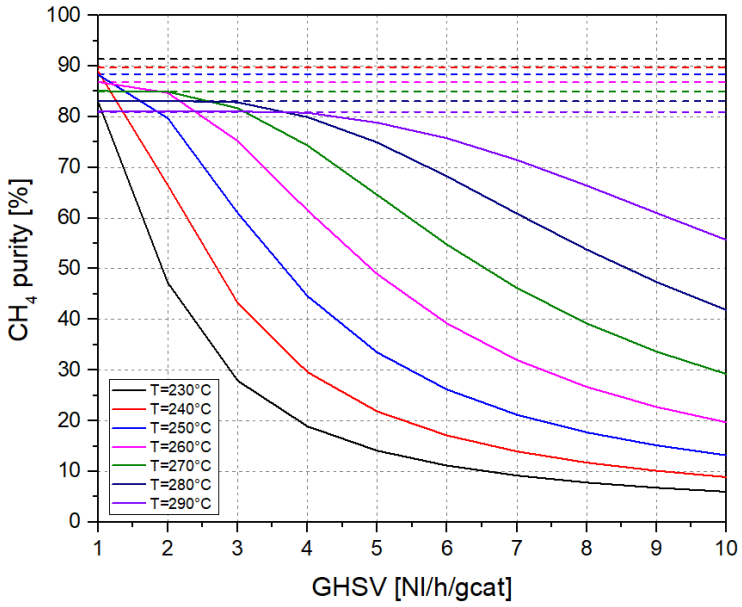

Figure 4.4. CO_2 conversion and CH_4 purity as function of GHSV for each temperature (T=230-290°C).

Reducing the GHSV, CO_2 conversion and CH_4 purity achieve higher values approaching the equilibrium line. At 250°C, in particular, it is evident the presence of an inflection working at 1 $Nl/h/g_{cat}$. The kinetics becomes thus limited by the thermodynamic constraints. A high value of conversion, 97.43%, however, can be achieved even at low temperature of $T_{in}=T_{coolant}=240°C$, working always at 1 $Nl/h/g_{cat.}$ The ratio between the CO_2 conversion obtainable in the reactor and the equilibrium one, shown in the Figure 4.4. but also reported as value in Table 4.6., allows to better identify whether the kinetics is far or close to the thermodynamic limits. As seen for lab-scale configurations, it is advantageous to work as close as possible to the equilibrium conditions maintaining the temperature as low as possible in order to achieve high conversion values.

Although there are no relevant discontinuities in parameters that take into account the material performances, these could become important when the thermal behaviour within the system is considered. It is therefore necessary also to assess the thermal aspects of detail. Among all the different parameters that could be taken into account, the maximum temperature achievable by the solid catalyst during the completion of the CO_2 methanation

process is the most relevant one. In addition to possible issues of the catalyst deactivation, from the thermodynamic point of view, a possible reversal of the Sabatier reaction at temperature above 500°C may occur as well as the possible ignition of undesired secondary reactions. Operative conditions that involve thermal instability up to reach temperatures of 500°C, or over, need to be avoid.

Tmax[°C]	200°C	210°C	220°C	230°C	240°C	250°C	260°C	270°C	280°C	290°C	300°C
1 [Nl/h/gcat]	203,62	215,43	228,17	242,47	259,82	285,39	563,45	588,45	601,49	613,57	623,85
2 [Nl/h/gcat]	202,54	213,76	225,55	238,20	252,27	268,89	291,76	548,02	603,81	621,29	628,29
3 [Nl/h/gcat]	201,97	212,90	224,24	236,18	249,04	263,36	280,43	304,08	550,18	612,85	626,64
4 [Nl/h/gcat]	201,62	212,37	223,45	234,98	247,20	260,44	275,40	293,62	320,49	571,69	626,58
5 [Nl/h/gcat]	201,38	212,01	222,92	234,19	246,01	258,62	272,47	288,43	308,68	343,69	614,80
6 [Nl/h/gcat]	201,20	211,75	222,53	233,63	245,17	257,36	270,52	285,23	302,74	326,77	606,53
7 [Nl/h/gcat]	201,07	211,56	222,24	233,20	244,55	256,44	269,13	283,04	299,00	319,02	351,13
8 [Nl/h/gcat]	200,96	211,40	222,02	232,87	244,07	255,73	268,08	281,43	296,39	314,27	338,77
9 [Nl/h/gcat]	200,88	211,28	221,83	232,61	243,68	255,17	267,26	280,20	294,46	310,97	331,95
10 [Nl/h/gcat]	200,81	211,17	221,68	232,39	243,37	254,72	266,59	279,22	292,96	308,52	327,43

Table 4.7. Maximum temperature of catalyst assessed in center line in a single 2D reactor model.

To give an overview on the performances obtainable at different conditions the analysis of CO_2 conversion and center line temperature profile along the axial coordinate of the reactor is reported in Figure 4.5. The analysis, in particular, has been conducted for each temperature [230:10:290]°C considered valid from an operative point of view being able to obtain conversions higher than 95%.

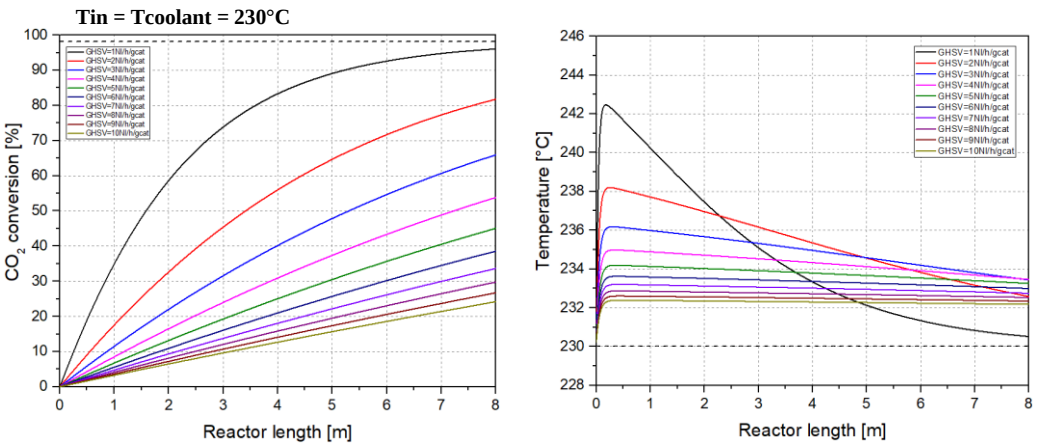

Tin = Tcoolant = 240°C

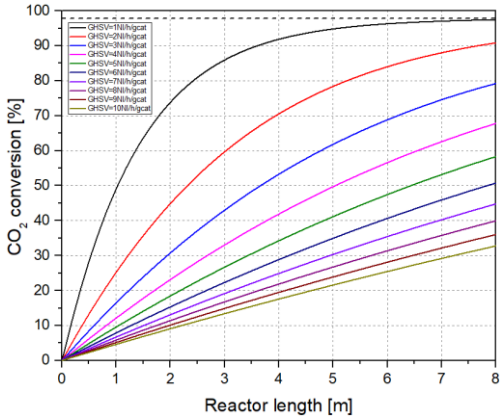

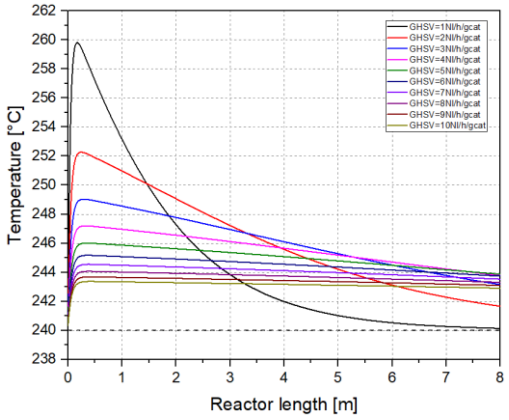

Tin = Tcoolant = 250°C

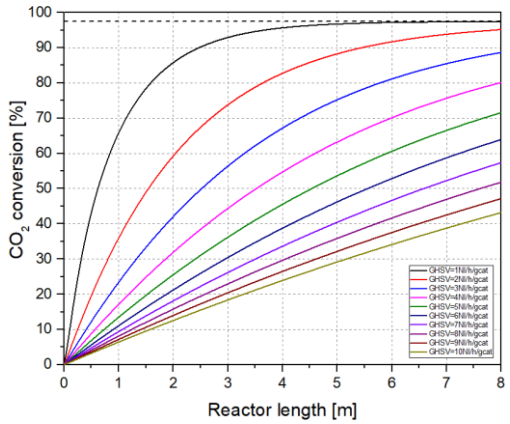

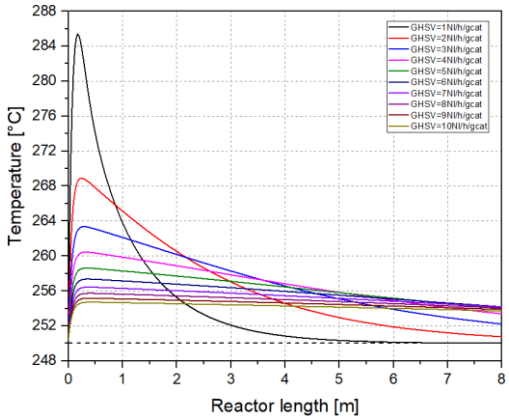

Tin = Tcoolant = 260°C

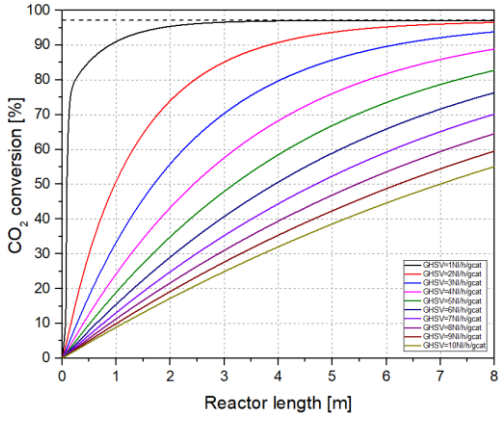

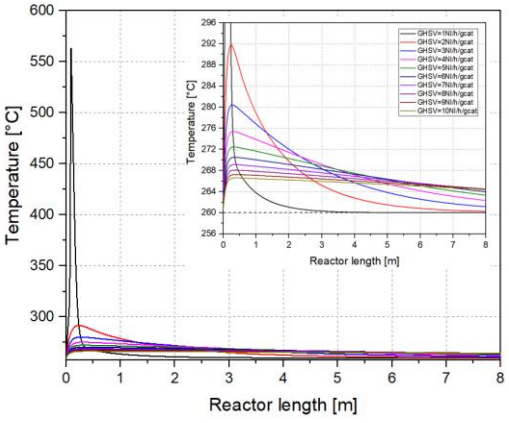

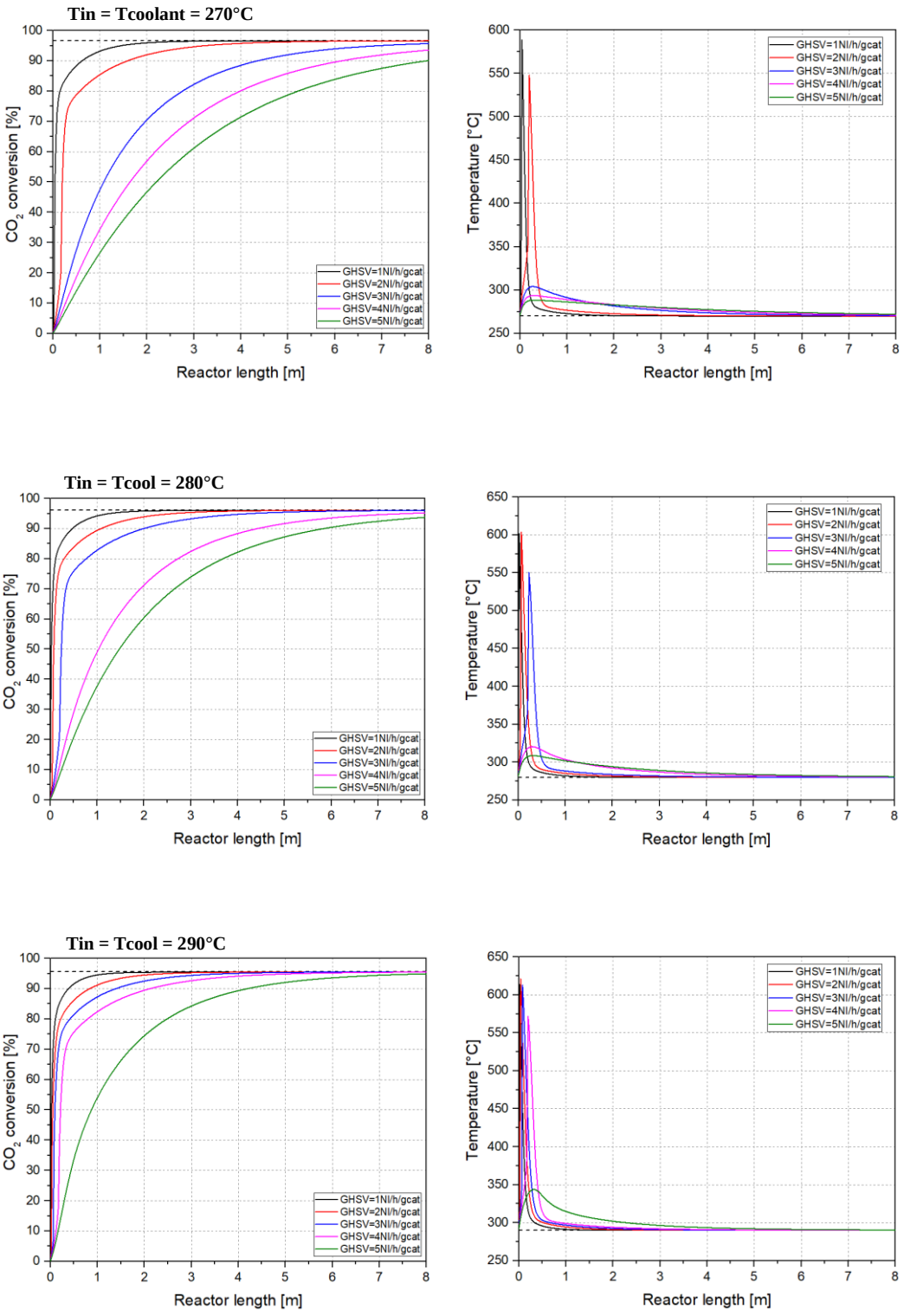

Figure 4.5. CO_2 conversion and center line temperature profile as function of reactor length for each temperature [230:10:290]°C at different GHSV=[1:1:10] Nl/h/gcat.

In the plots of Figure 4.5. from $T_{in}=T_{coolant}=270°C$ it was deemed necessary to report GHSV in the range [1:1:5] NL/g/g_{cat}. Starting from a higher thermal level, the reaction proceeds faster and the temperature profile is more pronounced. The plot at 260°C justifies this choice. The gas hourly space velocities higher than 6 NL/h/g_{cat} are discarded in order to better identify the discontinuity of the T_{max} parameter. In this way it is possible to evaluate at which inlet flow rates operate avoiding conditions that involve high hotspots and therefore thermal instability. For instance, at inlet temperature equal to 290°C, as the coolant one, moving from 5 to 4 NL/h/gcat a jump in maximum temperature achievable is present. This could not be noticed by evaluating the reactor in isothermal conditions however it is an important factor that need to be taken into consideration.

Looking at the case of 240°C, it is possible to observe an equilibrium condition only by operating with an inlet space velocity of 1 NL/h/g_{cat}. Through these additional plots (Figure 4.5.), it is also possible to notice the strict correlation between the conversion and the temperature profiles. At 1 NL/h/g_{cat} the conversion curve along the catalytic bed shows in the second half of the reactor a minimum variation of compound compositions. This translates into the possibility of reaching a temperature at the exit of the reactor equal to the coolant one. Indeed, it was expected that the heat released by the reaction was greater than the removed one until the thermodynamic limit was approached and then the temperature profile begun to fall. The kinetically controlled exothermic reactions, such as the CO_2 methanation process, require high temperatures in the initial phase to promote the kinetics and lower ones to acquire conditions very close to equilibrium favouring the thermodynamics. At 1 NL/h/g_{cat} the temperature profile seems to simulate correctly the desired behaviour. The conversion growth along the catalytic bed appears different for the others space velocities. In particular, the slope remains almost constant within the curve at a GHSV=10 NL/h/g_{cat}. The values remain moreover very low, far from the equilibrium ones. The heat of reaction remains almost constant and with a low absolute value. In this way it can be easily equated by the heat removed and thus no particular temperature hotspots are evident, rather the profile remains flat. Actually, at the begin, there is no presence of the driving force able to remove the heat released due to the CO_2 conversion

that, although very low, proceeds. Therefore, an initial increment of temperature inside the reactor is displayed. After some centimeters however the ΔT increases, enhancing the heat transfer. Soon the heat released becomes compensated by the heat removed. However, since the reaction is not complete and continue to proceed, the final temperature can even not stabilize at 240°C remaining some degrees above this value.

Evaluating both the mass and heat performances assessed through simulations, good results are obtained working at 240°C at 1 Nl/h/g_{cat}. Moreover, the temperature is maintained at reasonable values never overcoming ΔT=20°C.

Once a sufficiently performing condition has been identified, it was deemed necessary to determine whether it would be possible to increase the diameter of the tube. On one side smaller tube diameters allow to minimize radial temperature gradients but on the other by-pass phenomenon may increase. Simulations to study the effect of tube diameter are thus executed varying it in the range of [1:0.1:2] cm. The reference case coincides with an isobaric and non-isothermal single reactor working at 1 Nl/h/g_{cat} and T_{in}=$T_{coolant}$=240°C.

Performances	**1cm**	**1.1cm**	**1.2cm**	**1.3cm**	**1.4cm**	**1.5cm**	**1.6cm**	**1.7cm**	**1.8cm**	**1.9cm**	**2cm**
convCO_2[%]	97,433	97,475	97,522	97,792	97,747	97,696	97,658	97,636	97,588	97,568	97,549
PuCH_4[%]	88,344	88,511	88,696	89,648	89,767	89,799	89,820	89,834	89,849	89,858	89,865
prod.[mol/s]	0,0016	0,0019	0,0023	0,0027	0,0031	0,0036	0,0041	0,0046	0,0052	0,0058	0,0064
Tmax[°C]	259,82	265,41	274,25	492,86	583,92	602,95	612,83	614,26	627,88	629,66	631,10
real/eq.conv.	1,00	1,00	1,00	1,00	1,00	1,00	1,00	1,00	1,00	1,00	1,00

Table 4.8. Performances of 2D single reactor model varying the tube diameter.

From the Table 4.8., it can be seen that the conversion always remains around the same value of 97.5% as well as the CH_4 purity parameter. Varying the cross section does not influence the material performances and the approach to the equilibrium conditions is assessed in all cases. However, the productivity increases with an enlargement of the tube dimensions because the inlet flow rate becomes higher in order to maintain always a GHSV=1 NL/h/g_{cat}. From a thermal point of view, the most important parameter to analyze

remains the maximum temperature reached by the catalyst. For the same reasons previously described, it is necessary that the temperature stays below 500°C. A diameter over 1.4 cm is therefore not suitable for conducting the CO_2 methanation reaction in these conditions. The simulation performed with a reactor configuration of tube diameter equal to 1.3 cm, however, presents a temperature profile at centerline with a hotspot higher than 250°C. It is obviously a condition not stable to operate the reaction. Generally, indeed, the industrial ΔT reputed effective does not overcome 50°C.

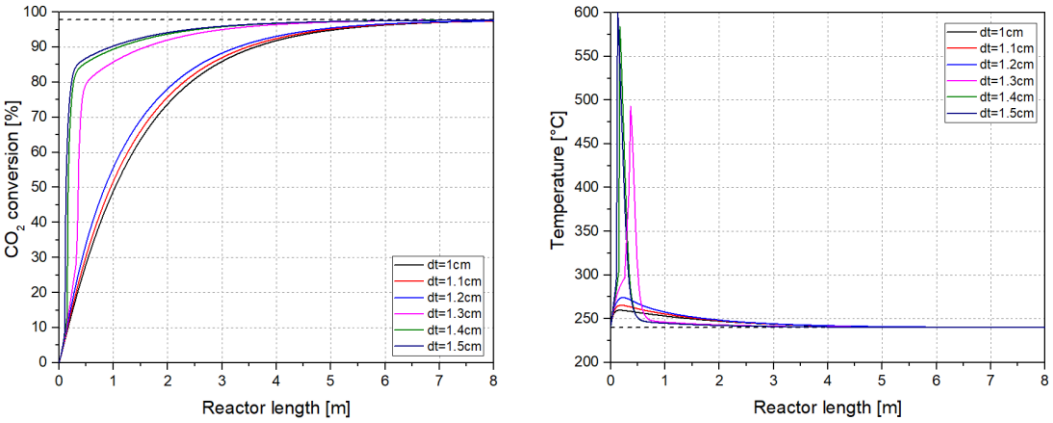

Figure 4.6. CO_2 conversion and center line temperature profile varying the tube diameter od a 2D single reactor model.

In Figure 4.6. plots depict the effect of the tube diameter, investigating it from 1 cm to 1.5 cm. The scale down of the range allows to better visualize all the different curves. In any case, the detachment of performance moving from 1.2 cm and 1.3 cm is reported. Also considering the extreme case of tube diameter equal to 1.5 cm, at least 6 meters of reactor length are necessary to achieve the equilibrium conversion value. Indeed, at tube diameters higher than 1.3 cm the 80% of CO_2 conversion is completed within the first meter then the reaction slows down becoming relevant the inverse reaction. To get the equilibrium conversion value, a high contact time is in any case necessary and for this reason it is not worth operating with high ΔT of hotspot.

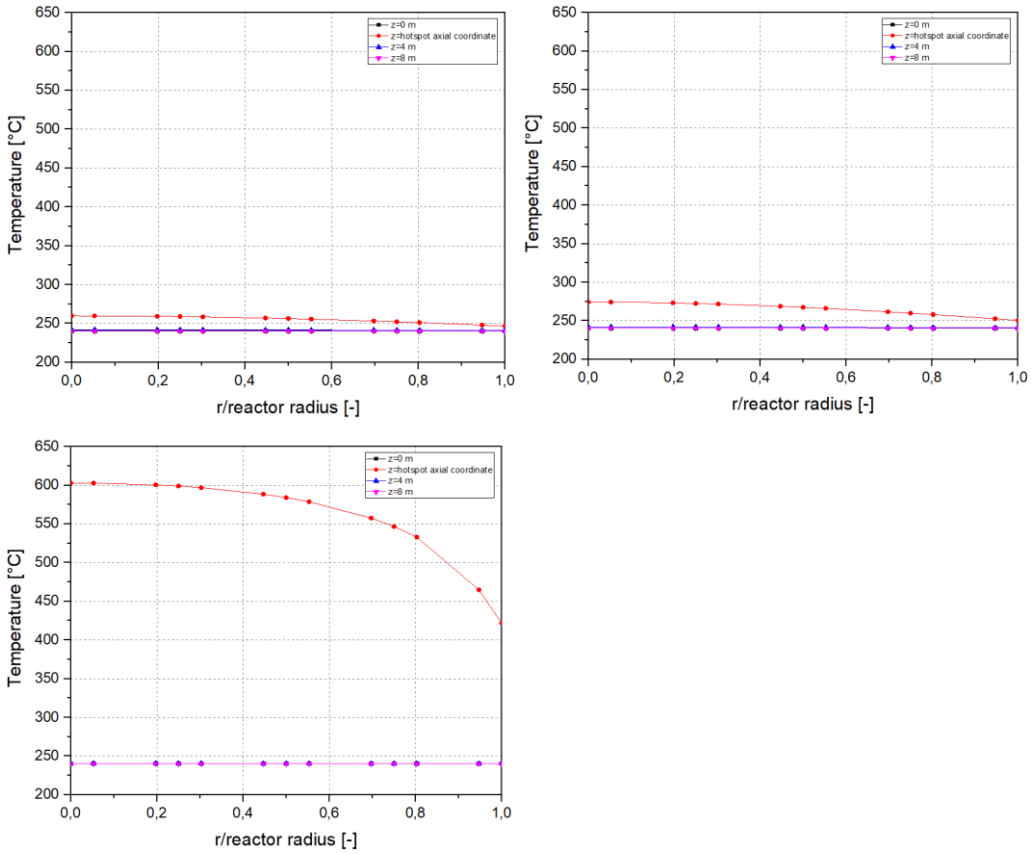

Figure 4.7. Radial temperature profile at different axial positions (z = 0 m, z = hotspot point, z = 4 m, z = 8 m) for tube with diameter d=1, 1.2, 1.5 cm.

Figure 4.6 coupled with Figure 4.7 proved the adequacy of the starting assumption of minimizing the thermal limitations by reducing the diameter of the tube. Evaluating the variation of temperature along the radial coordinate a $\Delta T=200°C$ is present for the configuration with tube radius equal to 1.5 cm. The analysis made possible to evaluate the permissible tube dimensions in the process conditions taken as a reference. Therefore, it is highlighted the possibility to work with a tube diameter of 1.2 cm. A possible alternative, which should not be completely discarded, could be working with a first reactor at 80% conversion even with a diameter of 1.2 cm and 2 meters of length. In this case, however, a series configuration will still be required.

4.3. Effect of intraporous diffusion limitations on process temperature

Going forward the analysis of the 2D isobaric and non-isothermal reactor, the intraporous diffusive limitations are now introduced. The 1D pseudo-homogeneous pellet model is considered only isobaric thus coupled mass and heat balances for reactor and pellet will be solved. In this way, it is also possible to assess how much the intraporous diffusive limitations can influence the thermal profile. It is expected a damp due to the greater importance of the limiting contribution of diffusion which therefore coincides with a decrease in the reaction speed.

The simulation is conducted at $T_{in}=T_{coolant}=240°C$ with an inlet space velocity equal to 1 $NL/h/g_{cat}$ while the individual reactor is configured as described at the beginning of Section 4.2. An added information that now need to be specified as input is the pore radius, imposed equal to 5 nm for 5%wt.Ru/γ-Al_2O_3 catalyst. The results display a CO_2 conversion of 97% and a CH_4 purity of 86.5%. The profiles of conversion and center line temperature along the axial coordinate, compared to the one obtained without accounting for the concentration gradient inside the pellet, show curves similar in Figure 4.8. However, in the first meter the solid temperature results less accentuated but this is strictly correlated to the higher ΔC_i of reagents present in the pellet at the beginning. Being the hydrogen and carbon dioxide diffusion limited in the first centimeters of the reactor length the reaction rate turns out to be less fast. Looking at the kinetic expression Lunde and Kester it can be noticed also the double effects of damping the reaction speed. At the same constant diffusion rate the effect is more relevant in the center of the pellet where the concentration deficit of the reagents is also coupled to an accumulation of products compared to the bulk phase. By evaluating a posteriori the diffusivity coefficients it is noticed that the limitations related to the Knudsen domain are the most relevant ones. In particular the different order of magnitude is:

$$D_{mix,i} \cong 10^{-4}\ m^2/s$$

$$D_{K,i} \cong 10^{-6}\ m^2/s$$

This is in accordance with the expectations since pore radius is very small and pressure low.

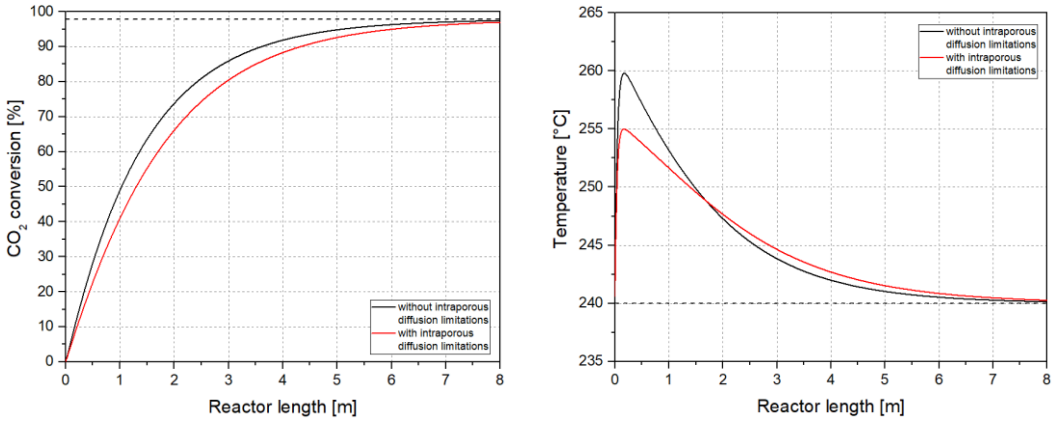

Figure 4.8. CO_2 conversion and center line temperature profile taking into account intraporous diffusion limitations.

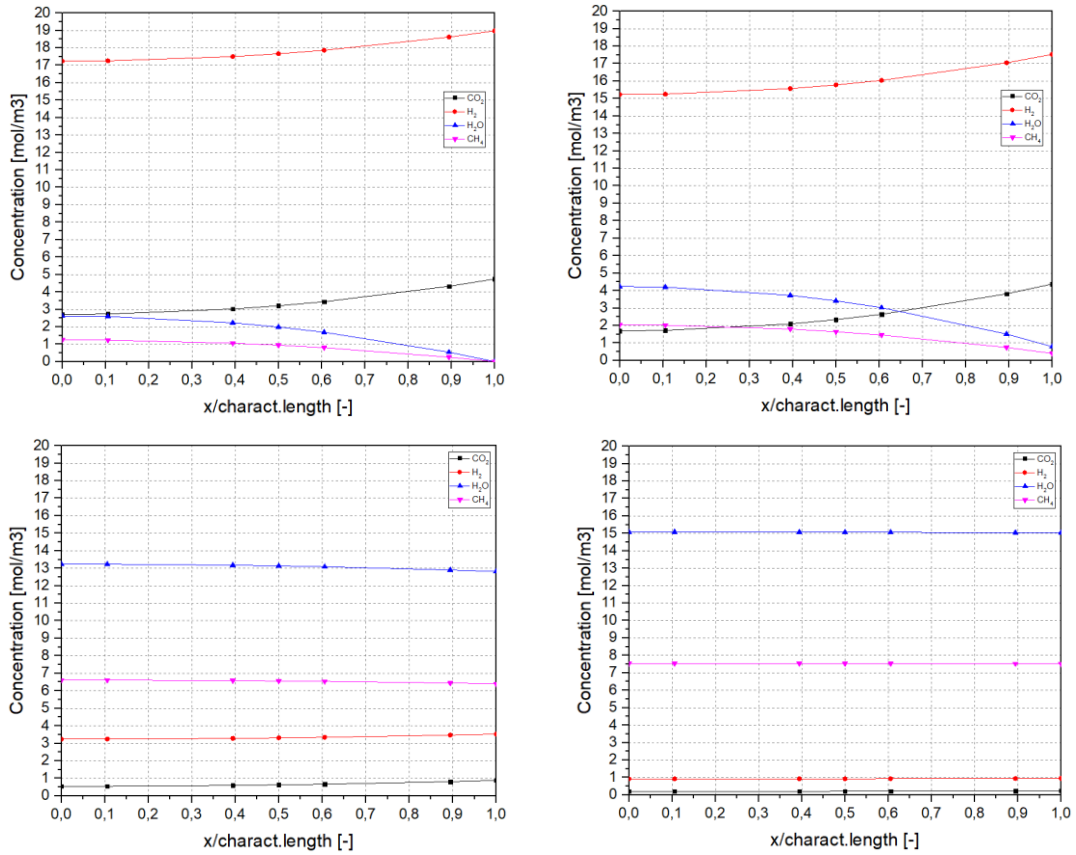

Figure 4.9. Concentration profiles along pellet coordinate in the center of the tube (r = 0) at different axial positions (z = 0 m, z = 0.17 m, z = 4 m, z = 8 m).

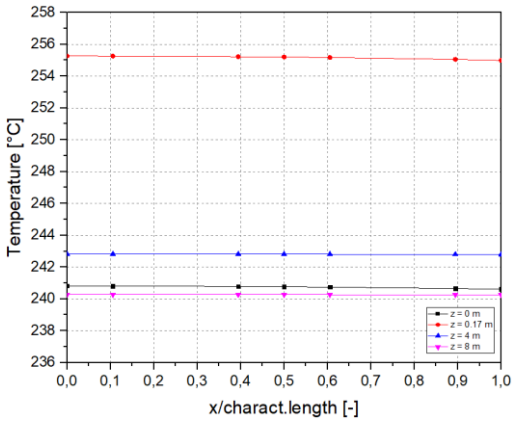

Figure 4.10. Temperature profile along pellet coordinate in the center of the tube (r = 0) at different axial positions (z = 0 m, z = 0.17 m, z = 4 m, z = 8 m).

Figure 4.10. is added to show the temperature profile along the pellet coordinate that is almost flat in any different position of reactor length: only in the hotspot (L=0.17m) axial point a ΔT=0.3°C is noticed. It is therefore absolutely allowed to assume the pellet as isothermal. So far it has been established that it is not possible to use a tube diameter higher than 1.2 cm under these conditions to obtain an acceptable thermal trend. However, considering also the intraporous diffusive limitations these profiles are slightly damped. Qualitatively it is possible to state that this phenomenon could allow to work with tubes of higher diameter even if a maximum limit will still be present.

4.4. Effect of pore radius on thermal and material performances

In Section 4.3 present above, it has been shown the possibility of exploiting the diffusive limitations to have a larger tube diameter, closer to an industrial standard configuration. However, this solution actually coincides with a less exploitation of the catalytic performance because a greater amount of catalyst need to be inserted in the reactor to achieve equal productivity. A further analysis is therefore conducted to establish how the catalyst must be morphologically structured to minimize the intraporous diffusive limitations, although this for the moment involves smaller tube diameters for greater thermal management. In the model is thus set a pore radius equal to 20 nm.

The following analysis investigate the importance of pore radius on the performances of CO_2 conversion and CH_4 purity since it is a variable present in the Knudsen diffusivity coefficients.

Perfomances	**without intraporous limitations**	**with intraporous diffusion limitations**	
		rp=20nm	**rp=5nm**
conv.CO_2[%]	97,433	97,328	96,958
PuCH_4[%]	88,344	87,916	86,432
Tmax[°C]	259,82	258,16	254,91

Table 4.9. Comparison of CO_2 conversion, CH_4 purity and maximum temperature taking into account intraporous diffusion limitations within pellet of pore radius=5nm or pore radius=20nm.

In Figure 4.12. a graphic representation of the change in concentration along the coordinate of the pellet is therefore reported also for the condition in which the support has a pore radius of 20 nm. The maximum value of CO_2 conversion reached is 97.33% while the purity is 87.9%. Considering the pore radius equal to 20 nm the CO_2 conversion and the temperature profiles along the reactor axial coordinate are almost equal to those that not take into account the diffusion limitations. This means that the negative contribution of intraporous gradients is almost negligible in these conditions.

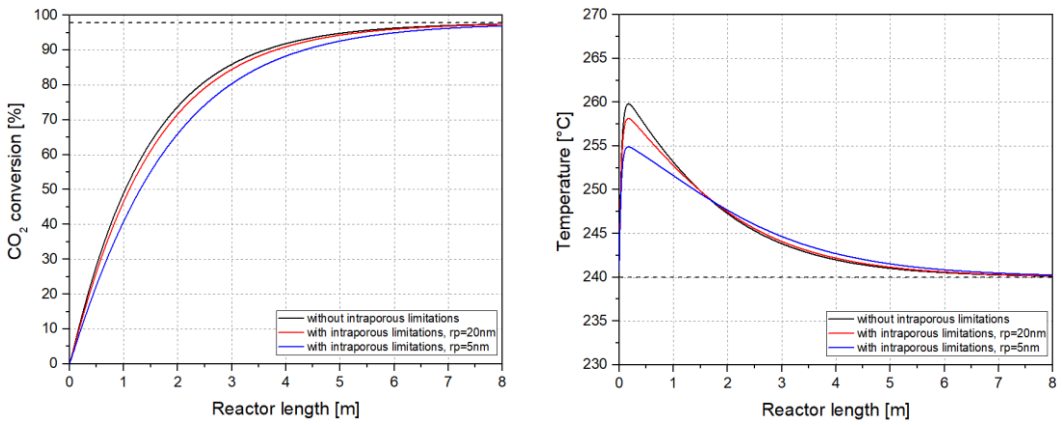

Figure 4.11. Comparison of CO_2 conversion and center line temperature profile taking into account intraporous diffusion limitations within pellet of pore radius=5nm or pore radius=20nm.

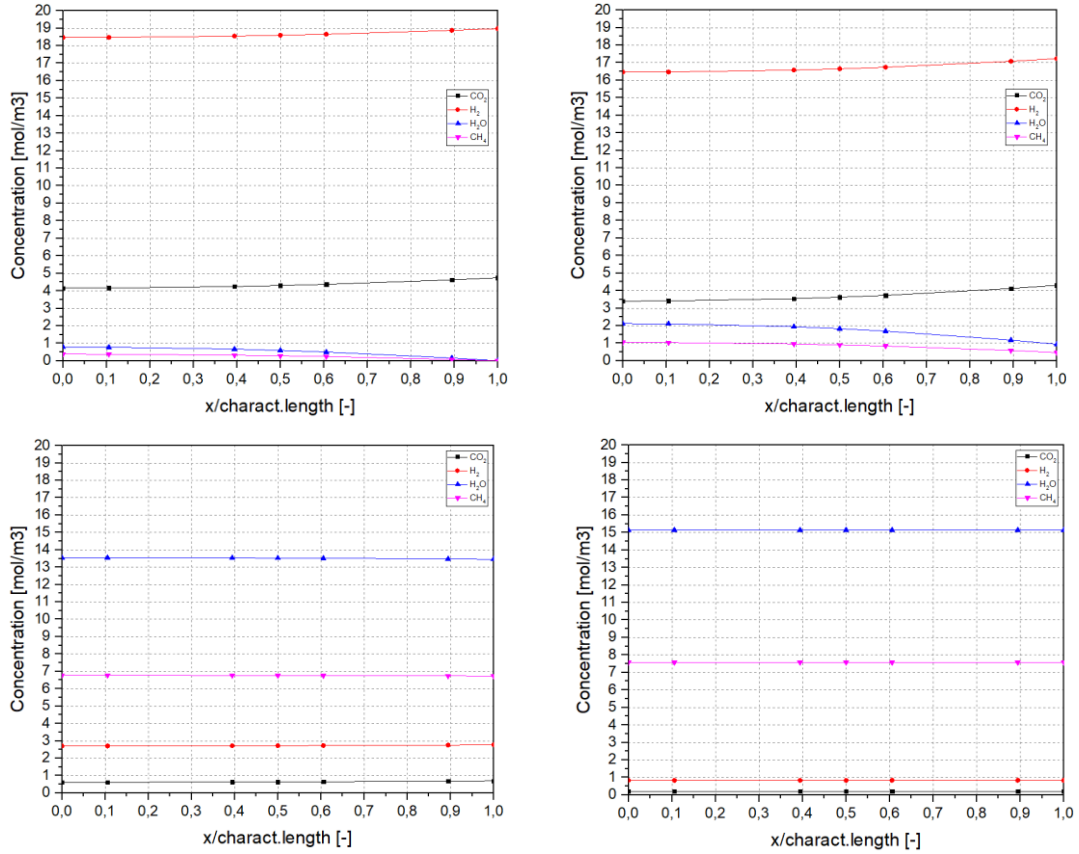

Figure 4.12. Concentration profiles along pellet coordinate in the center of the tube (r = 0) at different axial positions (z = 0 m, z = 0.17 m, z = 4 m, z = 8 m). Pore radius=20nm.

4.5. Simulation of the optimized configuration

Taking into account what has been presented in this work, it is useful also to simulate the configuration of two reactors in series with intermediate flash. The information that this type of analysis can give is the verification of which process conditions can be maintained valid evaluating the scheme also from the thermal point of view. The ideal process configuration identified in Section 3. is therefore considered. In addition, the operative effects that can influence the performances in terms of CO_2 conversion and CH_4 purity are analyzed.

4.5.1. First reactor performances

The first reactor operates in isobaric conditions at 1 GHSV Nl/h/g_{cat}, H_2/CO_2=4, P=1 atm and T_{in}=$T_{coolant}$=240°C. The intraporous diffusion limitations are still kept at zero. The obtainable performances are already described in detail in Section 4.2. but in Table 4.10. and in Figure 4.13. are ported again all the information necessary to frame the results of the reference case considered.

conv.CO_2[%]	97,433
PuCH_4[%]	88,344
Tmax[°C]	259,82

Table 4.10. Summary table of perfomances in single 2D reactor model.

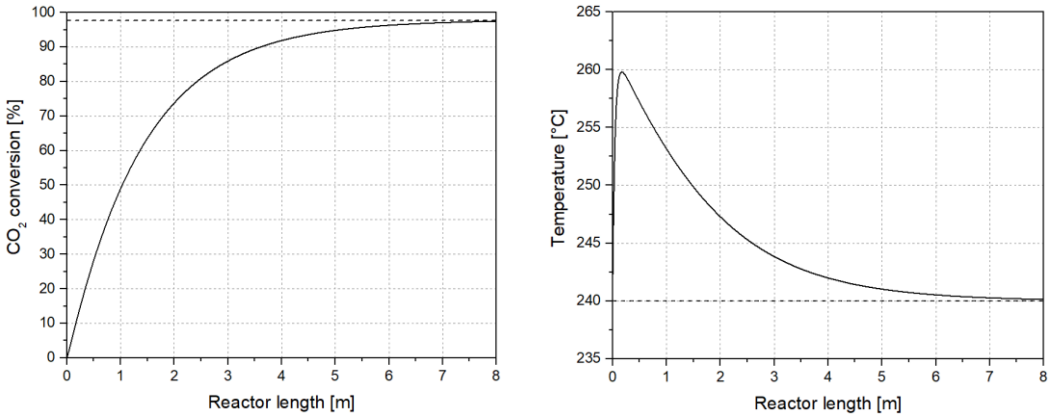

Figure 4.13. CO2 conversion and center line temperature profile of a 2D single reactor model.

4.5.2. Intermediate flash

The flowrates resulted from the first reactor are inserted within a water condenser working at atmospheric pressure and temperature equal to 1°C. To execute the phase equilibrium calculations Aspen Plus® V10 is used, exploiting the EoS Peng-Robinson. The vapour stream coincides with inlet conditions of second reactor.

flash performances					
F [mol/s]	0,00499	**V [mol/s]**	0,00181	**L [mol/s]**	0,00318
xCO_2_in	8,41E-03	**xCO_2_V**	2,32E-02	**xCO_2_L**	0,00E+00
xH_2_in	3,37E-02	**xH_2_V**	9,28E-02	**xH_2_L**	0,00E+00
xH_2O_in	6,39E-01	**xH_2O_V**	5,01E-03	**xH_2O_L**	1,00E+00
xCH_4_in	3,19E-01	**xCH_4_V**	8,79E-01	**xCH_4_L**	0,00E+00

Table 4.11. Performances of the intermediate flash.

4.5.3. Second reactor performances

Properties of reactor and pellet design of the model in gPROMS ModelBuilder® V5.0.2 is maintained equal to the first reactor configuration, reported in Section 4.2. What change in the second reactor is the investigated temperature range of $T_{in}=T_{coolant}=[150:10:240]°C$.

Performances	**150°C**	**160°C**	**170°C**	**180°C**	**190°C**	**200°C**	**210°C**	**220°C**	**230°C**	**240°C**
$convCO_2$ 2°reactor[%]	37,910	52,670	67,915	80,756	88,870	92,218	92,218	91,077	89,534	87,778
real/eq.conv. 2°reactor	0,39	0,54	0,71	0,85	0,94	0,99	1,00	1,00	1,00	1,00
Tmax 2°reactor[°C]	150,09	160,14	170,21	180,31	190,45	200,64	210,89	221,23	231,66	242,20

Table 4.12. Performances of second reactor in a series of 2D reactor models with intermediate flash.

The material performances assessed from the simulations highlight that high values of conversion within the second reactor can be obtained working at temperature equal to 210°C. In the second reactor can thus be achieved a CO_2 conversion per passage higher than 90%, approaching the thermodynamic equilibrium line at temperature relatively low. This consideration is also depicted in the Figure 4.14., where the conversion and center line temperature profile are shown.

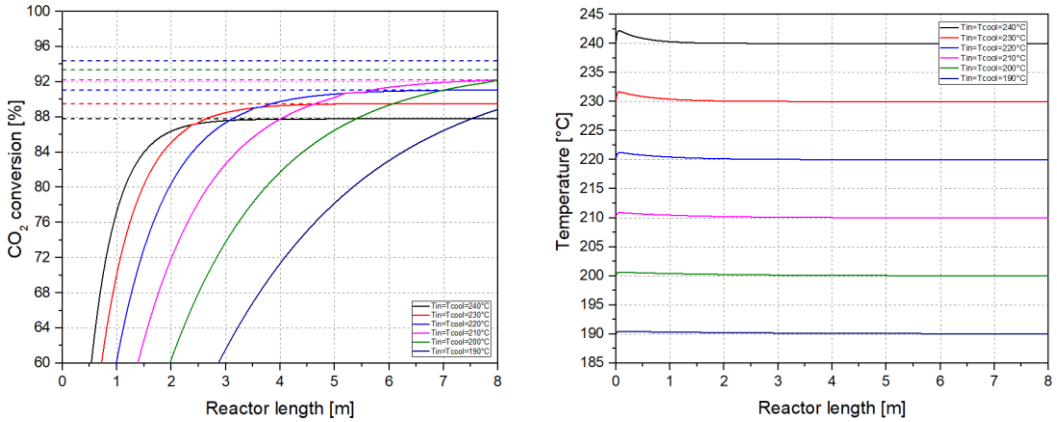

Figure 4.14. CO_2 conversion and center line temperature profile varying the temperature of second reactor.

The analysis of the thermal behaviour, as expected, does not give relevant added information. The major conversion of carbon dioxide is indeed obtained in the first reactor. The second one works with a very low inlet flow rate and already with a high inlet composition of methane. This means that the heat released does not contribute significantly in the temperature profile along the reactor coordinate. The refrigerant effect performed by the cooling medium, is thus higher and for this reason the profile is flat for each investigated temperature. In particular, the range analyzed is [190:10:240] °C since at these temperatures is achieved a 85%, or higher values, of CO_2 conversion.

4.5.4. Overall performance

After having considered all the equipment performance alone, it is possible to analyze the overall process scheme, valuing CO_2 conversion and CH_4 purity that can be reached.

Performances	**150°C**	**160°C**	**170°C**	**180°C**	**190°C**	**200°C**	**210°C**	**220°C**	**230°C**	**240°C**
convCO_2 [%]	93,614	95,132	96,700	98,021	98,855	99,800	99,800	99,771	99,731	99,686
real/eq.conv.	0,94	0,95	0,97	0,98	0,99	1,00	1,00	1,00	1,00	1,00
PuCH_4[%]	92,496	94,197	96,006	97,574	98,585	98,995	99,007	98,863	98,669	98,448
PuCH_4 without CO_2[%]	93,905	95,303	96,779	98,050	98,865	99,192	99,204	99,088	98,932	98,755

Table 4.13. Performances of a series of 2D reactor models with intermediate flash.

Evaluating the whole performances of the process scheme the total CO_2 conversion achieve a maximum value of 99.8% while the dry CH_4 purity a value of 99% working with the first reactor at 240°C and with the second one at 210°C. In the Table 4.13. it is also reported the dry CH_4 purity parameter that not consider the carbon dioxide molar fraction in the outlet stream. However, not a relevant improvement is assessed and this is due to the fact that a stoichiometric inlet ratio H_2/CO_2 was selected. The values reported in the Table 4.13. are also shown in the Figure 4.15. for a better comprehension of the obtained results.

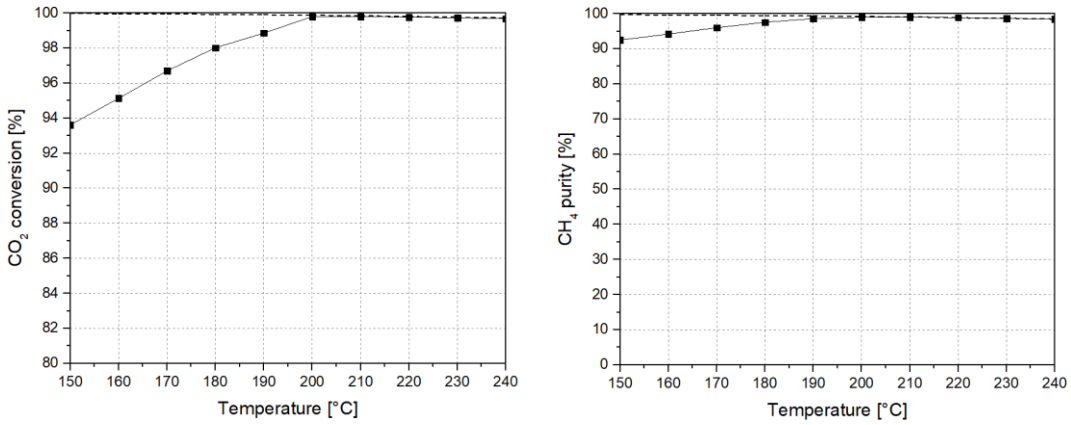

Figure 4.15. Performances of series of 2D reactor models with intermediate flash varying the temperature of second reactor.

4.5.5. Effect of flash operative conditions

After the analysis of the overall performance it was considered necessary to assess how the conditions of the water condenser are relevant in the acquisition of the results. The simulation is conducted as before with a first reactor working at 240°C but assuming a 100% ideal removal of water, thus the value of water molar fraction in the vapour stream from 5.01E-03 is imposed equal to 0.

Performances	150°C	160°C	170°C	180°C	190°C	200°C	210°C	220°C	230°C	240°C
conv.CO_2 2°reactor[%]	37,951	52,725	67,983	80,834	88,951	92,298	92,298	91,156	89,611	87,855
real/eq.conv. 2°reactor	0,39	0,54	0,70	0,84	0,94	0,98	1,00	1,00	1,00	1,00
PuCH_4[%]	92,496	94,197	96,007	97,574	98,586	98,995	99,007	98,863	98,669	98,448
PuCH_4 without CO_2[%]	93,903	95,301	96,778	98,048	98,863	99,190	99,202	99,086	98,930	98,752
Tmax 2°reactor[°C]	150,09	160,14	170,21	180,31	190,45	200,64	210,90	221,23	231,66	242,20
conv.CO_2 tot[%]	98,406	98,786	99,178	99,508	99,716	99,802	99,802	99,773	99,733	99,688
real/eq.conv.CO_2 tot	0,98	0,99	0,99	1,00	1,00	1,00	1,00	1,00	1,00	1,00

Table 4.14. Performances of a series of 2D reactor models with flash able to remove 100% water.

If the entire process scheme is subject to an intermediate total condensation of water actually no significance improvement on the performances could be assessed. This means that the determining conditions coincide in this case with the operative conditions of the two reactors. The water condenser operating at atmospheric pressure and temperature equal to 1 ºC is already sufficient for the purpose of the work.

4.5.6. Effect of pressure on the overall performance

In order to investigate possible improvements, the configuration of two reactors in series with intermediate condenser is also evaluated at higher pressure equal to 5 bar. An analysis in the temperature range of [150:10:230]°C and GHSV=[1:1:5]Nl/h/g_{cat} is thus performed to select the first reactor operative conditions.

convCO2[%]	150°C	160°C	170°C	180°C	190°C	200°C	210°C	220°C	230°C
1 [Nl/h/gcat]	46,043	65,342	83,462	94,640	98,714	99,218	99,100	98,965	98,799
2 [Nl/h/gcat]	25,086	38,297	55,409	74,025	88,888	96,539	99,118	99,025	98,875
3 [Nl/h/gcat]	17,089	26,570	39,799	56,628	74,636	88,885	96,327	99,006	98,910
4 [Nl/h/gcat]	12,931	20,256	30,770	44,973	62,199	79,278	91,377	97,152	98,891
5 [Nl/h/gcat]	10,391	16,336	24,989	37,014	52,515	69,902	85,096	94,272	98,874

PuCH4[%]	150°C	160°C	170°C	180°C	190°C	200°C	210°C	220°C	230°C
1 [Nl/h/gcat]	14,579	27,382	50,231	77,925	93,867	97,121	96,611	95,996	95,294
2 [Nl/h/gcat]	6,277	11,043	19,905	36,305	61,533	84,788	96,387	95,978	95,306
3 [Nl/h/gcat]	3,959	6,748	11,678	20,706	37,048	61,526	83,978	95,677	95,312
4 [Nl/h/gcat]	2,885	4,835	8,164	14,049	24,761	43,347	67,940	87,203	95,048
5 [Nl/h/gcat]	2,267	3,758	6,247	10,517	18,112	31,717	53,312	76,693	94,964

Tmax[°C]	150°C	160°C	170°C	180°C	190°C	200°C	210°C	220°C	230°C
1 [Nl/h/gcat]	152,20	163,61	175,95	190,05	208,54	664,73	668,44	672,16	675,91
2 [Nl/h/gcat]	151,54	162,50	174,04	186,55	200,91	219,74	689,93	693,53	697,15
3 [Nl/h/gcat]	151,20	161,93	173,09	184,92	197,92	213,20	234,78	697,68	704,72
4 [Nl/h/gcat]	150,99	161,58	172,51	183,96	196,27	210,10	227,16	257,41	708,74
5 [Nl/h/gcat]	150,84	161,34	172,12	183,33	195,21	208,23	223,42	244,15	711,28

real/eq.conv	150°C	160°C	170°C	180°C	190°C	200°C	210°C	220°C	230°C
1 [Nl/h/gcat]	0,46	0,66	0,84	0,95	0,99	1,00	1,00	1,00	1,00
2 [Nl/h/gcat]	0,25	0,38	0,56	0,74	0,89	0,97	1,00	1,00	1,00
3 [Nl/h/gcat]	0,17	0,27	0,40	0,57	0,75	0,89	0,97	1,00	1,00
4 [Nl/h/gcat]	0,13	0,20	0,31	0,45	0,62	0,80	0,92	0,98	1,00
5 [Nl/h/gcat]	0,10	0,16	0,25	0,37	0,53	0,70	0,86	0,95	1,00

Table 4.15. CO_2 conversion, CH_4 purity, maximum temperature and CO_2 conversion reached respect to the equilibrium one at pressure of 5 bar.

Working at 1 Nl/h/g_{cat} and T=190°C in the first reactor seems to be a valid option at least to identify if significant improvements of CH_4 purity and CO_2 conversion are obtainable. Thus the outlet stream of the first reactor, operated in this reference condition, is inserted within the phase equilibrium equipment that works in the same way at 5 bar.

flash performances					
F [mol/s]	0,00495	**V [mol/s]**	0,00172	**L [mol/s]**	0,00323
xCO_2_in	4,48E-03	**xCO_2_V**	1,15E-02	**xCO_2_L**	0,00E+00
xH_2_in	1,80E-02	**xH_2_V**	5,17E-02	**xH_2_L**	0,00E+00
xH_2O_in	6,52E-01	**xH_2O_V**	1,07E-03	**xH_2O_L**	1,00E+00
xCH_4_in	3,26E-01	**xCH_4_V**	9,36E-01	**xCH_4_L**	0,00E+00

Table 4.16. Performances of the intermediate flash at 5 bar.

The vapour stream of the flash enters in the second reactor. The temperature range investigated is $T_{in}=T_{coolant}$=[140:10:190]°C.

Performances	140°C	150°C	160°C	170°C	180°C	190°C
conv.CO_2 2°reactor[%]	85,079	98,529	99,982	99,982	99,972	99,972
real/eq.conv. 2°reactor	0,85	0,99	1,00	1,00	1,00	1,00
Tmax 2°reactor[°C]	140,15	150,23	160,36	170,54	180,79	191,12

Table 4.17. Performances of second reactor in a series of 2D reactor models with flash at 5bar.

Performances	140°C	150°C	160°C	170°C	180°C	190°C
PuCH_4[%]	98,5123	99,2946	99,4014	99,3965	99,3963	99,3960
PuCH_4 without CO_2[%]	98,689	99,312	99,402	99,397	99,397	99,397
conv.CO_2 tot[%]	99,8195	99,9822	99,9998	99,9998	99,9997	99,9997
real/eq.conv.CO_2 tot	0,998	1,000	1,000	1,000	1,000	1,000

Table 4.18. Overall performances of a series of 2D reactor models with flash at 5bar.

It is necessary to point out that in the Table 4.18. some data are reported with more decimals than necessary only to highlight the correct trend of purity and clearly show the maximum value achievable. A trend almost flat after the achieving of equilibrium conditions is in accordance with what expected. Moreover, at the end the conversion of carbon dioxide goes almost to completion thus the value of methane purity that accounts of a complete removal of CO_2 outlet stream does not have any relevant significance. The best operative conditions at 5 bar coincides with gas inlet space velocity equal to 1 Nl/h/g_{cat} in the first reactor that works at T=190°C while the second reactor operates at T=160°C. The temperatures at which it is possible to operate the two reactors at pressure equal to 5 bar are certainly lower than the ones assessed in the same configuration at atmospheric pressure. The temperature of the second reactor is indeed a compromise to reach the conditions of thermodynamic equilibrium without affecting too much the kinetics.

From a qualitative point of view, the performances remains similar to those obtained in Section 4.5.4. but the thermodynamic benefit that is obtained working at lower temperature is important since it is possible to obtain an overall CH_4 purity of 99.4%.

Section 5: Conclusions

The performances of the calcinated 5%wt.Ru/γ-Al_2O_3 catalyst, developed by the research group of Laboratory of Catalysis and Catalytic Processes of Politecnico di Milano, were investigated from the laboratory to the industrial scale.

The process simulator Aspen Plus® V10 was used firstly to achieve a kinetic model validation through the comparison with experimental data obtained in isothermal conditions. Therefore, it was exploited as suitable tool for extend the investigation of operativity. The evaluation of the performance in terms of CO_2 conversion and CH_4 purity in different configurations allowed to identify the most suitable process scheme in which conduct the analysis. The results, in particular, revealed the beneficial effect of working with multiple reactors in series with an intermediate water condenser. Regarding the catalyst, the first major advantage of its utilization lies into the possibility of selectively conducting the Sabatier reaction while the other one is certainly the high activity that allows to obtain purity of methane over 99%. Therefore, the catalyst was also tested in configurations already validated at pilot scale highlighting its adequacy on different CO_2 methanation processes. To increase the level of detail of the system analysis, a specific model constituted by a 2D heterogeneous packed bed reactor coupled with 1D pellet description was introduced. The simulations were thus conducted in gPROMS ModelBuilder® V5.0.2. Abandoning the assumption of operating in isothermal conditions, the first reactor turned out to be more critic from the thermal point of view. In this way it has been possible to identify adequate operative conditions without run into regions of thermal instability and to investigate possible improvements on the reactor and pellet

configuration. As conclusion of the work the overall process scheme were analyzed taking into account 2D isobaric and non-isothermal reactors with the purpose to establish if the configuration can be industrialized.

Content of methane in the outlet stream of the process configuration of two reactors in series with intermediate flash could achieve value over 98% even at atmospheric pressure, condition in which it was also proven that the kinetic model is validated. The results obtained are therefore in accordance with the restrictions in the production of SNG that require high CH_4 molar fraction. During the course of the development of the thesis it was considered useful to evaluate the maximum performance obtainable also by investigating higher pressure ranges. This has been done to provide a broader overview and set maximum limits of methane purity. Colleagues that works in the laboratory are currently exploring the capabilities of the intermediate condensing system at higher GHSV values with a double ruthenium catalyst bed operating the test rig up to 10 bar. The kinetic parameters implemented within the model will be then updated using larger dataset obtainable by studying the system under pressure. Regarding the modelling of the reactor, in the future, pressure drops will be considered and the possible external diffusive phenomena, which could occur at low spatial velocities, will be assessed. The perspective then coincides with the assessment of an intensified reactor configuration to improve the heat exchange.

Appendix

Data elaboration was executed by colleagues at Laboratory of Catalysis and Catalytic Processes of Politecnico di Milano during research activities on 5wt.% Ru/γ-Al_2O_3 catalyst. For the sake of clarity about this work, the experimental values used in the simulations are reported below.

test # 138						
P [atm]	T [°C]	H_2/CO_2 [-]	GHSV [NL/h/gcat]	y inert [%]	CO_2 conversion [%]	CH_4 purity [%]
1	150	3,94	0,25	2,05	36,98	9,85
1	200	3,94	0,25	2,05	94,44	88,17
1	250	3,94	0,25	2,05	94,74	89,49
1	310	3,94	0,25	2,05	91,56	79,40
1	150	3,94	0,5	2,05	16,86	3,69
1	200	3,94	0,5	2,05	87,64	65,89
1	250	3,94	0,5	2,05	94,77	89,33
1	310	3,94	0,5	2,05	91,81	78,95
1	150	3,94	1	2,05	8,24	1,67
1	200	3,94	1	2,05	60,47	24,77
1	250	3,94	1	2,05	94,87	89,09
1	310	3,94	1	2,05	92,07	79,44
1	200	3,94	5	2,05	15,67	3,61
1	250	3,94	5	2,05	62,60	26,52
1	310	3,94	5	2,05	92,57	81,5
1	350	3,94	5	2,05	90,97	75,42
1	250	3,94	50	2,05	7,77	1,62
1	270	3,94	50	2,05	14,53	3,16
1	290	3,94	50	2,05	24,72	5,84
1	310	3,94	50	2,05	38,73	10,79
1	330	3,94	50	2,05	55,62	20,02
1	350	3,94	50	2,05	70,96	34,25
1	370	3,94	50	2,05	80,79	48,89
1	390	3,94	50	2,05	83,22	53,51
1	410	3,94	50	2,05	82,37	51,67
1	430	3,94	50	2,05	80,23	47,09

test # 143							
P [atm]	T_{R1} [°C]	T_{R2} [°C]	H_2/CO_2 [-]	GHSV [NL/h/gcat]	y inert [%]	CO_2 conversion [%]	CH_4 purity [%]
1	250	100	3,94	0,25	2,05	98,36	96,92
1	250	125	3,94	0,25	2,05	98,10	96,92
1	250	150	3,94	0,25	2,05	98,19	97,19
1	250	175	3,94	0,25	2,05	98,26	97,99
1	250	200	3,94	0,25	2,05	98,06	96,84
1	310	100	3,94	0,25	2,05	95,28	87,09
1	310	125	3,94	0,25	2,05	97,13	88,98
1	310	150	3,94	0,25	2,05	98,42	93,36
1	310	175	3,94	0,25	2,05	98,35	95,84
1	310	200	3,94	0,25	2,05	97,95	96,24
1	250	100	3,94	0,5	2,05	97,35	93,02
1	250	125	3,94	0,5	2,05	97,70	94,78
1	250	150	3,94	0,5	2,05	98,14	96,75
1	250	175	3,94	0,5	2,05	98,15	96,45
1	250	200	3,94	0,5	2,05	98,19	96,37
1	310	100	3,94	0,5	2,05	94,94	84,62
1	310	125	3,94	0,5	2,05	95,35	86,49
1	310	150	3,94	0,5	2,05	96,91	91,42
1	310	175	3,94	0,5	2,05	97,77	95,27
1	310	200	3,94	0,5	2,05	98,15	96,50
1	250	100	3,94	1	2,05	96,27	89,20
1	250	125	3,94	1	2,05	96,64	90,97
1	250	150	3,94	1	2,05	97,46	92,93
1	250	175	3,94	1	2,05	97,69	94,90
1	250	200	3,94	1	2,05	97,97	95,58
1	310	100	3,94	1	2,05	94,44	83,09
1	310	125	3,94	1	2,05	95,33	85,95
1	310	150	3,94	1	2,05	96,42	90,37
1	310	175	3,94	1	2,05	97,47	94,85
1	310	200	3,94	1	2,05	97,58	94,60

test # 149								
P [atm]	T_{flash} [°C]	T_{R1} [°C]	T_{R2} [°C]	H_2/CO_2 [-]	GHSV [NL/h/gcat]	y inert [%]	CO_2 conversion [%]	CH_4 purity [%]
1	10	250	150	3,94	0,25	2,05	98,48	98,19
1	10	250	175	3,94	0,25	2,05	98,57	98,42
1	10	250	200	3,94	0,25	2,05	98,56	98,34
1	10	250	225	3,94	0,25	2,05	98,50	98,14
1	10	310	150	3,94	0,25	2,05	98,09	97,03
1	10	310	175	3,94	0,25	2,05	98,54	98,26
1	10	310	200	3,94	0,25	2,05	98,58	98,24
1	10	310	225	3,94	0,25	2,05	98,40	97,86
1	10	310	250	3,94	0,25	2,05	98,22	97,38
1	10	250	150	3,94	0,5	2,05	98,37	97,82
1	10	250	175	3,94	0,5	2,05	98,53	98,37
1	10	250	200	3,94	0,5	2,05	98,54	98,33
1	10	250	225	3,94	0,5	2,05	98,46	98,10
1	10	310	150	3,94	0,5	2,05	97,54	95,22
1	10	310	175	3,94	0,5	2,05	98,45	98,06
1	10	310	200	3,94	0,5	2,05	98,48	98,19
1	10	310	225	3,94	0,5	2,05	98,38	97,88
1	10	310	250	3,94	0,5	2,05	98,22	97,35
1	10	250	150	3,94	1	2,05	97,59	95,41
1	10	250	175	3,94	1	2,05	98,42	98,02
1	10	250	200	3,94	1	2,05	98,52	98,27
1	10	250	225	3,94	1	2,05	98,42	98,01
1	10	310	150	3,94	1	2,05	96,52	91,78
1	10	310	175	3,94	1	2,05	98,17	97,29
1	10	310	200	3,94	1	2,05	98,44	98,08
1	10	310	225	3,94	1	2,05	98,37	97,84
1	10	310	250	3,94	1	2,05	98,22	97,36
1	10	250	150	3,94	3	2,05	80,72	49,26
1	10	250	175	3,94	3	2,05	84,52	56,92
1	10	250	200	3,94	3	2,05	92,53	78,63
1	10	250	225	3,94	3	2,05	97,72	95,77
1	10	250	250	3,94	3	2,05	97,83	96,08
1	10	310	150	3,94	3	2,05	95,69	89,10
1	10	310	175	3,94	3	2,05	97,48	94,98
1	10	310	200	3,94	3	2,05	98,43	97,10
1	10	310	225	3,94	3	2,05	98,41	97,96
1	10	310	250	3,94	3	2,05	98,26	97,53

1	10	250	150	3,94	4	2,05	69,63	33,52
1	10	250	175	3,94	4	2,05	73,05	37,90
1	10	250	200	3,94	4	2,05	81,09	50,33
1	10	250	225	3,94	4	2,05	92,75	79,62
1	10	250	250	3,94	4	2,05	97,42	94,74
1	10	310	150	3,94	4	2,05	95,71	89,19
1	10	310	175	3,94	4	2,05	97,28	94,34
1	10	310	200	3,94	4	2,05	98,38	97,87
1	10	310	225	3,94	4	2,05	98,42	97,97
1	10	310	250	3,94	4	2,05	98,29	97,56

Bibliography

[1] D. Hafemeister, Physics of Societal Issues: Calculations on National Security, Environment and Energy 2014, 8, 277-285.

[2] IEA, Global Energy & CO_2 Status Report, 2019.

https://www.iea.org/reports/global-energy-co2-status-report-2019/emissions

[3] BP Statistical Review of World Energy 2019, 68th edition.

https://www.bp.com/content/dam/bp/business-sites/en/global/corporate/pdfs/energy-economics/statistical-review/bp-stats-review-2019-full-report.pdf

[4] I. Omae, Aspects of carbon dioxide utilization. Catalysis Today, 2006, 115(1–4), 33–52.

[5] M.E. Boot-Handford, J.C. Abanades, E. J. Anthony, M. J. Blunt, S. Brandani, N.M. Dowell, J.R. Fernandez, M. Ferrari, R. Gross, J.P. Hallett, R.S. Haszeldine, P. Heptonstall, A. Lyngfelt, Z. Makuch, E. Mangano, R.T.J. Porter, M. Pourkashanian, G.T. Rochelle, N. Shah, J.G. Yaoa, P.S. Fennell, Carbon capture and storage update, Energy Environmental Science, 2014, 7, 130–189.

[6] S.N. Pandey, K.G. Sanjeev, T. Abhishek, K. Arun, Post combustion carbon capture technology, National Conference on Eco friendly Manufacturing for Sustainable Development, 19-21, 2010.

[7] B.M. Abraham, J.G. Asbury, E.P. Lynch, Coal-oxygen process provides CO_2 for enhanced recovery, Oil and Gas Journal, 1982, 80, 68–70.

[8] M. Christie, R. Victor, J. Li, B.V. Hassel, Advanced oxyfuel boilers and process heaters for cost effective CO_2 capture and sequestration, Annual Technical Progress Report, Praxair, Inc. 2006.

[9] J.D. Figueroa, T. Fout, S. Plasynski, H. McIlvried, R.D. Srivastava, Advances in CO_2 capture technology, The U.S. Department of Energy's Carbon Sequestration Program, International Journal of Greenhouse Gas Control 2008, 9–20.

[10] E.S. Sanz-Pérez, C.R. Murdock, S.A. Didas, C.W. Jones, Direct capture of CO_2 from ambient air, Chemical Reviews 2016, 116, 11840–11876.

[11] J.Gibbins, H.Chalmers, Carbon capture and storage. Energy Technology for Sustainable Development Group, Proc. IMechE, 224, Part C: J. Mechanical Engineering Science, 2009.

[12] C. Vogt, M. Monai, G.J. Kramer, B.M. Weckhuysen, The renaissance of the Sabatier reaction and its applications on Earth and in space, Nature Catalysis, 2, 188-197, 2019.

[13] Northern Lights – Part of The Full-Scale CCS Project. https://northernlightsccs.com/en/about

[14] V.A. Kuuskra, M.L. Godec, P. Dipietro, CO_2 Utilization from "Next Generation" CO_2 Enhanced Oil Recovery Technology, Energy Procedia 37, 2013, 6854 – 6866.

[15] S. Al-Hajeri, S. Negahban, G. Al-Yafei, A. Basry: Design and Implementation of the First CO_2-EOR Pilot in Abu Dhabi, SPE West Asia EOR Conference, Oman, 11-13, April 2010.

[16] E. Alper, O.Y. Orhan, CO_2 utilization: Developments in conversion processes, Petroleum 3, 2017, 109-126.

[17] A. Bazzanella, D. Kräme, Technologies for Sustainability and Climate Protection, Chemical Processes and Use of CO_2. DECHEMA Gesellschaft für Chemische Technik und Biotechnologie. https://dechema.de/en/energyandclimate/_/CO2_Buch_engl.pdf

[18] P. F. Tropschuh, E. Pham, Sustainable Automotive Technologies 2013: Proceedings of the 5th International Conference ICSAT 2013, Switzerland, 2013,185–190.

[19] M.D. Max, K. Sheps, S.R. Tatro, L. Brazel, J. Osegovic, Sea Water desalination as beneficial factor of CO_2 sequestration, Proceedings of the 6th International Conference on Gas Hydrates (ICGH 2008), Canada, 6-10, 2008.

[20] A. Al-Mamoori, A. Krishnamurthy, A.A. Rownaghi, F. Rezaei, Carbon Capture and Utilization Update, Energy Technology 2017, 5, 834-849.

[21] M. El-Shafie, S. Kambara, Y. Hayakawa, Hydrogen Production Technologies Overview. Journal of Power and Energy Engineering, 2019, 7, 107-154.

[22] C.M. Kalamaras, A.M. Efstathiou, Hydrogen Production Technologies: Current State and Future Developments. Hindawi Publishing Corporation Conference Papers in Energy Volume 2013.

[23] A. Buttler, H. Spliethoff, Current status of water electrolysis for energy storage, grid balancing and sector coupling via power-to-gas and power-to-liquids: A review, Renewable and Sustainable Energy Reviews, 82, 2440–2454, 2018.

[24] A. Ursua, L.M. Gandıa, P. Sanchis, Hydrogen Production from Water Electrolysis: Current Status and Future Trends. Proceedings of the IEEE, 100, 2, 2012.

[25] R. Phillips, C.W. Dunnill, Zero gap alkaline electrolysis cell design for renewable energy storage as hydrogen gas. Royal Society of Chemistry 2016,6, 100643-100651.

[26] World Energy Council Report on E-Storage: Shifting from Cost to Value Wind and Solar Applications, 2016.

https://www.worldenergy.org/assets/downloads/World-Energy-Resources-E-storage-wind-and-solar-presentation-World-Energy-Council.pdf

[27] IEA, Renewables 2019.

https://www.iea.org/reports/renewables-2019

[28] M.D. Porosoff, B. Yan, J.G. Chen, Catalytic reduction of CO2 by H2 for synthesis of CO, methanol and hydrocarbons: challenges and opportunities, Energy Environmental Science, 9, 62–73, 2016.

[29] Z. Wang, R.R. Roberts, G.F. Naterer, K.S. Gabriel, Comparison of thermochemical, electrolytic, photoelectrolytic and photochemical solar-to-hydrogen production technologies, International Journal of Hydrogen Energy 37, 2012, 16287-16301.

[30] Linde Gas Division, "The cleanest energy carrier ever" hydrogen solutions from Linde Gas. https://www.the-linde-group.com/en/images/HydrogenBrochure_EN_tcm14-10196.pdf

[31] A. Züttel, Materials for hydrogen storage, MaterialsToday, Elsevier Ltd 2003.

[32] A.J. Colozza, Hydrogen Storage for Aircraft Applications Overview. NASA/CR-2002-211867. https://ntrs.nasa.gov/archive/nasa/casi.ntrs.nasa.gov/20020085127.pdf

[33] Y. Wang, Recent advances in additive-enhanced magnesium hydride for hydrogen storage. Progress in Natural Science: Materials International 27, 2017, 41–49.

[34] F.V. Vázquez, J. Koponen, V. Ruuskanen, C. Bajamundi, A. Kosonen, P. Simell, J. Ahola, C. Frilund, J. Elfving, M. Reinikainen, N. Heikkinen, J. Kauppinen, P. Piermartini, Power-to-X technology using renewable electricity and carbon dioxide from ambient air: SOLETAIR proof-of-concept and improved process concept, Journal of CO2 Utilization, 28, 235–246, 2018.

[35] C. Schnuelle, J. Thoeming, T. Wassermann, P. Thier, A. von Gleich, S. Goessling-Reisemann, Socio-technical-economic assessment of power-to-X: Potentials and limitations for an integration into the German energy system, Energy Research and Social Science, 51, 187–197, 2019.

[36] S. Rönsch, J. Schneider, S. Matthischke, M. Schlüter, M. Götz, J. Lefebvre, P. Prabhakaran, S. Bajohr, Review on methanation.: From fundamentals to current projects, Fuel 166, 276–296, 2016.

[37] W. Li, H. Wang, X. Jiang, J. Zhu, Z. Liu, X. Guo, C. Song, A short review of recent advances in CO2 hydrogenation to hydrocarbons over heterogeneous catalysts, Royal Society of Chemistry, 8, 7651–7669, 2018.

[38] M. Götz, J. Lefebvre, F. Mörs, A. McDaniel Koch, F. Graf, S. Bajohr, R. Reimert, T. Kolb, Rewable Power to Gas : A technological and economic review, Renewable Energy, 85,1371–1390, 2016.

[39] C. Wulf, J. Linßen, P. Zapp, Review of Power-to-Gas projects in Europe, Energy Procedia, 155, 367–378, 2018.

[40] A. Goguet, F.C. Meunier, D. Tibiletti, J.P. Breen, R. Burch, Spectrokinetic investigation of Reverse Water-Gas-Shift Reaction intermediates over a Pt/CeO_2 catalyst, Journal of Physical Chemistry B, 108, 52, 20240-20246.

[41] B. Ernsta, S. Libsa, P. Chaumetteb, A. Kiennemanna, Preparation and characterization of Fischer–Tropsch active Co/SiO_2 catalysts, Applied Catalysis A: General 186, 1999, 145–168.

[42] J. Liu, C. Li, F. Wang, S. He, H. Chen, Y. Zhao, M. Wei, D.G. Evans, X. Duan, Enhanced low temperature activity of CO_2 methanation over highly dispersed Ni/TiO_2 catalyst, Catalyst Science and Technology, 2013,3, 2627-2633.

[43] C.H. Bartholomew, Mechanisms of catalyst deactivation, Applied Catalysis A: General 212, 2001, 17–60.

[44] B. Miao, S.S.K. Ma, X. Wang, H. Su, S.H. Chan, Catalysis mechanisms of CO_2 and CO methanation, Catalyst Science and Technology, 2016, 6, 4048–4058.

[45] G. Garbarino, D. Bellotti, P. Riani, L. Magistri, G. Busca, Methanation of carbon dioxide on Ru/Al_2O_3 and Ni/Al_2O_3 catalysts at atmospheric pressure: Catalysts activation, behaviour and stability, International Journey of Hydrogen Energy, 40, 2015, 9171-9182.

[46] M. Younas, L.L. Kong, M.J.K Bashir, H. Nadeem, A. Shehzad, S. Sethupathi, Recent advancements, fundamental challenges and opportunities in catalytic methanation of CO_2. Energy Fuels 2016, 30, 8815–8831.

[47] Z. Kowalczyk, K. Stołecki, W. Rarog-Pileckaa, E. Miskiewicza, E. Wilczkowska, Z. Karpinski, Supported ruthenium catalysts for selective methanation of carbon oxides at very low CO_x/H_2 ratios, Applied Catalysis A: General 342, 2008, 35–39.

[48] K. Jalama, Carbon dioxide hydrogenation over nickel-, ruthenium- and copper-based catalysts: Review of kinetics and mechanism, Catalysis Reviews, 59, 2, 95-164.

[49] J.L. Falconer, Adsorption and methanation of carbon dioxide on a nickel/silica catalyst, Journal of Catalysis 1980, 62, 2, 280-285.

[50] S. Eckle, H.G. Anfang, R.J. Behm, Reaction intermediates and side products in the methanation of CO and CO_2 over supported Ru catalysts in H_2-rich Reformate Gases, Journal of Physical Chemistry 2011, 4, 1361-1367.

[51] M. Marwood, R. Doepper, A. Renken, In situ surface and gas phase analysis for kinetic studies under transient conditions: the catalytic hydrogenation of CO_2, Applied Catalysis A: 151, 1997, 223–246.

[52] J. Witte, A. Calbry-Muzyka, T. Wieseler, P. Hottinger, S.M.A. Biollaz, T.J. Schildhauer, Demonstrating direct methanation of real biogas in a fluidized bed reactor, Applied Energy 240, 359–371, 2019.

[53] J. Li, L. Zhou, P. Li, Q. Zhu, J. Gao, F. Gu, F. Su, Enhanced fluidized bed methanation over a Ni/Al_2O_3 catalyst for production of synthetic natural gas, Chemical Engineering Journal, 183–189, 2013.

[54] M. Bailera, P. Lisbona, L.M. Romeo, S. Espatolero, Power to Gas projects review: Lab, pilot and demo plants for storing renewable energy and CO_2, Renewable and Sustainable Energy Reviews, 69, 292–312, 2017.

[55] Solar Fuel GmbH, United States Patent Application Publication, Method for producing a methane-rich product gas and reactor system usable for that purpose, US 2013/0041051A1.

https://patents.google.com/patent/US20130041051A1/en?oq=US+2013%2f0041051A1.

[56] G. Iaquaniello, S. Setini, A. Salladini, M. De Falco, CO_2 valorization through direct methanation of flue gas and renewable hydrogen: A technical and economic assessment, International Journal of Hydrogen Energy 43, 2018, 17069-17081.

[57] MAN Diesel & Turbo SE, United States Patent Application Publication, Shell and tube reactor for carrying out catalytic gas phase reactions, US 8961909B2.

https://patents.google.com/patent/US8961909B2/en?oq=US+8%2c961%2c909+B2

[58] L. Maggioni, C. Pieroni, ISAAC Report on the Biomethane Injection into National Gas Grid, 2016.

http://www.isaac-project.it/wp-content/uploads/2017/07/D5.2-Report-on-the-biomethane-injection-into-national-gas-grid.pdf

[59] IEA, Limits on Hydrogen Blending in Natural Gas Networks, 2018.

https://www.iea.org/data-and-statistics/charts/limits-on-hydrogen-blending-in-natural-gas-networks-2018

[60] P.E. Hintze, A.J. Meier, M.G. Shah., Sabatier System Design Study for a Mars ISRU Propellant Production Plant, International Conference on Environmental Systems 2018.

https://ntrs.nasa.gov/archive/nasa/casi.ntrs.nasa.gov/20180004697.pdf

[61] A.M. Gambelli, B. Castellani, A. Nicolini, F. Rossi, Gas hydrate formation as a strategy for CH_4/CO_2 separation: Experimental study on gaseous mixtures produced via Sabatier reaction, Journal of Natural Gas Science and Engineering 71, 2019, 102985.

[62] L. Jürgensena, E.A. Ehimenc, J. Bornb, J.B. Holm-Nielsen, Dynamic biogas upgrading based on the Sabatier process: Thermodynamic and dynamic process simulation, Bioresource Technology, 178, 2015, 323–329.

[63] P.J. Lunde, F.L. Kester, Rates of methane formation from carbon dioxide and hydrogen over a ruthenium catalyst, Journal of Catalysis: 30, 1973, 423–429.

[64] M.A.A. Aziz, A.A. Jalil, S. Triwahyono, A. Ahmad, CO_2 methanation over heterogeneous catalysts: recent progress and future prospects, Green Chemistry, 2015, 17, 2647–2663.

[65] M. Matrascia, Once through processes exploiting Ru-based catalysts for CO_2 hydrogenation to SNG, Thesis 2018-2019, Energy Engineering of Politecnico di Milano.

[66] K.P. Brooks, J. Hu, H. Zhu, R.J. Kee, Methanation of carbon dioxide by hydrogen reduction using the Sabatier process in microchannel reactors, Chemical Engineering Science 2007, 62, 1161-1170.

[67] L. Falbo, M. Martinelli, C.G. Visconti, L. Lietti, C. Bassano, P. Deiana, Kinetics of CO_2 methanation on a Ru-based catalyst at process conditions relevant for Power-to-Gas applications, Applied Catalysis B: Environmental 225, 2018, 354–363.

[68] N. Wakao, S. Kaguei, Heat and Mass Transfer in Packed Beds, Gordon and Breach Science Publishers, 1983, 2, 72-86.

[69] W.C. Yang, Handbook of fluidization and fluid-particle systems, CRC Press, 2003, 6, 38-39.

[70] D.W. Green, R.H. Perry, Perry's chemical engineers' handbook, seventh edition, 1997, 5-50.

[71] J.R. Welty, C.E. Wicks, R.E. Wilson, G.L Rohrer, Fundamentals of momentum, heat, and mass transfer, John Wiley & Sons Inc., 2007, 24, 410-412.

[72] A.S. Lamine, L. Gerth, H.L. Gall, G. Wild, Heat transfer in a packed bed reactor with cocurrent downflow of a gas and a liquid, Chemical Engineering Science 1996, 51,15, 3813-3827.

[73] R. Pfeffer, Heat and Mass Transport in Multiparticle Systems, Industrial & Engineering Chemistry Fundamentals 1964, 3, 4, 380-383.

[74] V. Specchia, G. Baldi, S. Sicardi, Heat transfer in packed bed reactors with one phase flow, Chemical Engineering Communications, 4, 361-380, 1980.

[75] F. Hartig and F. J. Keil, Large-scale spherical fixed bed reactors: modeling and optimization, Industrial & Engineering Chemistry Research, 32, 424-437, 1993.

[76] C.N. Satterfield, Mass Transfer in Heterogeneous Catalysis. M.I.T. PRESS Cambridge, 1970, 1.7, 41.

[77] R.S. Brodkey, H.C. Hershey, Transport Phenomena: A Unified Approach, Part I – Basic concepts in Transport Phenomena, Volume 1, 5.3.6, 182-183.

[78] S. Yagi, D. Kunii, N. Wakao, Studies on axial effective thermal conductivities in packed beds, American Institute of Chemical Engineers (A.I.Ch.E.) Journal, 6, 543-546, 1960.

[79] A. Montebelli, Carlo Giorgio Visconti, Gianpiero Groppi, Enrico Tronconi, Cristina Ferreira, Stefanie Kohler, Enabling small-scale methanol synthesis reactors through the adoption of highly conductive structured catalysts, Catalysis Today, 215, 176– 185, 2013.